University of Alberta

Autoregulation of RNA helicase operon expression

by

Albert Remus R. Rosana

A thesis submitted to the Faculty of Graduate Studies and Research
in partial fulfillment of the requirements for the degree of

Master of Science
in
Microbiology and Biotechnology

Department of Biological Sciences

Fall 2013
Edmonton, Alberta

Abstract

The cyanobacterium *Synechocystis* sp. PCC 6803 encodes for an RNA helicase, *crhR*, whose expression is regulated by the redox status of the electron transport chain and further enhanced by temperature downshift. In this study, the effect of *crhR* inactivation was investigated in response to temperature alteration. The inactivation of CrhR has drastic morphological and physiological effects particularly under cold stress, including a rapid cessation of photosynthesis, impaired cell growth, decrease in viability, cell size and DNA content and accumulation of structural abnormalities. Extensive transcript and protein analyses between wild type and mutant cells revealed that CrhR activity is linked to its autoregulation of expression involving complex network acting at the transcriptional and post-transcriptional levels. Furthermore, autoregulation is extended to the *rimO-crhR* operon where processing and degradation contributes to differential accumulation of the cistrons. Lastly, the potential association of CrhR in a degradosome-polysome complex in the thylakoid membrane is proposed.

Acknowledgement

I would like to extend by deepest appreciation and sincerest gratitude to the many individuals who contributed to the successful completion of this chapter in my life. These individuals deserved my humble thanks that made this thesis possible.

Dr. George W. Owttrim, my mentor who gave me the opportunity to conduct research under his tutelage. His unreserved guidance, support and encouragement allowed me to grow both professionally and personally as a scientist.

Dr. Danuta Chamot for imparting invaluable techniques especially the paranoia of RNA research. Dana's constant guidance on molecular biology techniques made this journey navigable.

My supervisory committee, Dr. Lisa Y. Stein and Dr. Michael Deyholos for their valuable suggestions and advice.

Oxana Tarassova, Reem Skeik and Denise Whitford made this whole journey so enjoyable. The camaraderie we all shared, the scientific craziness, the exhausting laughter, the unforgettable travels, sumptuous food trips and of course the love for 'gambling' will always be a part of my life that I will cherish.

My family, Papa, Mama, Tin-tin and Mommy Ella who always supported me in all my endeavour. For believing in me especially when I doubt myself, for loving me and encouraging me to finish the battle. I love you all.

And finally to the Lord God, who made everything possible. Thank you very much.

Table of Contents

List of Tables

List of Figures

Page

List of Abbreviations

A	Absorbance
aadA	aminoglycoside-3′-adenyltransferase
Ab	Antibody
ArgC	Arginine C
ARRR	Albert Remus Romero Rosana
asRNA	antisense Ribonucleic acid
ATCC	American Type Culture Collection
ATP	Adenosine triphosphate
bp	base pair
*BstE*II	*Bacillus stearothermophilus* ET II
BTP	bis[tris(hydroxymethyl)methylamino] propane
DEAD	asp-glu-ala-asp
DExD/H	asp-glu-amino acid-asp/his
DNA	Deoxyribonucleic acid
DNase I	Deoxyribonuclease I
dNTP	Deoxyribonucleotide triphosphate
DOOR	Database of Prokayotic Operons
DSM	Deutsche Sammlung von Mikroorganismen
°C	degree Celsius
CA	carbonic anhydrase
CCM	CO_2-concentrating mechanism
cDNA	Complementary Deoxyribonucleic acid
CFU	Colony forming units
Chl *a*	Chlorophyll a
Ci	Inorganic carbon
CO_2	Carbon dioxide
CrhR	Cyanobacterial RNA helicase redox
CrhC	Cyanobacterial RNA helicase cold
Cyb_6f	Cytochrome b_6f complex
ECL	Enhanced chemiluminescence
EcoRI	*Escherichia coli RI*
F	Forward
FACS	Fluorescence Activated Cell Sorting
GWO	George W Owttrim
H+	Hydrogen ion
h	hour
HCl	Hydrochloric acid

HCO_3	Bicarbonate
*Hinc*II	*Haemophilus influenzae Rc II*
His-CrhR	Histidine-tagged Cyanobacterial RNA helicase Redox
HMDS	Hexamethyldisilazane
*Hpa*I	*Haemophilus parainfluenzae I*
HPLC	High Performance Liquid Chromatography
IDT	Integrated DNA Technologies
IEM	Immuno Electron Microscopy
IgG	Immunoglobulin G
IRES	Internal Ribosome Entry Site
Kan	kanamycin
kbp	kilo base pair
kDa	kilo Dalton
$KHCO_3$	Potassium bicarbonate
knt	kilo nucleotide
LiCl	Lithium chloride
LPF	Laura Patterson-Fortin
M	Molar
MiaB	tRNA methylthiolase
min	minute
mg	milligram
ml	milliliter
MLV	Murine Leukemia Virus
mM	milliMolar
MT	Mutant
MV	Methyl viologen
NaCl	Sodium chloride
NADPH	Nicotinamide Adenine Dinucleotide Phosphate Hydrogen
ncRNA	non-coding Ribonucleic acid
NIES	National Institute for Environmental Studies
NIH	National Institute of Health
nm	nanometer
nt	nucleotide
O_2	Oxygen
OD	Optical density
OM	Outer membrane
ORF	Open reading frame
OsO_4	Osmium tetroxide
PAG	Polyacrylamide gel

PAGE	Polyacrylamide gel electrophoresis
PBS	Phosphate buffered saline
PC	Phycocyanin
PCC	Pasteur Culture Collection
PCR	Polymerase Chain Reaction
PI	Propidium iodide
PM	Plasma membrane
*Pml*I	*Pseudomonas maltophilia I*
PQ	Plastoquinone
PS	Photosystem
R	Reverse
RACE	Rapid Amplification of cDNA Ends
RCA	Rolling Circle Amplification
RimO	Ribosomal modification
RNA	Ribonucleic acid
RNase A	Ribonuclease A
RNase H	Ribonuclease H
RNP	Ribonucleoprotein
rnpB	RNase P RNA gene B
rpm	revolution per minute
Rps1	Ribosomal protein S1
ROS	Reactive Oxygen Species
ROSE	Repression of Heat Shock gene Expression
s	second
S	Supplementary
*Sac*II	*Streptomyces achromogenes II*
SDS	Sodium dodecyl sulphate
SEM	Scanning Electron Microscopy
SmaI	*Serratia marcescens I*
Sp	Spectinomycin
Spec	Spectinomycin
sRNA	small RNA
TEM	Transmission Electron Microscopy
TM	Thylakoid membrane
tRNA	Transfer Ribonucleic acid
U	Unit (s)
UTR	Untranslated region
UV	Ultraviolet
WT	Wild type
*Xba*I	*Xanthomonas badrii I*

Δ*crhR*	delta-*crhR* (mutant) – complete deletion strain
Δ*crhR*TR	delta-*crhR* (mutant) – 2-76 strain
ΔG	delta Gibbs free energy
µL	microliter
µg	micrograms
µmol	micromole

Chapter 1: Introduction

1.1. Cyanobacteria as model organism

Cyanobacteria are a diverse group of Gram-negative oxygenic photoautotrophic bacteria found in almost all environments with water and illumination (Whitton and Potts, 2012). They are a major contributor of primary productivity in an aquatic environment and their significant impact to nutrient cycling is well-documented (Grewe and Pulz, 2012). Geologic evidence indicates that cyanobacteria are one of the most ancient forms of life dating the Pre-Cambrian era (Tandeau de Marsac and Houmard, 1993; Knoll, 2008) and are a major contributor to the oxygenation and transformation of the Earth's atmosphere (Des Marais, 2000) A significant proportion of this molecular oxygen is produced in the marine environment whose major photoautotrophic players include cyanobacteria (Kasting and Siefert, 2002). Furthermore, the early reduction of atmospheric nitrogen was thought to be performed largely by nitrogen-fixing cyanobacteria (Berman-Frank *et al.*, 2003).

Cyanobacteria are largely cosmopolitan and ubiquitous microorganisms. Although cyanobacteria have shown high metabolic plasticity to able to colonize a number of habitats, their success can be ascribed to several unique characteristics. Variations in abiotic factors such as temperature, salinity and osmotic pressure, light fluctuations, water availability and nutrient scarcity limit the growth of a microorganism. Therefore, cyanobacteria have been equipped with an arsenal of adaptive features to survive, colonize, dominate and occupy a niche in all environments.

Cyanobacteria inhabit and dominate some of the most extreme environments on Earth such as the cryosphere, geothermal hotsprings, deserts, high-radiation surfaces, oligotrophic and eutrophic waters to name a few (Quesada and Vincent, 2012; Ward *et al*., 2012; Hu *et al*., 2012; Castenholz and Garcia-Pichel, 2012). They are found in ice-based environments or cryosphere including snow, lake ice, glacier ice, and ice-shelves and seasonally achieve high biomass. In such an environment, where extreme cold and low water activity result in severe constraints on growth and survival, microbial strategy for

successful colonization of these environments doesn't rely on adaptive mechanisms toward optimum growth but rather an increased tolerance to such extreme temperature. Entering dormancy and maintenance of minimum metabolic activity accounts for their widespread occurrence in the cryosphere (Quesada and Vincent, 2012).

The permissible temperature for cyanobacterial suboptimal to optimal growth has a wider range compared to other aquatic photosynthetic organisms such as eukaryotic algae (Castenholz and Waterbury, 1989). As such, temperature serves as a basic growth requirement allowing cyanobacterial colonization across the globe. A significant density of phytoplankton population in the open ocean is represented by two genera of picocyanobacteria *Prochlorococcus* sp. and *Synechococcus* sp. (Zwirglmaier *et al.*, 2007). The homocystous nitrogen fixing cyanobacterium, *Trichodesmium* contributes significantly to global nitrogen fixation in open marine ecosystem (Capone *et al*., 1997). Although a majority of cyanobacterial species are concentrated in tropical and subtropical regions with ambient temperatures, a number of species are reported in geothermal hotsprings (Phoenix *et al.*, 2000, Ward *et al.*, 2012) and shallow hydrothermal vents (Sorokin *et al.*, 1998) where temperatures can reach 100^{o}C. Therefore, the ability of an organism to respond, tolerate and adapt to fluctuations in environmental parameters such as temperature helps to ensure survival.

1.2 RNA Helicases and abiotic stress response

RNA helicases are molecular drivers that catalyze the reorganization of RNA secondary structures due to its innate ability to unwind double stranded RNA and anneal complimentary single stranded RNA molecules (Linder *et al*., 2011) potentially leading to RNA strand exchange (Chamot *et al*., 2005). RNA helicases not only modify RNA secondary structure but some have also been shown to disrupt ribonucleoprotein complexes by displacing the protein subunits. (Jankowsky *et al*., 2001; Linder *et al*., 2001; Jankowsky and Fairman, 2008). Recently, RNA helicases were proposed to function as ATP-dependent RNA

clamps, serving as a nucleation sites for larger protein complex recruitment (Linder and Jankowsky, 2011). These activities of RNA helicases require the energy from the hydrolysis of ATP (Linder and Jankowsky, 2011). The association of the helicase and ATP is required to bind the helicase to the RNA substrate while ATP hydrolysis removes the helicase from the RNA (Liu *et al*., 2008; Chen *et al*., 2008). Using single-molecule FRET approach, the *Bacillus* DEAD-box RNA helicase, YXiN, showed a close protein conformation resulting from the cooperative binding of ATP and the substrate RNA (Theissen *et al*., 2008). Upon binding of RNA and ADP, the helicase adopt an open confirmation. On the other hand, in the presence of ATP, the enzyme revealed a compact helicase structure established at the junction of the interdomain cleft of the two helicase core.

The majority of RNA helicases are categorized into helicase superfamily 2 (SF2) which is a collation of five subfamilies represented by DEAH, DExH and three DEAD-box protein subfamilies (Owttrim, 2013). The largest of the subfamilies is the group of DEAD-box RNA helicase with a conserved domain (Asp-Glu-Ala-Asp motif) (Fairman-Williams *et al*., 2010) and two RecA-like domains making up the conserved helicase core (Caruthers and McKay, 2002). Evolution suggests the importance of this group of proteins having high conservation across all three domains of life including many viruses (Jankowsky and Putnam, 2010; Owttrim, 2013 and Iost *et al*., 2013). In eukaryotes, RNA helicases play critical roles in all aspects of RNA metabolism such as transcription, translation initiation, ribosome assembly, mRNA splicing and RNA maturation and degradation (Rocak and Linder, 2004; Cordin *et al*., 2006). Conversely, prokaryotic RNA helicases function in related processes including ribosome biogenesis, RNA turnover and translation initiation (Iost *et al.,* 2013).

Regulation of bacterial gene expression is often modulated at the transcriptional and post transcriptional levels (Nogueira and Springer, 2000; Gualerzi *et al*., 2003; Kaberdin and Blassi, 2013) and a few genes at the translational level (Urban and Vogel, 2007; Milon and Rodnina, 2012). The emerging field of small regulatory RNAs including antisense, 5'and 3'

untranslated region (UTRs), internal sRNAs (Frolich and Vogel, 2009) and the recently characterized long antisense RNAs termed excludons (Sesto *et al*., 2012; Wurtzel *et al*, 2012) have been increasingly recognized as significant players in controlling global gene expression. The broad activity of DEAD-box RNA helicases drive RNA metabolism at different levels mainly through the modulation and remodeling of RNA secondary structures (Linder, 2006).

1.3 CrhR RNA helicase biology

1.3.1 Regulation of CrhR RNA helicase

The genome of the photosynthetic model cyanobacterium *Synechocystis* sp. PCC 6803 encodes only one DEAD-box RNA helicase, *crhR*, cyanobacterial RNA helicase redox (Kujat and Owttrim, 2000). The basic mechanisms regulating expression and the biochemical activity of CrhR are well-documented. *crhR* expression is tightly regulated by the redox status of the electron transport chain (Kujat and Owttrim, 2000). The redox poise at the junction of the plastoquinone pool and the $cytb_6f$ complex controls the induction of expression of *crhR* (Kujat and Owttrim, 2000, **Fig. 1.1**). Several additional stress conditions were also shown to induced *crhR* expression including salt stress, osmotic stress and temperature downshift (Vinnemeier and Hagemann, 1998; Mikami *et al*., 2002; Prakash *et al*., 2010). These factors simulate water stress which are all indirectly linked to the enhanced reduction of the chain (Chinnusamy *et al.*, 2007, Owttrim, 2013) and hence contribute to *crhR* induction. The signal transduction pathway governing the relay of the reduced status resulting in enhanced *crhR* expression is still unknown. There is no established two-component kinase-response regulator associated with the helicase cold-induction of expression. DNA microaaray analysis revealed the *crhR* is not under the direct control of the temperature responsive Hik33 sensor kinase, that controls expression of some cold-inducible genes in *Synechocystis* (Suzuki *et al*., 2000). This suggests that an

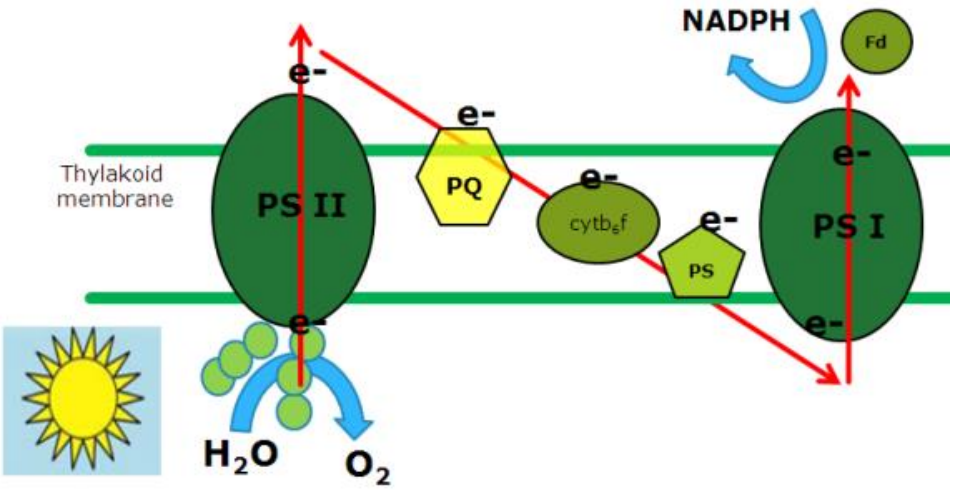

Figure 1.1. Organization of the photosynthetic electron transport chain. Photolysis of water occurs at the PSII complex where electrons (-e) are then shuttled through a series electron carriers (PQ- plastoquinone, cytb6f – cytochrome b6f complex, PS-plastocyanin) into PSI and final reduction via ferredoxin transfer to NADPH.

unknown mechanism(s) is orchestrating the signal response and induction of expression of *crhR*. Interestingly, a LexA-orthologue was discovered to bind the promoter region of *crhR* at 30^{o}C (Patterson-Fortin *et al*., 2006; Patterson-Fortin and Owttrim, 2008). The expression profile of this LexA-related protein is divergent from CrhR, with up regulation observed during conditions when *crhR* is induced. These results suggest that the LexA orthologue functions as a negative regulator of *crhR* gene expression.

1.3.2 Catalytic function of CrhR RNA helicase

Biochemical analysis of CrhR helicase revealed a distinct catalytic function. Nucleic acid helicase activity is often associated with unwinding of duplexes. CrhR RNA helicase though is unique since it catalyzes not only the unwinding of double-stranded RNA but also the annealing of complementary single-stranded RNA *in vitro* (Chamot *et al*., 2005). It is the fourth known RNA helicase shown to possess both unwinding and annealing abilities in a bidirectional ATP-dependent manner (Rossler *et al*., 2001; Chamot *et al*., 2005). As for all true RNA helicases, CrhR ATPase activity was RNA-dependent while the helicase function was shown to catalyze bidirectional unwinding although with low processivity. Conversely, the annealing activity of CrhR can create intermolecular duplexes. The annealing ability of RNA helicases is not conversed in cyanobacteria as indicated by the cold-inducible RNA helicase, CrhC in *Anabaena* sp. PCC 7120 (Yu and Owttrim, 2000). Furthermore, the simultaneous catalysis via unwiding and annealing of RNA targets occurs via RNA strand exchange (Chamot *et al*., 2005), a reaction also performed by the yeast DEAD box RNA helicase, Ded1 (Yang and Jankowsky, 2005).

1.3.3 *crhR* inactivation studies

CrhR helicase RNA target substrates are still unknown. Inactivation strategies coupled with transcript, microarray and proteomic analysis were

utilized to elucidate the role of CrhR. Subtractive RNA hybridization approach established an association between *crhR* and its upstream genes *slr0082* and *slr0081*, as well as *cpn60* which encodes a molecular chaperone GroEL in response to salt stress (Vinnemeier and Hagemann, 1999). Microarray analysis on the other hand, revealed potential regulation by CrhR over the hypothetical gene *slr0082* and two glutamine synthetase inactivating factor genes, *gifA* and *gifB* (Prakash *et al*., 2010). Interestingly, transcripts for three molecular chaperones (GroEL1, 2 and GroES) were down-regulated during cold stress in Δ*crhR*, suggesting probable control over the expression of these heat-shock genes (Prakash *et al*., 2010). Over the years, it has becoming evident that the disparity between transcript and protein levels makes it difficult to draw a generalization amongst transcriptomic data. As such, the proteome from wild type and Δ*crhR* was analyzed in response to temperature downshift (Rowland *et al*., 2011). Using 2D-gel protein analysis, a number of putative interacting proteins were proposed in accordance to cold-inducible polypeptides between wild type and Δ*crhR* (Rowland *et al*., 2011). A low to moderate correlation was established between the regulated proteins in this network and the previously generated transcriptome (Prakash *et al*., 2010), supporting the incongruence between transcriptomic and proteomic data.

At the physiological level, very little is known about the role of CrhR in *Synechocystis*. During this thesis, the absence of functional CrhR was reported to result-in the imbalance of the photosystem stoichiometry during cold stress (Sirresha *et al*., 2012). The photosystem I (PSI) trimer was significantly reduced in the absence of CrhR while photosystem transcripts *psaA* and *psaB* were strongly downregulated suggesting a functional role of CrhR in energy re-distribution in the cell during cold stress (Sirresha *et al*., 2012). Furthermore, almost all aspects cellular biosynthetic pathways were affected by *crhR* mutation (Rowland *et al*., 2011) including transcription, translation, photosynthesis, amino acid and carbohydrate metabolism. Mutant cells are relatively yellower than wild type cells (Rowland *et al*., 2011) suggesting alteration of pigment level or composition. Cold induction of mutant cells from 30 to 15^{o}C resulted in a

reduction of both photosynthetic and respiratory activities and lead to inability to eliminate lipid peroxides (Li *et al*., 2011). In cyanobacteria, one of the common response to cold stress is the up-regulation of fatty acid desaturases to increase the degree of lipid unsaturation (Los *et al*., 1997, Sakamoto *et al.*, 1997) thus improving the fluidity of the cellular membranes. In wild type cells, cold stress up-regulate fatty acid desaturase (*desA, desB* and *desD*) synthesis (Sakamoto and Bryant, 1997). On the other hand, cold-stressed Δ*crhR* cells resulted in downregulation of *desB* transcript which is further supported by the reduced levels of polyunsaturated fatty acids (Li *et al*., 2011).

1.4 Cyanobacterial operons

An operon is defined as a collation of two or more functional genes under the control of the same regulator or promoter that are transcribed as a primary polycistronic transcript (Jacob *et al.*, 1960). The coordination of cold response gene expression is seemingly governed by a limited number of operons. Generally in prokaryotes, the induction of stress responsive genes is orchestrated by sigma factors such as the *E. coli* master stress gene regulator σ^S accounting for the initiation of stress-induced regulon expression (Hengge-Aronis, 2002; Weber *et al*., 2005). Conversely, a limited number of genes are induced in response to cold stress in bacteria, however a cold-specific sigma factor or two component signal transduction pathway initiating global gene regulation has not been identified (Guiliodori *et al*., 2007). On a genome scale, genes within transcriptional operons frequently respond more similarly to cold shock conditions than monocistronic genes randomly selected from the genome (Gao *et al*., 2006). Expression of individual genes within operons is frequently not coordinated, resulting in differential transcript accumulation of operon members. Therefore, the control over polycistronic message expression suggests a complex cascade of signal transduction often leading to a combination of transcriptional, posttransciptional, translation and posttranslational controls (Kaberdin and Blassi, 2013; Milon and Rodnina, 2012).

The expression of polycistronic transcripts is a system that frequently ensures that the protein products of its gene members are synthesize for a coordinated function. In general, the member transcripts are processed to give rise to monocistronic mRNAs for translation, although some polycistronic transcripts . Endonucleases, such as RNase E or RNase III process the cistron separating the members into monocistronic transcripts in a nucleotide-specific manner (Kaberdin and Blasi, 2013). The cleaved mRNA may undergo further maturation through the alteration of either end, via 3'-5'exonuclease (Mohanty and Kushner, 2010) or a 5'-3' degradation (Even *et al*., 2005). The intrinsic stability or half-life of the mature monocistronic transcript defines the availability of the mRNA molecule as a template for translation (Gegenheimer and Apirion, 1981; King *et al*., 1986; Rauhut and Klug, 1999, Shyu *et al*., 2008, Pedersen *et al*., 2011; Arraiano *et al*., 2010). In bacteria, different operons are co-expressed in response to different environmental stimuli. Examples of which includes the *ibpAB* heat shock operon in *E. coli* (Gaubig *et al*., 2011), *oxyR-recG* oxidative stress operon in *Pseudomonas aeruginosa* (Ochsner *et al*., 2000), *desKR* cold shock operon in *Bacillus* (Beckering *et al*., 2002) and the *isiAB* operon during salt-stress and iron starvation in *Synechocystis* (Vinnemeier *et al*., 1998).

Several operon structures were reported in *Synechocystis*. The best studied cyanobacterial operons are the *atp1* and *atp2* operons which encode subunits of the F_OF_1 ATP-synthase (Lill and Nelson, 1991). In *Synechocytis*, the F_OF_1 ATP-synthase is made up of nine subunits with a hypothetical protein encoded in a gene located upstream of *atp1*. Another operon, the *isiAB* dicistronic operon, is upregulated in response to iron limitation. A similar induction is also observed during salt stress although *isiA* transcript accumulates 10-fold higher than the dicistronic message (Vinnemeier *et al*., 1998). It is apparent that multiple stress affect operon expression in cyanobacteria. In the case of *crhR*, its upstream gene, *slr0082* is separated by only 130 bp which potentially suggests that the two genes are co-transcribed as a dicistronic operon. This organization is supported by a substractive RNA hybridization approach revealing a ~3 kb mRNA transcript in

salt-stress *Synechocystis* cells detected by both *slr0082* and *crhR* probes (Vinnemeier and Hagemann, 1999).

1.5 Thesis objectives

The primary objective of this thesis is to further advance the understanding of CrhR RNA helicase expression in response in environmental temperature alterations. Using wild type and Δ*crhR* cells, the regulation of *crhR* at different levels was investigated. The work presented here utilized the model cyanobacterium *Synechocystis* sp. PCC 6803 that encodes only one DEAD-box RNA helicase whose regulated expression is linked to the light-driven changes in the redox status of the electron transport system (Kujat and Owttrim, 2000). This cellular phenomenon is further augmented by conditions that results in the reduction of the chain such as temperature downshifts and salt (Vinnemeier and Hagemann, 1999) and as well as osmotic stress (Mikami *et al*., 2002). So far, the cold-induction of *crhR* was performed on different ranges of temperature downshifts (Vinnemeier and Hagemann, 1999; Prakash *et al*., 2010; Li *et al*., 2011) which makes the definition of cold shock and the data generated from such experiments variable. The cold response is a function of both the choice of temperature and time. Therefore, the need to identify the temperature switch and time for induction for maximum *crhR* induction is of paramount importance. This basic requirement is addressed in this thesis, which is then utilized in dissecting the physiological, morphological roles and temperature regulation, proposed to be the standard temperature in elucidating the function of CrhR RNA helicase in cold acclimation of *Synechocystis*.

The first objective was to characterize the morphological and physiological aberrations in the cell resulting from the inactivation of the *crhR* gene. The observed phenotypic effects were compared between wild type *Synechocystis* cells and the *crhR* mutant (designated as 2-76). In Chapter 2, a combination of microscopic, flow cytometric and mass spectrometry analyses revealed distinct morphological and physiological differences between the two

strains. Furthermore, the mutation resulted in a decrease in cell viability, cell size and DNA content which are physiologically ascribed to reduced photosynthetic capacity and carbon fixation (Rosana *et al.*, 2012a). This is the first account showing the potential involvement of an RNA helicase in photosynthesis.

The second goal is to dissect the stress-enhanced expression of *crhR* gene in wild type and mutant cells resulting from temperature downshifts both at the transcript and protein level. In Chapter 3, coupled northern and western analyses revealed that autoregulation governs the expression of this RNA helicase. *crhR* transcript was rapidly synthesized upon temperature downshift in both strains with transient expression found in wild type while persistently high mRNA levels were detected in the mutant. Conversely, wild type CrhR protein was rapidly synthesized in response to cold shock while the inactivation caused unregulated level of truncated CrhR polypeptide. Transcript and protein half-life analysis indicates a profound effect of temperature-dependent stabilization of macromolecules. To date, this is the most extensive analysis performed on *crhR* expression, both at the transcript and protein level, revealing the complex interplay of CrhR-dependent and independent pathways leading to temperature acclimation in *Synechocystis*.

Thirdly, analysis of the autoregulatory nature of *crhR* expression under cold stress was also extended on the potential involvement of CrhR RNA helicase in the regulation of its upstream gene *slr0082*. Chapter 4 presents the operon processing data where Northern and 5' RACE analyses revealed co-transcription of *slr0082* and *slr0083* (*crhR*) as a dicistronic transcript with a strong constitutive promoter responding to temperature downshift. A complex network of mRNA processing events, involving CrhR RNA helicase, resulted in generation of mature transcripts with variable length and stability. Although both mature monocistronic transcripts are transiently expressed upon cold stress, the rapid degradation of *slr0082* and significant stabilization of *slr0083* add yet another complex layer of regulation of cold-inducible gene expression in cyanobacterium. Furthermore, the accumulation of two mature stable RNAs from the processed, unstable *slr0082* transcript potentially can act as a small regulatory RNA suggesting differential

stability not only between the individual monocistronic mRNAs but also within specific sequences within a single gene's open reading frame.

Lastly, an extended appendix is included in this thesis presented in Chapter 6. This section describes several projects completed as part of either preliminary analysis, bioinformatics predictions or data generated by directing student interns in the laboratory. The multifaceted control over CrhR expression is also represented at the translational and posttranslational levels. Using differential translational inhibitor antibiotics, affecting either translation initiation or elongation, *crhR* translation revealed an unknown mechanism that by-passed the effect of initiation antibiotics but not elongation inhibitors. The involvement of RNA helicases, and potentially CrhR, on the ribosomal apparatus function or biogenesis is increasingly becoming evident in recent years (Iost *et al*., 2013). Using a combination of bioinformatic predictions and sucrose gradient approach, CrhR was found to co-sediment with ribosomal complexes. Furthermore, mass spectrometry revealed not only the ribosomal subunits but also degradosome-related polypeptides and thylakoid membrane proteins. These interesting data potentially will lead to the first account of a DEAD-box RNA helicase for a photosynthetic bacterium showing an RNA helicase interacting with a ribosome-degradosome complex localized in the thylakoid membrane. Finally, operon analysis was extended using bioinformatics tools. Evolutionary conservation of the *rimO-crhR* operon structure was established using predictive databases which were confirmed by RACE analysis in this study.

Overall, the regulation of *crhR* in response to temperature stress revealed a complex network involving autoregulation together with controls at the transcriptional, posttranscriptional and translational and potentially posttranslational levels. As the only DEAD-box RNA helicase in *Synechocystis*, CrhR, its multi-level regulation is seemingly correlated to it performing various functions in the cell and these investigative endeavours provided several future directions for elucidating photosynthetic RNA helicase functions.

1.6 References

Arraiano, C. M., Andrade, J. M., Domingues, S., Guinote, I. B., Malecki, M., Matos, R. G., and Viegas, S. C. 2010. The critical role of RNA processing and degradation in the control of gene expression. FEMS Microbiol Rev. **34**(5): 883-923.

Beckering CL, Steil L, Weber MHW, Volker U and Marahiel M. 2002. Genomewide transcriptional analysis of the cold shock response in *Bacillus subtilis*. J Bacteriol. **184** (22): 6395-6402.

Berman-Frank, I., Lundgren, P., Chen, Y., Küpper, H., Kolber, Z., Bergman, B., and Falkowski, P. 2001. Segregation of nitrogen fixation and oxygenic photosynthesis in the marine cyanobacterium Trichodesmium. Science **294**(5546): 1534-1537.

Capone, D.G., Zehr, J.P., Paerl, H.W., Bergman, B., and Carpenter, E.J. 1997. Trichodesmium, a globally significant marine cyanobacterium. Science **276**(5316): 1221-1229.

Caruthers, J.M., and McKay, D.B. 2002. Helicase structure and mechanism. Curr Opin Struct Biol. **12**(1): 123-133.

Castenholz, R., and Waterbury, J. 1989. Oxygenic photosynthetic bacteria. Group I. Cyanobacteria. Bergey's manual of systematic bacteriology **3**: 1710-1806.

Chamot, D., Colvin, K.R., Kujat-Choy, S.L., and Owttrim, G.W. 2005. RNA structural rearrangement via unwinding and annealing by the cyanobacterial RNA helicase, CrhR. J. Biol. Chem. **280**(3): 2036-2044.

Chen, Y., Potratz, J.P., Tijerina, P., Del Campo, M., Lambowitz, A.M., and Russell, R. 2008. DEAD-box proteins can completely separate an RNA duplex using a single ATP. Proc Natl Acad Sci U S A, **105:** 20203-20208.

Chinnusamy, V., Zhu, J., and Zhu, J. 2007. Cold stress regulation of gene expression in plants. Trends Plant Sci. **12**(10): 444-451.

Cordin, O., Banroques, J., Tanner, N.K., and Linder, P. 2006. The DEAD-box protein family of RNA helicases. Gene **367**: 17-37.

Des Marais, D.J. 2000. When did photosynthesis emerge on Earth? Science. **289**(5485): 1703-1705.

Dismukes, G., Klimov, V., Baranov, S., Kozlov, Y.N., DasGupta, J., and Tyryshkin, A. 2001. The origin of atmospheric oxygen on Earth: the innovation of oxygenic photosynthesis. Proc Natl Acad Sci. **98**(5): 2170-2175.

Even, S., Pellegrini, O., Zig, L., Labas, V., Vinh, J., Bréchemmier-Baey, D., and Putzer, H. 2005. Ribonucleases J1 and J2: two novel endoribonucleases in *B. subtilis* with functional homology to *E. coli* RNase E. Nucleic Acids Res. **33**(7): 2141-2152.

Fairman-Williams, M.E., Guenther, U., and Jankowsky, E. 2010. SF1 and SF2 helicases: family matters. Curr Opin Struct Biol. **20**(3): 313-324.

Falkowski, P.G., and Godfrey, L.V. 2008. Electrons, life and the evolution of Earth's oxygen cycle. Phil Trans Royal Soc B: Biol Sci. **363**(1504): 2705-2716.

Fröhlich, K.S., and Vogel, J. 2009. Activation of gene expression by small RNA. Curr Opin Microbiol. **12**(6): 674-682.

Gao, H., Yang, Z. K., Wu, L., Thompson, D. K., and Zhou, J. 2006. Global transcriptome analysis of the cold shock response of *Shewanella oneidensis* MR-1 and mutational analysis of its classical cold shock proteins. J Bacteriol. **188**(12): 4560-4569.

Gaubig, L. C., Waldminghaus, T., and Narberhaus, F. 2011. Multiple layers of control govern expression of the Escherichia coli *ibpAB* heat-shock operon. Microbiol. **157**(1): 66-76.

Gegenheimer, P and Apirion, D. 1981. Processing of procaryotic ribonucleic acid. Microbiol Rev. **45**(4): 502.

Grewe, C.B., and Pulz, O. 2012. The Biotechnology of Cyanobacteria. *In* Ecology of Cyanobacteria II. Springer. 707-739.

Giuliodori, A. M., Brandi, A., Giangrossi, M., Gualerzi, C. O., and Pon, C. L. 2007. Cold-stress-induced *de novo* expression of *infC* and role of IF3 in cold-shock translational bias. RNA. **13**(8): 1355-1365.

Gualerzi, C.O., Maria Giuliodori, A., and Pon, C.L. 2003. Transcriptional and post-transcriptional control of cold-shock genes. J Mol Biol. **331**(3): 527-539.

Hengge-Aronis, R. 2002. Signal transduction and regulatory mechanisms involved in control of the σS (RpoS) subunit of RNA polymerase. Microbiol Mol Biol Rev. **66**(3): 373-395.

Iost, I., Bizebard, T., and Dreyfus, M. 2013. Functions of DEAD-box proteins in bacteria: Current knowledge and pending questions. Biochim Biophys Acta (BBA)-Gene Regulatory Mechanisms. http://dx.doi.org/10.1016/j.bbagrm.2013.01.012

Jacob, F., Perrin, D., Sánchez, C., and Monod, J. 1960. L'opéron: groupe de gènes à expression coordonnée par un opérateur. CR Acad Sci Paris. **250**: 1727-1729.

Jankowsky, E., and Putnam, A. 2010. Duplex unwinding with DEAD-box proteins. *In* Helicases. Springer. 245-264.

Jankowsky, E., and Fairman, M.E. 2008. Duplex unwinding and RNP remodeling with RNA helicases. *In* RNA-Protein Interaction Protocols. Springer. 343-355.

Jankowsky, E., Gross, C.H., Shuman, S., and Pyle, A.M. 2001. Active disruption of an RNA-protein interaction by a DExH/D RNA helicase. Sci. **291**(5501): 121-125.

Kaberdin, V.R., and Bläsi, U. 2013. Bacterial helicases in post-transcriptional control. Biochim Biophys Acta (BBA)-Gene Regulatory Mechanisms. http://dx.doi.org/10.1016/j.bbagrm.2012.12.005.

Kåhrström, C.T. 2012. Bacterial Transcription: Introducing the excludon. Nat Rev Microbiol. doi:10.1038/nrmicro2822

Kasting, J.F., and Siefert, J.L. 2002. Life and the evolution of Earth's atmosphere. Science **296**(5570): 1066-1068.

King, T. C., Sirdeskmukh, R. A. V. I., and Schlessinger, D. 1986. Nucleolytic processing of ribonucleic acid transcripts in procaryotes. Microbiol Rev. **50**(4): 428.

Knoll, A.H. 2008. Cyanobacteria and earth history. Cyanobacteria: Molecular Biology, Genomics and Evolution : 1-19.

Kujat, S.L., and Owttrim, G.W. 2000. Redox-regulated RNA helicase expression. Plant Physiol. **124**(2): 703-714.

Li, Q., and Xu, X. D. 2011. The role of CrhR, the RNA helicase gene, in cold acclimation of *Synechocystis* sp. PCC 6803. Acta Hydrobiol Sinica. **3**: 009.

Lill, H., and Nelson, N. 1991. The atp1 and atp2 operons of the cyanobacterium *Synechocystis* sp. PCC 6803. Plant Mol Biol. **17**(4): 641-652.

Linder, P., Tanner, N.K., and Banroques, J. 2001. From RNA helicases to RNPases. Trends Biochem. Sci. **26**(6): 339-341.

Linder, P. 2006. Dead-box proteins: a family affair—active and passive players in RNP-remodeling. Nucleic Acids Res. **34**(15:, 4168-4180.

Linder, P., and Jankowsky, E. 2011. From unwinding to clamping the DEAD box RNA helicase family. Nat Rev Mol Cell Biol. **12**(8): 505-516.

Liu F., Putnam, A., and Jankowsky, E. 2008. ATP hydrolysis is required for DEAD-box protein recycling but not for duplex unwinding, Proc Natl Acad Sci **105:** 20209-20214.

Los, D.A., Ray, M.K., and Murata, N. 1997. Differences in the control of the temperature-dependent expression of four genes for desaturases in *Synechocystis* sp. PCC 6803. Mol Microbiol. **25**(6): 1167-1175.

Mikami, K., Kanesaki, Y., Suzuki, I., and Murata, N. 2002. The histidine kinase Hik33 perceives osmotic stress and cold stress in Synechocystis sp. PCC 6803. Mol Microbiol. **46**(4): 905-915.

Milón, P., and Rodnina, M.V. 2012. Kinetic control of translation initiation in bacteria. Crit Rev Biochem Mol Biol. **47**(4): 334-348.

Mohanty, B. K., and Kushner, S. R. 2010. Processing of the *Escherichia coli* leuX tRNA transcript, encoding tRNA Leu5, requires either the 3′→ 5′ exoribonuclease polynucleotide phosphorylase or RNase P to remove the Rho-independent transcription terminator. Nucleic Acids Res. **38**(2): 597-607.

Nogueira, T., and Springer, M. 2000. Post-transcriptional control by global regulators of gene expression in bacteria. Curr Opin Microbiol. **3**(2): 154-158.

Ochsner, U. A., Vasil, M. L., Alsabbagh, E., Parvatiyar, K., and Hassett, D. J. 2000. Role of the *Pseudomonas aeruginosa oxyR-recG* operon in oxidative stress defense and DNA repair: OxyR-dependent regulation of *katB-ankB, ahpB, andahpC-ahpF*. J Bacteriol. **182**(16): 4533-4544.

Owttrim, G.W. 2013. RNA helicases: Diverse roles in prokaryotic response to abiotic stress. RNA Biol. **10**(1): 96-110.

Owttrim, G.W. 2006. RNA helicases and abiotic stress. Nucleic Acids Res. **34**(11): 3220-3230.

Patterson-Fortin, L.M., and Owttrim, G.W. 2008. A *Synechocystis* LexA-orthologue binds direct repeats in target genes. FEBS Let. **582**(16): 2424-2430.

Patterson-Fortin, L.M., Colvin, K.R., and Owttrim, G.W. 2006. A LexA-related protein regulates redox-sensitive expression of the cyanobacterial RNA helicase, crhR. Nucleic Acids Res. **34**(12): 3446-3454.

Pedersen, M., Nissen, S., Mitarai, N., Svenningsen, S. L., Sneppen, K., and Pedersen, S. 2011. The functional half-life of an mRNA depends on the ribosome spacing in an early coding region. J Mol Biol. **407**(1), 35-44.

Phoenix, V.R., Adams, D.G., and Konhauser, K.O. 2000. Cyanobacterial viability during hydrothermal biomineralisation. Chem. Geol. **169**(3): 329-338.

Prakash, J.S., Krishna, P.S., Sirisha, K., Kanesaki, Y., Suzuki, I., Shivaji, S., and Murata, N. 2010. An RNA helicase, CrhR, regulates the low-temperature-inducible expression of heat-shock genes *groES*, *groEL1* and *groEL2* in *Synechocystis* sp. PCC 6803. Microbiology **156**(2): 442-451.

Rocak, S., and Linder, P. 2004. DEAD-box proteins: the driving forces behind RNA metabolism. Nat Rev Mol Cell Biol **5**(3): 232-241.

Rosana ARR, Ventakesh M, Chamot D, Patterson-Fortin LM, Tarassova O, Espie GS and Owttrim GW. 2012a. Inactivation of a low temperature induced RNA helicase in *Synechocystis* sp. PCC 6803: Physiological and morphological consequences. Plant Cell Physiol **53**: 646–658.

Rosana ARR, Chamot D, and Owttrim GW. 2012b. Autoregulation of RNA helicase expression in response to temperature stress in *Synechocystis* sp. PCC 6803. PLoS ONE **7**(10): e48683.

Rössler, O. G., Straka, A., and Stahl, H. 2001. Rearrangement of structured RNA via branch migration structures catalysed by the highly related DEAD-box proteins p68 and p72. Nucleic Acids Res. **29**(10): 2088-2096.

Rowland, J.G., Simon, W.J., Prakash, J.S., and Slabas, A.R. 2011. Proteomics reveals a role for the RNA helicase *crhR* in the modulation of multiple metabolic pathways during cold acclimation of *Synechocystis* sp. PCC6803. J Proteome Res. **10**(8): 3674-3689.

Sakamoto, T., Higashi, S., Wada, H., Murata, N., and Bryant, D.A. 1997. Low-temperature-induced desaturation of fatty acids and expression of desaturase genes in the cyanobacterium *Synechococcus* sp. PCC 7002. FEMS Microbiol. Lett. **152**(2): 313-320.

Sakamoto, T., and Bryant, D. A. 1997. Growth at low temperature causes nitrogen limitation in the cyanobacterium *Synechococcus* sp. PCC 7002. Arch Microbiol. 169(1): 10-19.

Sesto, N., Wurtzel, O., Archambaud, C., Sorek, R., and Cossart, P. 2012. The excludon: a new concept in bacterial antisense RNA-mediated gene regulation. Nat Rev Microbiol. **11**(2): 75-82.

Sireesha, K., Radharani, B., Krishna, P. S., Sreedhar, N., Subramanyam, R., Mohanty, P., and Prakash, J. S. 2012. RNA helicase, CrhR is indispensable for the energy redistribution and the regulation of photosystem stoichiometry at low temperature in *Synechocystis* sp. PCC6803. Biochim Biophys Acta (BBA)-Bioenergetics. http://dx.doi.org/10.1016/j.bbabio.2012.04.016

Sorokin, Y.I., Sorokin, P.Y., and Zakuskina, O.Y. 1998. Microplankton and its functional activity in zones of shallow hydrotherms in the Western Pacific. J. Plankton Res. **20**(6): 1015-1031.

Suzuki, I., Los, D.A., Kanesaki, Y., Mikami, K., and Murata, N. 2000. The pathway for perception and transduction of low-temperature signals in *Synechocystis*. Science Signaling **19**(6): 1327.

Tandeau de Marsac, N., and Houmard, J. 1993. Adaptation of cyanobacteria to environmental stimuli: new steps towards molecular mechanisms. FEMS Microbiol. Lett. **104**(1): 119-189.

Theissen, B., Karow, A.R., Köhler, J., Gubaev, A., and Klostermeier, D. 2008. Cooperative binding of ATP and RNA induces a closed conformation in a DEAD box RNA helicase. Proc Natl Acad Sci. **105**(2): 548-553.

Urban, J.H., and Vogel, J. 2007. Translational control and target recognition by *Escherichia coli* small RNAs in vivo. Nucleic Acids Res. **35**(3): 1018-1037.

Vinnemeier, J., Kunert, A., and Hagemann, M. 1998. Transcriptional analysis of the *isiAB* operon in salt-stressed cells of the cyanobacterium *Synechocystis* sp. PCC 6803. FEMS Microbiol Let. **169**(2): 323-330.

Vinnemeier, J., and Hagemann, M. 1999. Identification of salt-regulated genes in the genome of the cyanobacterium *Synechocystis* sp. strain PCC 6803 by subtractive RNA hybridization. Arch Microbiol. **172**(6): 377-386.

Ward, D.M., Castenholz, R.W., and Miller, S.R. 2012. Cyanobacteria in geothermal habitats. *In* Ecology of Cyanobacteria II. Springer. 39-63.

Weber, H., Polen, T., Heuveling, J., Wendisch, V. F., and Hengge, R. 2005. Genome-wide analysis of the general stress response network *in Escherichia coli*: σS-dependent genes, promoters, and sigma factor selectivity. J Bacteriol. **187**(5): 1591-1603.

Whitton, B.A., and Potts, M. 2012. Introduction to the cyanobacteria. *In* Ecology of Cyanobacteria II. Springer. 1-13.

Yang, Q., and Jankowsky, E. 2005. ATP-and ADP-dependent modulation of RNA unwinding and strand annealing activities by the DEAD-box protein DED1. Biochemistry. **44**(41): 13591-13601.

Yu, E., and Owttrim, G.W. 2000. Characterization of the cold stress-induced cyanobacterial DEAD-box protein CrhC as an RNA helicase. Nucleic Acids Res. **28**(20): 3926-3934.

Zwirglmaier, K., Heywood, J.L., Chamberlain, K., Woodward, E.M.S., Zubkov, M.V., and Scanlan, D.J. 2007. Basin-scale distribution patterns of picocyanobacterial lineages in the Atlantic Ocean. Environ. Microbiol. **9**(5): 1278-1290.

Chapter 2: Inactivation of a low temperature-induced RNA helicase in *Synechocystis* sp. PCC 6803: Physiological and morphological consequences

A version of this chapter has been published.
Albert Remus R. Rosana, Meghana Ventakesh, Danuta Chamot,
Laura M. Patterson-Fortin, Oxana Tarassova,
George Espie and George W. Owttrim.
2012. Plant Cell Physiol. 53:646-658

2.1 Introduction

RNA helicases are ubiquitous enzymes conserved from viruses to humans forming an extended superfamily of proteins termed DEAD or DExD/H (Rocak and Linder 2004, Cordin *et al*., 2006; Fairman-Williams *et al*., 2010). Members of this protein family function as molecular motors catalyzing the rearrangement of RNA secondary structure, associated with all aspects of RNA metabolism including translation initiation, mRNA degradation, RNA splicing, ribosome assembly, small RNA metabolism and transcription (Rocak and Linder 2004, Linder and Owttrim 2009, Jankowsky 2011). These activities regulate gene expression and have profound effects on cellular growth and development in eukaryotes and stress responses in prokaryotes (Owttrim 2006; Barral *et al*., 2009; Ewen-Campen *et al*., 2010). Bacterial responses to low temperature stress are well-studied phenomena on the molecular level (Shivaji and Prakash, 2010). However, a cold-specific sigma factor and two component signal transduction pathways, associated with regulation of cold stress gene expression in other prokaryotic regulatory systems, do not control all genes involved in this response in cyanobacteria (Suzuki *et al*., 2000; Shivaji and Prakash 2010). Thus, the mechanisms by which prokaryotic organisms respond to cold stress are not entirely understood. A common feature of the prokaryotic cold stress response involves RNA helicase activity as bacterial genomes almost invariably encode an RNA helicase whose expression is induced at low temperature (Jones *et al*., 1996; Chamot *et al*., 1999; Chamot and Owttrim, 2000; Yu and Owttrim, 2000; El-Fahmawi and Owttrim, 2003; Hunger *et al*., 2006). In *Escherichia coli*, three of the five DEAD-box RNA helicases perform roles in ribosome biogenesis, although the exact nature of the role has not been elucidated (Charollais *et al*., 2003; Charollais *et al*., 2004; Trubetskoy *et al*., 2009; Jagessar and Jain, 2010). One of these, CsdA, is involved in 50S ribosome biogenesis (Charollais *et al*., 2004) and is also induced in response to cold stress (Jones *et al*., 1996). Recent analysis indicates that CsdA performs an unknown role in the conversion of 40S precursor particles into 50S subunits (Peil *et al*., 2008). Thus, similar to the

majority of RNA helicases, the molecular aspects of RNA helicase interaction have been studied while the physiological and morphological functions performed by cold stress-induced RNA helicases remain unclear (Jankowsky, 2011).

CrhR is a DEAD box RNA helicase in the model photosynthetic cyanobacterium *Synechocystis* sp. PCC 6803 whose expression and biochemical activity are well studied. *crhR* expression is regulated by the redox status of the electron transport chain, with expression induced in response to conditions that elicit reduction of the chain, including salt and cold stress (Kujat and Owttrim, 2000). Relay of the reduced status of the electron transport chain occurs through an unknown mechanism but regulates binding of a LexA-related protein to the *crhR* promoter (Patterson-Fortin *et al*., 2006; Patterson-Fortin and Owttrim, 2008). Biochemically, CrhR is distinct as it is one of only three RNA helicases known to catalyze both double-stranded RNA (dsRNA) unwinding and complementary single-stranded RNA (ssRNA) annealing through a mechanism which can combine both processes, generating RNA stand exchange (Chamot *et al*., 2005).

We have mutated the gene encoding CrhR in *Synechocystis* sp. PCC 6803 as a means by which to continue analysis of the physiological function performed by this helicase. Here we show that mutation of *crhR* has profound effects on cellular physiology and metabolism. Although these effects are exacerbated in response to cold stress, they do not occur directly in response to cold stress as they are observed at all temperatures. Cell growth is dramatically affected at 20°C, an effect that correlates with changes in cell size and division capabilities and photosynthetic performance associated with a reduced capacity for electron transport and CO_2 fixation. The results indicate an intimate link between CrhR RNA helicase activity and photosynthetic capacity, a relationship that is crucial at low temperature. To our knowledge, this is the first report of an RNA helicase that is associated with photosynthetic capacity.

2.2 Materials and Methods

2.2.1 Bacterial strains and culture conditions

The *Synechocystis* sp. strain PCC 6803 strains used in this study included the WT and two strains in which *crhR* (slr0083) was inactivated, the Δ*crhR* mutant (2-76) and 6AO6 (a kind gift from Kintake Sonoike). *Synechocystis* was cultured photoautotrophically in BG-11 liquid medium at 30°C under continuous illumination (30 μmol photons m^{-2} s^{-1}) with continuous bubbling with sterile, humidified air (Chamot and Owttrim, 2000). Glucose (5 mM) was added when indicated to support photoheterotrophic growth. Medium supporting mutant cyanobacterial growth was supplemented with sodium thiosulfate (0.3%), tricine (10 mM, pH 8.0) and antibiotics when required [a mixture of spectinomycin and spectinomycin (50 μg ml^{-1}each) for the Δ*crhR* mutant and chloramphenicol (8 μg ml^{-1}) for 6AO6]. Cold-stressed cells were produced by incubation as above at 20°C for the indicated periods (Chamot and Owttrim, 2000). Cell growth was measured by a change in light scattering of liquid cultures at an optical density (OD) of 750 nm. Cell viability was determined by determining colony-forming units (CFU) after exposing mid-log phase cells to 20°C for the indicated times, followed by growth on plates at 30°C. Results are reported as a survival fraction in relation to the CFU ml^{-1} value at time zero for each strain.

The effect of *crhR* inactivation was studied in two mutants created using different strategies. The Δ*crhR* mutant was constructed by replacement of the 1.42 kbp *Pml*I–*Hpa*I fragment with the aminoglycoside-3′-adenyltransferase (*aadA*) cassette from pHP45Ω (Prentki and Krisch 1984). In 6AO6, *crhR* was inactivated by random insertion of the Transprimer 2 sequence from pGPS2.1 by K. Sonoike as described by the manufacturer (New England Biolabs). Confirmation of complete segregation of the *crhR* gene was performed by PCR using primers GWO39 (5′-TGACGATGTGAAAACC-3′), GWO40 (5′-TGTGTGGCTTCAGGC-3′) and GWO41 (5′-CCGGGGGAGGTAGAGA-3′) for 2-76, and using GWO73 (5′-AGACCCTGGATGTGCTGAT-3′) and GWO74 (5′-TTGGGAAGAATCCTTAGGC-3′) for 6AO6 (data not shown). We determined the location of the Transprimer 2 insertion by amplifying the entire *crhR* ORF

plus the Transprimer 2 insert from 6AO6 genomic DNA using GWO73 and GWO74 and sequencing the product with primer GWO39 (5′-TGACGATGTGAAAACC-3′). The Transprimer 2 inserted at bp 2,888,242 of the *crhR* ORF, 76 bp upstream of the start of the Δ*crhR* deletion (*Pml*I site).

In the Δ*crhR* mutation, a portion of the 3′ region of the downstream gene,*argC*, was deleted which could potentially affect cell morphology and physiology. This did not appear to be the case for a number of reasons. Firstly, the Δ*crhR* mutant is not an arginine auxotroph. Secondly, the phenotypic and morphological defects observed in the Δ*crhR* mutant were not rescued by inclusion of arginine in the growth media (data not shown), even though cyanobacteria contain high-affinity arginine transporters (Flores and Herrero, 1994). These results indicate that *Synechocystis* differs from *Anabaena* in which *argC* mutation results in arginine auxotrophy (Floriano *et al*., 1992). Finally, for all physiological and morphological assays investigated, an identical phenotype was observed in the 6AO6 mutant which contains the WT *argC* gene.

2.2.2 Photosynthetic oxygen evolution

Cells were harvested and washed three times by centrifugation (12,500 ×*g* for 15 s, Beckman microfuge E) in Ci-free 25 mM 1,3-bis[tris(hydroxymethyl)methylamino] propane (BTP)/23.5 mM HCl buffer, pH 8.0, and were used at a final concentration of 7–15 μg Chl *a* ml^{-1}. Photosynthesis was measured as O_2 evolution in a Clark-type O_2 electrode (Hansatech, Norfolk, UK) at 20–30°C (Espie *et al*., 1988b). The rates of CO_2 supply for photosynthesis from HCO_3^- dehydration at the experimental pHs were calculated as described previously (Espie *at al*., 1988a). Light was provided by a tungsten/halogen projector lamp at 400 μmol photons m^{-2} s^{-1}, measured using a Li-Cor Li-185 light meter and quantum sensor. Photosynthesis was initiated, first by the addition of 25 mM NaCl to activate/energize HCO_3^- transport (Espie *et al*., 1988b), followed by the addition of known amounts of $KHCO_3$ to cells at the CO_2 compensation

point. Results shown are the average of triplicates. MV (1 mM, Sigma) was added as indicated.

2.2.3 Mass spectrometric measurements of photosynthetic CO_2 uptake

Washed cell suspensions (4 ml) were transferred to a glass reaction vessel, containing a magnetic stirrer, and the chamber was closed with a plexiglass stopper leaving no head space. The reaction chamber was connected to the ion source of a magnetic sector mass spectrometer (model MM 14-80 SC; VG Gas Analysis) by an inlet covered with a dimethyl silicone membrane that allowed dissolved gases to pass, but not ions such as HCO_3^-. The illuminated (400 μmol photons m^{-2} s^{-1}) cells were allowed to consume residual Ci photosynthetically before experiments commenced and then were darkened. The appropriate concentration of ^{13}C-labeled CO_2/HCO_3^- substrate was added, which also served as an internal calibration standard for the instrument. The mass spectrometer was operated in 'peak-jumping' mode to allow for the sequential measurement of the dissolved O_2 (*m/z* = 32) and $^{13}CO_2$ (*m/z* = 45) in the cell suspension (Espie *et al*., 1988a; Espie *et al*., 1988b; Miller *et al*., 1988).

2.2.4 Intracellular Ci concentration

The volatile intracellular Ci pool was estimated by mass spectrometry as the ^{13}Ci released from cells upon darkening (Miller *et al*., 1988). Bovine CA (10 μg ml^{-1}) was present in cell suspensions to ensure that the measured [$^{13}CO_2$] was directly proportional to the [$H^{13}CO_3^-$] to enable the calculation of total ^{13}Ci released. The intracellular Ci concentration was determined by partitioning the released ^{13}Ci into the intracellular volume of *Synechocystis* sp. PCC 6803, which was previously determined to be 60 ± 4 μl mg^{-1} Chl, *n* = 12 (So *et al*., 2002).

2.2.5 Cell morphology

Cell size and DNA content was determined using FACS with a BD Biosciences FACS Canto II equipped with FACS Diva 6.1 software. Forward scattering and propidium iodide (PI) fluorescence were used to estimate cell size and DNA content, respectively. Briefly, cell size was estimated in mid-log phase cells in which the Chl was removed by treatment with 75% ethanol in 1× phosphate-buffered saline (PBS) at 4°C for 2 h. For DNA content, ethanol-treated cells were stained with PI (50 μg ml^{-1} in 1× PBS) for 2 h at 4°C. RNA was removed by inclusion of RNase A (500 μg ml^{-1}). PI fluorescence was measured at 617 nm using an excitation wavelength of 535 nm. Phycocyanin content was also estimated in ethanol-treated cells using FACS by measuring fluorescence at 617 nm. For FACS analysis, 10,000 cells were counted in triplicate for each measurement, with results shown obtained from three independent experiments. Chl *a* content was determined spectrophotometrically after extracting cells (0.5 $OD_{750\ nm}$) in 100% methanol overnight at −20°C (Porra *et al*., 1989). Phycobiliproteins were released from the methanol-treated cell pellets by treatment with lysozyme (Santiago-Santos *et al*., 2004) and the phycocyanin content calculated by absorption at 615 and 652 nm (Bennett and Bogorad, 1973). Chl autofluorescence in untreated *Synechocystis* cells was performed using a Leica TCS SP2 confocal microscope equipped with a He-Ne laser, excitation wavelength 543 nm and emission wavelength 590 nm, and filter N2.1.

2.2.6 Electron microscopy

For SEM, samples were fixed overnight in 2% glutaraldehyde–0.1 M cacodylate buffer, washed twice with cacodylate buffer and subjected to dehydration in an increasing ethanol series (50–100%) followed by a series of incubations in ethanol–hexamethyldisilazane (HMDS) (75 : 25, 50 : 50, 25 : 75, 0 : 100, 0 : 100 ethanol : HMDS). Following air-drying overnight, samples were mounted in SEM stubs and coated with a gold–palladium mixture using a Hummer 6.2 Sputter Coater (Anatech). Samples were viewed using a Philips

Scanning Electron Microscope Model XL30 and analyzed using Scandium software.

Cells were prepared for transmission electron microscopy (TEM) by rapid freezing in liquid nitrogen (−120°C) under high pressure (2,100 bar) in a Bal-Tec HPM100. The freeze substitution procedure involved low temperature infiltration at −85°C in 1% glutaraldehyde and 1% tannic acid in HPLC grade acetone for 72 h followed by three washes in anhydrous acetone for 1 h each at −85°C. Cells were stained with 1% OsO_4 in acetone for 1 h at −85°C, and staining was continued for 2 h each after slow warming over 6 h to −20°C then 4°C and finally at room temperature. Cells were embedded in Spurr's resin after washing in anhydrous acetone. Samples were sectioned on a Reichert–Jung Ultra Cut E microtome and stained with 5% uranyl acetate−2.7% lead citrate at room temperature for 15 min. Sections were viewed using a Morgagni 268 TEM (Philips) and Morgagni 268 3.0 software.

IEM was performed as described in El-Fahmawi and Owttrim (2003) using anti-Rubisco antibody (a gift from Dr. Spencer Whitney, Australian National University).

2.3 Results

2.3.1 crhR inactivation

The Δ*crhR* mutant was created by replacing a portion of the *crhR* open reading frame (ORF) with a cassette encoding resistance to spectinomycin, as shown in Fig. 2.1A. The absence of wild-type (WT) copies of the *crhR* gene was confirmed by PCR and Southern analysis (Fig. 2.1B, 2.1C). In agreement with this, Western analysis revealed the absence of full-length CrhR protein in the Δ*crhR* mutant while an ~27 kDa truncated version of CrhR was observed (Fig. 2.1D), as anticipated from the design of the inactivation cassette. The expected truncated version of CrhR (~25 kDa) was also detected in the 6AO6 mutant (data not shown).

2.3.2 Cell growth

Growth of both the Δ*crhR* mutant and the *crhR*::Transprimer 2 insertional inactivant, 6AO6 (data not shown), was reduced ~20% compared with WT cells at 30°C, with a doubling time of about 37 h compared with 30 h for WT cells (Fig. 2.2A). Although a decrease in growth temperature from 30 to 20°C significantly slowed the photoautotrophic growth of WT cells (doubling time = 39 h), the mutant displayed almost no growth over the 6 d period of the experiment (Fig. 2.2A). Furthermore, growth of the cold-sensitive Δ*crhR* mutants could not be rescued by the provision of 5 mM glucose that supports mixotrophic growth in WT cells (data not shown).

Cell viability was determined as an initial examination of the physiology creating the dramatic effect of low temperature on cell growth in the absence of CrhR. Since the Δ*crhR* mutant did not grow at low temperature, cells were exposed to 20°C for periods from 1 to 6 d and then plated at 30°C to determine viability. While viability of WT cells decreased in response to extended exposure to 20°C, the effect on the Δ*crhR* mutant was more severe, with viability decreasing progressively at the reduced temperature (Fig. 2.2B). This suggests that CrhR RNA helicase activity is required for *Synechocystis* viability at low temperature.

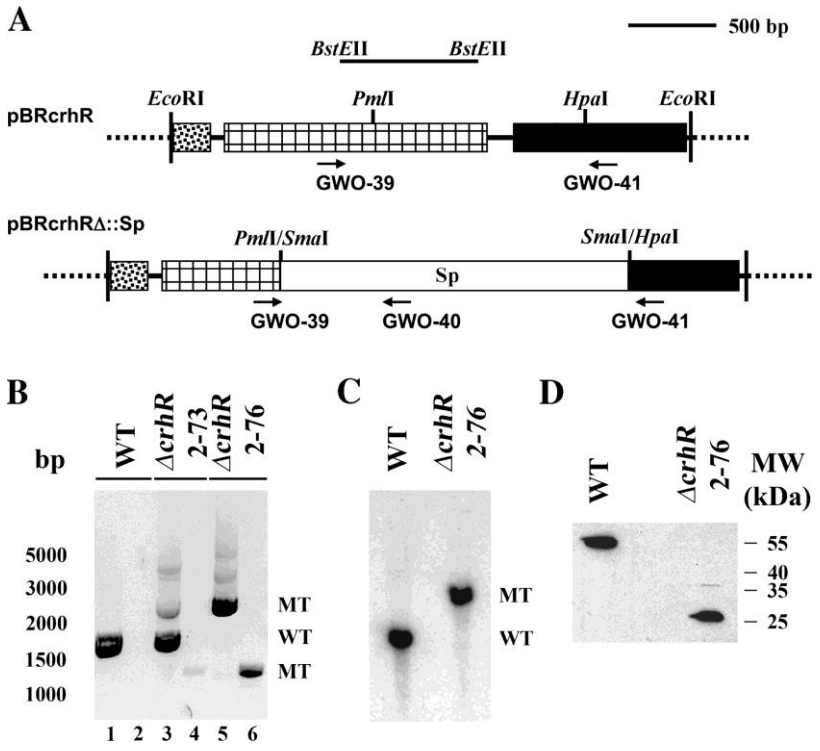

Figure 2.1 *crhR* mutagenesis.

(A) Schematic representation of the *crhR* inactivation strategy. The *crhR* ORF was partially deleted by insertion of an antibiotic cassette coding for resistance to spectinomycin (Sp) into the *crhR* ORF in pBR322. Primer sites utilized for PCR confirmation of the mutant are indicated. The *Bst*EII fragment used as a probe for Southern analysis is indicated as a solid line above the pBRcrhR sequence.

(B) PCR confirmation of *crhR* mutation. PCR was performed on genomic DNA isolated from the WT and two independent *Synechocystis* transformants, 2-73 and 2-76. The primer pair GWO39:41 (lanes 1, 3 and 5) amplify a 1,623 bp fragment from the WT gene (lanes 1 and 3) or a 2,205 bp fragment from the mutant gene (lane 5), while GWO39:40 (lanes 2, 4 and 6) produces a 1,200 bp fragment only from the mutant gene which was detected in lanes 4 and 6 but not from WT DNA (lane 2). The analysis indicates that 2-76 is completely inactivated while 2-73 is a merodiploid. 2-73 was used as an internal control to verify that WT copies of the *crhR* gene were detectable using the PCR protocol.

(C) Southern confirmation of *crhR* mutation. *Eco*RI-digested WT and the Δ*crhR* mutant mutant genomic DNA (5 μg) was probed with an internal 784 bp *Bst*EII fragment of the *crhR* gene.
(D) Western confirmation of *crhR* mutation. Total soluble protein (30 μg) probed with anti-CrhR antibody identified the 55 kDa CrhR protein in the WT while the Δ*crhR* mutant lacked the 55 kDa WT protein and a 27 kDa truncated version of CrhR was detected.

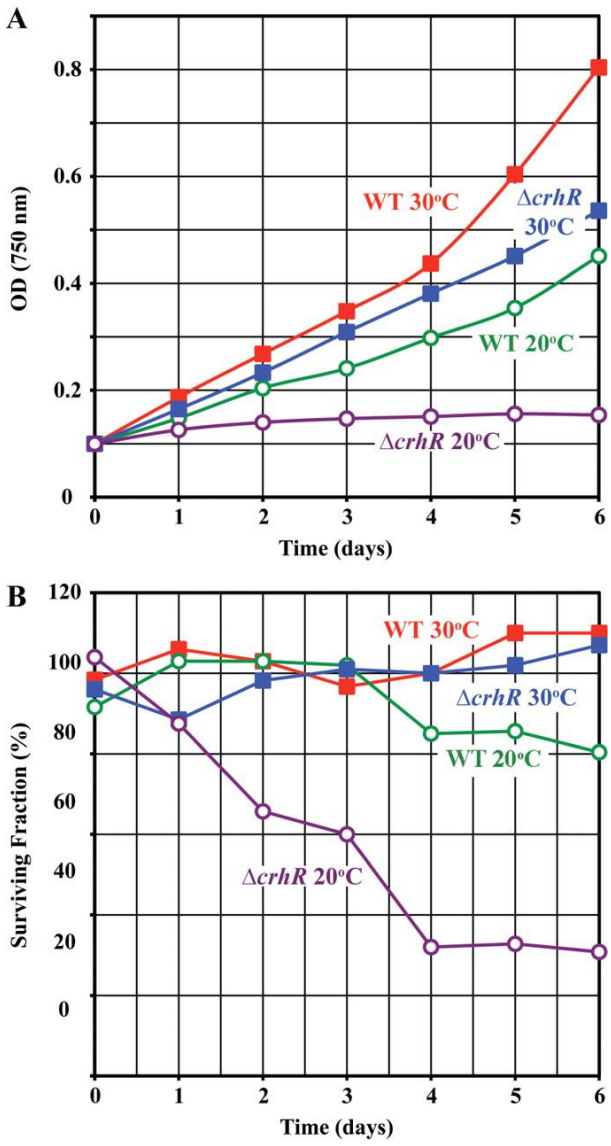

Figure 2.2 Growth and viability.

(A) Cell growth. Growth of the WT and the Δ*crhR* mutant strains was determined spectrophotometrically by measuring the OD_{750} of cultures grown at 20 and 30°C.

(B) Cell viability. Cell viability was measured using colony plate counts after the indicated growth period. After low temperature exposure, the diluted cells were plated and grown at 30°C. WT 30°C, red squares; WT 20°C, green circles; Δ*crhR* 30°C, blue squares; Δ*crhR* 20°C, purple circles.

2.3.3 Photosynthetic oxygen evolution

The inability of the Δ*crhR* mutant to grow at 20°C may be related to temperature-sensitive deficiencies in the photosynthetic apparatus that selectively prevent carbon assimilation. We examined photosynthesis in WT and Δ*crhR* mutant cells, at 20 and 30°C, by measuring CO_2 uptake and photosynthetic O_2 evolution (Fig. 2.3). A 10°C decrease in temperature reduced the inorganic carbon (Ci) saturated rate of O_2 evolution by 20–25% in WT *Synechocystis* (Fig. 2.3A). The Δ*crhR* mutant exhibited impaired photosynthetic O_2 evolution at both 30 and 20°C (Fig. 2.3A). At 30°C, the Ci saturated rate of O_2 evolution declined by 15–20% compared with the WT. At 20°C, however, photosynthesis was nearly abolished at all external Ci concentrations tested.

To determine if this effect was reversible, O_2 evolution was measured in Δ*crhR* mutant cells grown at 30°C, then rapidly shifted to 20°C for 18 min (Fig. 2.3B). This temperature downshift rapidly impaired oxygen evolution, the Δ*crhR* mutant achieving a Ci saturated evolution rate of 10 μmol $O_2 mg^{-1}$ Chl h^{-1} compared with 80 μmol $O_2\, mg^{-1}$ Chl h^{-1} in the WT. Warming the Δ*crhR* mutant from 20 to 30°C progressively accelerated O_2evolution, leading to a maximum rate of 88 μmol $O_2\ mg^{-1}$ Chl h^{-1}, a value similar to the pre-treatment rate (Fig. 2.3B).

2.3.4 Ci transport and accumulation

Efficient photosynthesis in cyanobacteria requires the concurrent participation of a CO_2-concentrating mechanism (CCM) to supply substrate to Rubisco. In *Synechocystis* PCC 6803, the CCM includes active, Na^+-dependent and Na^+-independent HCO_3^- transporters that concentrate Ci internally and high and low affinity CO_2 uptake systems that are essential for retention of the accumulated Ci pool (Price *et al*., 2008). In addition, proteinaceous carboxysomes, where Rubisco is encapsulated and where CO_2 is generated from accumulated Ci by a co-localized carbonic anhydrase (CA), are also required for carbon fixation under normal growth conditions (So *et al*., 2002).

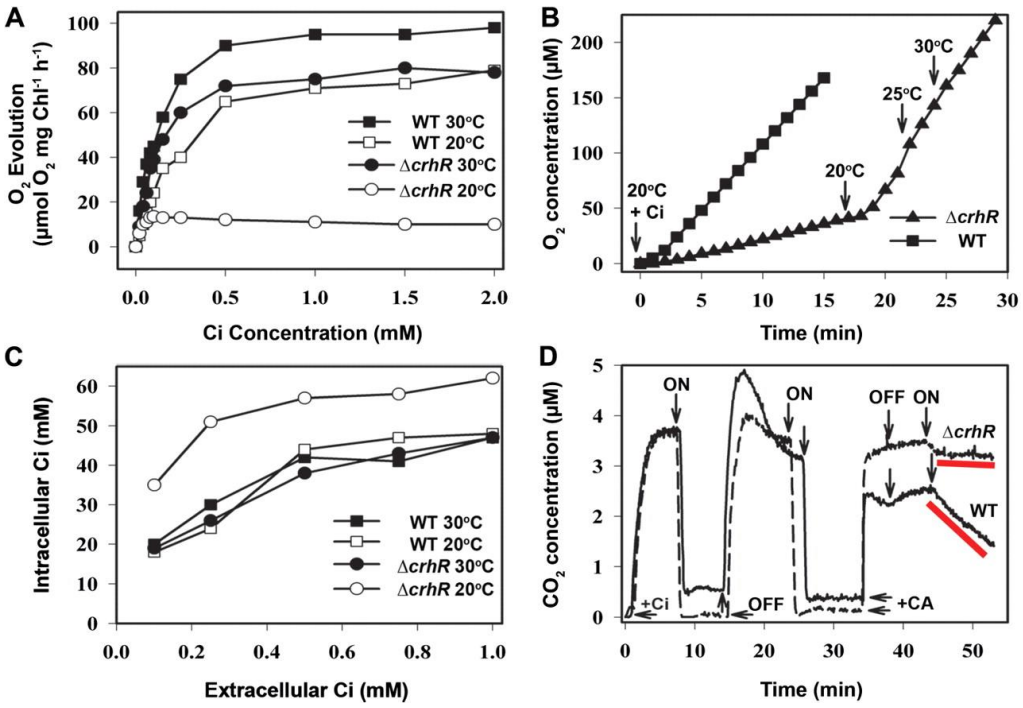

Figure 2.3 Photosynthetic oxygen evolution, Ci uptake and accumulation.

(A) The rate of photosynthetic oxygen evolution was measured in response to increasing external Ci in WT (square symbols) and Δ*crhR* (circle symbols) at 20°C (open symbols) and 30°C (filled symbols), as indicated. Cells were suspended in BTP/HCl buffer pH 8.0 containing 25 mM NaCl and illuminated with 300 μmol photons m^{-2} s^{-1}.

(B) Effect of a temperature shift from 20 to 30°C on photosynthetic O_2 evolution. Photosynthetic oxygen evolution was measured in WT cells (circles) at 20°C as described in A using 500 μM Ci to initiate photosynthesis. The same procedure was used to measure oxygen evolution in Δ*crhR* cells for 18 min at 20°C (triangles), at which time the temperature in the Δ*crhR* mutant chamber was allowed to increase to 30°C.

(C) Steady-state intracellular Ci pool in WT (square symbols) and Δ*crhR* cells (circle symbols) at 20 (open symbols) and 30°C (filled symbols). The intracellular Ci pool as a function of external Ci was measured by mass spectrometry under conditions identical to those described in A.

(D) Light-dependent CO_2 uptake and photosynthetic carbon fixation. WT (solid line) and Δ*crhR* (dashed line) cells were provided with 200 μM ^{13}Ci (3.75 μM $^{13}CO_2$) at zero time (+Ci), in BTP/HCl buffer, pH 8.0, containing 25 mM NaCl at 20°C. The light (300 μmol photons m^{-2} s^{-1}) was turned on or off as indicated, and $^{13}CO_2$ uptake or efflux, respectively, was measured continuously by mass spectrometry. During a period of illumination, carbonic anhydrase (+CA, 25 μg ml^{-1}) was added to the suspensions, causing rapid equilibration between $^{13}CO_2$ and $H^{13}CO_3^-$ in the medium, and then the light was turned off. The difference in the absolute $^{13}CO_2$ concentration in the dark between WT and Δ*crhR* cells, at this point, represents differences in photosynthetic $^{13}CO_2$ fixation during the previous light periods. Subsequent illumination revealed very different rates of $^{13}CO_2$disappearance from the medium, with WT cells showing robust photosynthetic consumption of $^{13}CO_2$ while Δ*crhR* cells displayed minimal consumption, as indicated by the red lines.

Similar to the WT, the Δ*crhR* mutant displayed HCO_3^- transport capacity at 30°C as the photosynthesis rate exceeded the CO_2 supply rate by 5-fold at low external Ci (Fig. 2.3A) (Espie *et al*., 1988a, Espie *et al*., 1988b). Although the low rates of photosynthesis at 20°C did not provide conclusive evidence for ongoing HCO_3^- transport in the Δ*crhR* mutant, the accumulation of a large pool of intracellular Ci (Fig. 2.3C) was consistent with this occurrence. Reduced oxygen evolution could result from the inability of the Δ*crhR* mutant actively to concentrate Ci at 20°C. Mass spectrometric measurements of intracellular Ci showed, however, that the intracellular pool in the Δ*crhR* mutant at 20°C was larger than even that in the WT at 30°C (Fig. 2.3C). This apparent anomaly can be explained by the fact that Ci was accumulated in the Δ*crhR* mutant but photosynthetic carbon fixation was not consuming it at an appreciable rate at 20°C. In the other three cases, accumulated Ci was drawn down at proportionately higher rate by photosynthetic carbon fixation, leading to lower steady-state Ci accumulation than in the case of the Δ*crhR* mutant at 20°C. Thus, at 20°C, the Δ*crhR* mutant actively transported and accumulated Ci but was incapable of utilizing the intracellular Ci pool for photosynthetic carbon fixation.

The rapid disappearance of CO_2 from the medium upon illumination (Fig. 2.3D) was indicative of high affinity CO_2 uptake known to be mediated by the inducible, NADPH-driven, NDH-1_3–CupA thylakoid membrane complex (Zhang *et al*., 2004; Ogawa and Mi, 2007; Battchikova *et al*., 2011). Little difference in the initial rate of CO_2 disappearance from the medium in the light was observed between the WT and the Δ*crhR* mutant at 20°C. Interestingly, the Δ*crhR* mutant drew down the external Ci concentration below the level found for WT cells, even in the absence of ongoing photosynthetic carbon fixation. This probably reflected differences in steady-state NADPH utilization. In WT cells, there was a competition for NADPH between CO_2 uptake and carbon fixation, while in the mutant, with reduced photosynthetic demand, there is potentially relatively more NADPH available for CO_2 uptake.

The observed rise in CO_2 levels upon darkening was due to release of the internal Ci pool and to equilibration of CO_2/HCO_3^- in the medium following the

cessation of light-dependent CO_2 uptake. These processes are expected to be thermodynamically passive in nature. The more rapid rise and 'overshoot' in the CO_2 concentration in the medium for WT cells compared with the Δ*crhR* mutant may reflect somewhat different rates of intracellular conversion of HCO_3^- to CO_2 and its subsequent release to the medium (Fig. 2.3D). The addition of exogenous CA to illuminated cells caused a rapid increase in the CO_2 concentration in the medium, with a much smaller rise in CO_2 following darkening. These results indicated that both the WT and the Δ*crhR* mutant created a chemical disequilibrium between HCO_3^- and CO_2 in the medium due to the selective uptake of CO_2. This process necessitates the expenditure of energy from the electrochemical potential for H^+ and NADPH produced by light-driven electron transport. Subsequent illumination of WT and Δ*crhR* mutant cells in the presence of CA revealed distinct patterns of Ci utilization. In this experiment, the addition of CA maintained chemical equilibrium between HCO_3^- and CO_2 so that changes in the CO_2 signal (*m/z* = 45) were directly proportional to changes in total Ci in the medium. In WT cells, illumination resulted in a continuous decrease in total Ci, resulting from a combination of steady-state CO_2 uptake and photosynthetic CO_2 fixation (Fig. 2.3D, red lines). In the Δ*crhR* mutant, in contrast, the much lower steady-state rate of Ci decline in the presence of CA compared with WT cells was indicative of a low level of photosynthetic CO_2 assimilation at 20°C (Fig. 2.3D, red lines).

2.3.5 Photosynthetic electron transport

The deficiencies in photosynthetic oxygen evolution and carbon fixation observed in the Δ*crhR* mutant could potentially result from a defect in electron transport. The activity of the electron transport chain was estimated by measuring the effect of methyl viologen (MV) on photosynthetic oxygen exchange (Table 2.1). The rate of oxygen consumption in the presence of MV reflects unimpeded electron flow from water to MV. Oxygen evolution in the *crhR* mutant was reduced ~10% at 30°C, similar to the decrease in growth rate (Table 2.1). In

contrast, oxygen evolution was reduced ~50% in the mutant at 20°C. This did not result from an increase in respiration in the mutant, as although a temperature downshift affected the ratio of photosynthetic oxygen evolution to respiratory oxygen uptake, the effect was similar in WT and mutant cells (Table 2.1). In contrast, the ratio of photosynthetic oxygen evolution to oxygen consumption in the presence of MV was significantly reduced in the *crhR* mutant at both temperatures (Table 2.1). Thus, while MV stimulated electron flow in both cell types, the stimulation was significantly increased in the *crhR* mutant. These results suggest that electrons are not flowing through the electron transport chain at maximum capacity in the Δ*crhR* mutant at both temperatures.

2.3.6 Photosynthetic pigment composition

The Δ*crhR* mutant was visually distinct from WT cells, being more yellow in color, suggesting differences in photosynthetic pigmentation. This could result from changes in light-harvesting pigment composition. The concentration of both Chl *a* and phycocyanin decreased in both cell types in response to low temperature, as revealed by both spectrophotometric and autofluorescence analysis (Fig. 2.4). Chl *a* and phycocyanin content responded similarly to low temperature in WT and Δ*crhR* mutant cells, decreasing approximately 1.5-fold (Fig. 2.4A). While both cell types exhibited reduced pigment content at low temperature, the reduction was more significant in the mutant at both growth temperatures (Fig. 2.4A). Similar results were also obtained by estimating Chl levels using fluorescence-activated cell sorting (FACS) to measure Chl-generated autofluorescence (data not shown). This analysis also indicated that low temperature reduced Chl levels by 1.4- and 1.9-fold in WT and Δ*crhR*mutant cells, respectively. Alteration of the pigment level concurrent with *crhR* mutation was also revealed by fluorescent and confocal microscopy (Fig. 2.4B and 2.4C, respectively). The Δ*crhR* mutant was also noticeably smaller than the WT, as indicated by autofluorescence detected by confocal microscopy, a procedure that does not involve ethanol dehydration of the cells before analysis (Fig. 2.4C).

Table 2.1 Oxygen exchange in WT and ΔcrhR cells

Strain	30°C		20°C	
	PS/respiration	PS/MV	PS/respiration	PS/MV
Wild type	201/72 2.48 ± 0.34	201/35 5.52 ± 0.98	98/27 3.55 ± 0.6	98/17 5.95 ± 1.15
Δ*crhR*	185/81 2.2 ± 0.65	185/50 3.55 ± 0.49	52/15 3.79 ± 0.3	52/11 4.4 ± 1.28
% Δ*crhR*/WT	88.7	64.3	106.8	73.9

Measurements were performed a minimum of four times, as described in Fig. 2.3 Representative rates of oxygen exchange (μmol oxygen evolved or consumed/mg Chl *a*/h) are given on the first line and the ratio (± SD) below.

PS, photosynthetic oxygen evolution; MV, oxygen consumption in the presence of MV (1 mM).

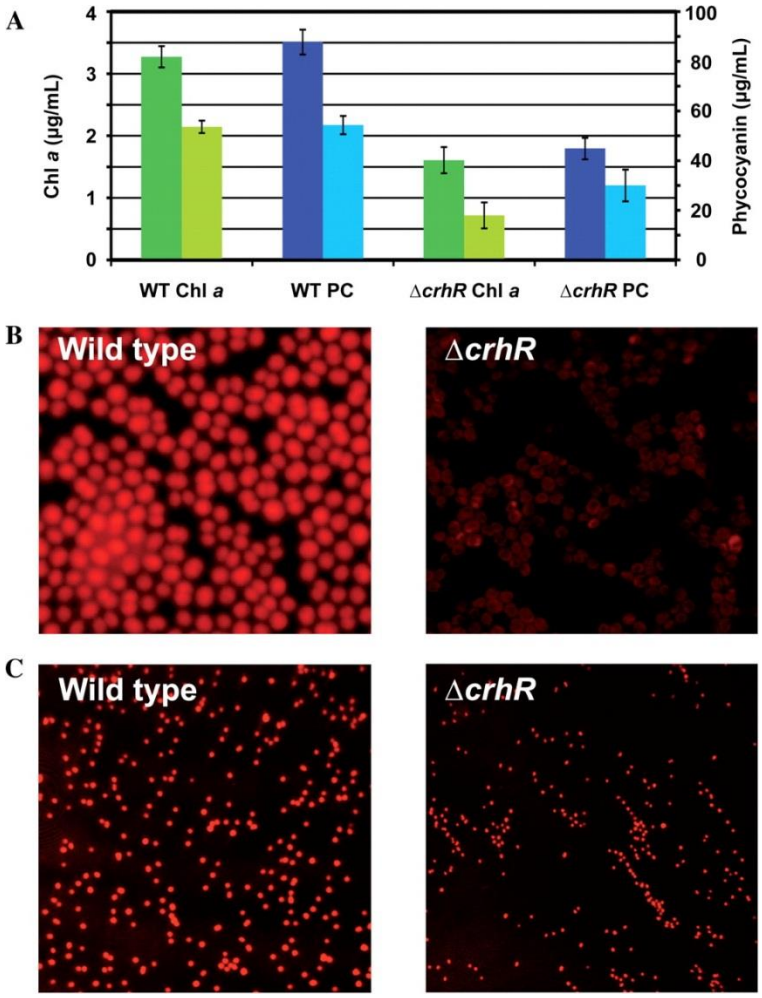

Figure 2.4 Photosynthetic pigment composition.

(A) Spectrophotometric determination of Chl *a* (green bars) and phycocyanin (blue bars) composition in the WT and the Δ*crhR* mutant grown at 30°C (dark bars) and 20°C (light bars) for 24 h.

(B) Fluorescent analysis. Cells grown at 20°C as described in A were visualized by fluorescent microscopy using the natural fluorescence of Chl. The WT cells are noticeably larger and exhibit elevated autofluorescence compared with the Δ*crhR* mutant.

(C) Fluorescent analysis. Autofluorescence of cells grown at 20°C as described in A were visualized by confocal microscopy. The Δ*crhR* mutant cells are smaller and exhibit less Chl autofluorescence than the WT.

2.3.7 Cellular morphology

Table 2.2 summarizes the effects of temperature on various features of WT and Δ*crhR* mutant cells. FACS estimation of cell size by forward light scattering indicated that WT cells alter in size in response to temperature change. A 10°C reduction in growth temperature yielded WT cells which tended to increase in size by ~25%. In contrast, temperature does not affect the size of Δ*crhR* mutant cells which are consistently smaller than those of the WT, ~34 and 18% smaller than the WT at 20 and 30°C, respectively.

Cell size alterations were correlated with a change in the proportion of cells visibly in the process of cell division (Table 2.2). *Synechocystis* cells were present in a culture as either single cells (singlets) or partially divided cells (doublets) that have initiated cytokinesis. At 30°C, the majority of WT cells were singlets, a situation which was reversed by a 10°C reduction in growth temperature. This cold-induced alteration in cell morphology was not observed for the Δ*crhR* mutant, as single cells existed predominantly at both temperatures. In an attempt to determine if the Δ*crhR* mutant was initiating cell division, DNA content per cell was estimated using propidium iodide (PI) fluorescence (Table 2.2). Similar levels were observed in the Δ*crhR* mutant irrespective of temperature. This level increased in WT cells by 23 and 34% at 20 and 30°C, respectively. Thus, the Δ*crhR* mutant does not appear to be initiating DNA replication in preparation for cell division. Overall, the Δ*crhR* mutant had the smallest size and the lowest DNA concentration, and predominantly occurred as single cells. The results suggest that the mutant was not growing to a size at which cell division was initiated and that DNA replication was not occurring.

Table 2.2 Cellular features of WT and Δ*crhR* cells

	Singlet/doublet composition (% ± SD[a])			
	30°C		20°C[b]	
	Singlets	Doublets	Singlets	Doublets
Strain				
WT	91.5 ± 0.5	8.5 ± 0.5	16.0 ± 6.0	84.0 ± 6.0
Δ*crhR*	94.7 ± 1.5	5.3 ± 1.5	88.6 ± 3.3	11.4 ± 3.3
DNA content[c]				
WT	4,241 ± 1037		3,612 ± 486	
Δ*crhR*	2,810 ± 484		2,764 ± 620	
Cell size[d]				
WT	1,916 ± 109		2,544 ± 483	
Δ*crhR*	1,578 ± 101		1,679 ± 236	

[a] n = 1,000.

[b] Cells were exposed to cold stress at 20°C for 24 h before analysis.

[c] FACS PI stain fluorescence (arbitrary units), n = 10,000.

[d] FACS forward scattering (arbitrary units), n = 10,000.

2.3.8 Ultrastructure analysis

The strains also differed on the ultrastructural level. Scanning electron microscopy (SEM) analysis indicated that WT cells possessed a deeply furrowed cell surface at both temperatures (Fig. 2.5A, C) while the Δ*crhR*mutant exhibited less furrowing at 30°C (Fig. 2.5B), a feature which is absent at 20°C (Fig. 2.5D). Thus, the Δ*crhR* mutant appears to differ in some aspect of cell wall architecture and/or formation. The SEM micrographs also reflected the singlet–doublet differences between the two cell types, as shown in Table 2.2.

Analysis of intracellular ultrastructure indicated that WT *Synechocystis* appeared very similar when grown at either 30 or 20°C, containing a variety of intracellular structures including ribosomes, carboxysomes, thylakoid membranes, etc. (Fig. 2.6A, B). In contrast, while the Δ*crhR* mutant cells appeared relatively normal at 30°C (Fig. 2.6C), intracellular abnormalities were apparent at 20°C where the internal structures appeared highly disorganized (Fig. 2.6D–H). The cells were deficient in internal structures, including ribosomes, carboxysomes and thylakoid membranes. Numerous small vesicular structures were observed which potentially originated from thylakoid membranes. In addition, a variety of irregularly shaped aggregates of differing electron density accumulated in the cytoplasm. A gradient of effect was apparent, as although the majority of cells exhibit significant structural alterations, some cells appeared relatively normal (Fig. 2.6F, G). When present, carboxysomes in the Δ*crhR*mutant were abnormal, appearing to be fused into larger, less consistently shaped structures. However, these aberrantly shaped carboxysomes retained Rubisco, as revealed by immunoelectron microscopy (IEM; Fig. 2.6G, H).

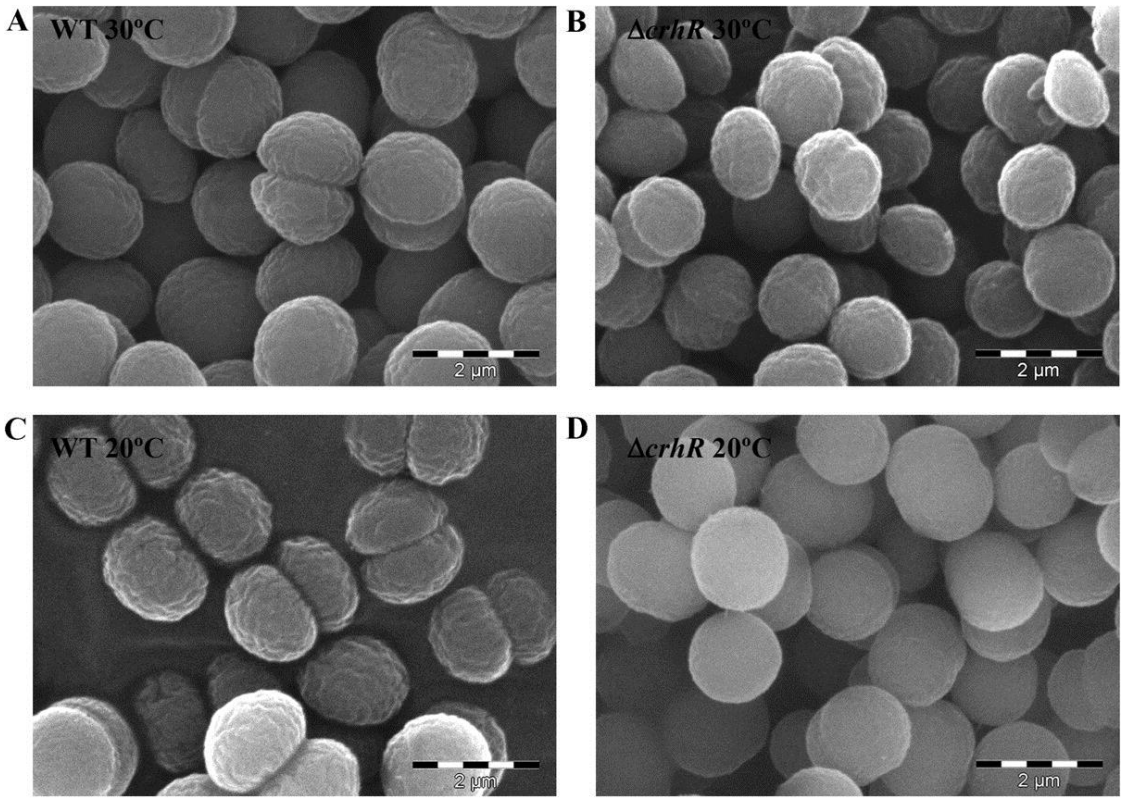

Figure 2.5 Ultrastructure analysis.

SEM micrographs of ethanol/HMDS-dehydrated cells fixed with glutaraldehyde and coated with gold/palladium. Cold-stressed cells were exposed to 20°C for 24 h before analysis.

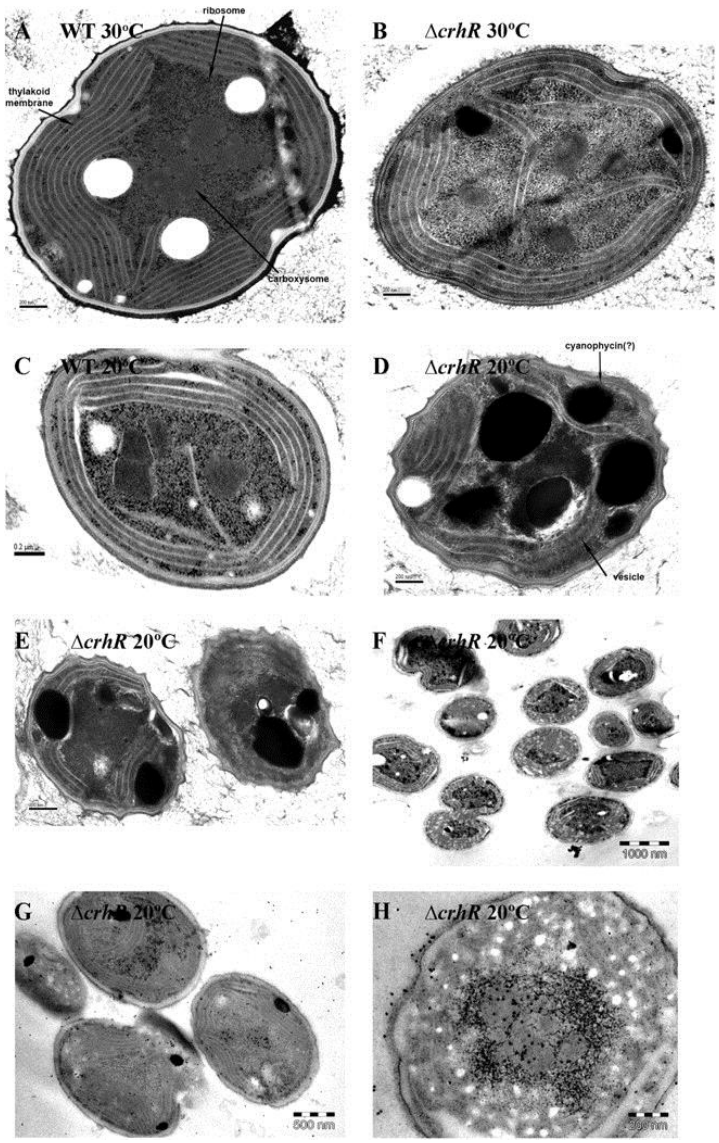

Figure 2.6 Ultrastructure analysis.

Representative TEM micrographs of cells rapidly frozen under high pressure, fixed with glutaraldehyde and stained with OsO_4 are shown. Cells were grown at 30°C (A and B) or cold stressed at 20°C for either 12 (F and G) or 24 h (C–E and H) before analysis. G and H are IEM images of cell sections probed with anti-Rubisco antibody.

2.4 Discussion

Synechocystis is predominantly a photoautotroph, and thus the ability to photosynthesize is crucial for survival. Inactivation of the RNA helicase,*crhR*, has dramatic effects on *Synechocystis* physiology and morphology. It is important to note that effects are observed under both normal (30°C) and cold stress (20°C) conditions, suggesting that CrhR performs crucial function(s) at both temperatures and thus the results do not derive solely from a defect in the cold stress response. Exacerbation of the effects induced by a 10°C reduction in growth temperature may correlate with increased *crhR* expression at low temperature, presumably a result of a cold-enhanced increase in the reduction of the electron transport chain (Miskiewicz *et al*., 2000; Ensminger *et al*,. 2006). However, we cannot rule out a contribution by a low temperature effect on *crhR* transcription or mRNA stability (Kujat and Owttrim 2000). A similar observation that RNA helicase inactivation has effects at all temperatures has recently been reported for RNA helicases associated with ribosome biogenesis in *E. coli* (Jagessar and Jain 2010).

The *crhR* mutant exhibits a number of physiological abnormalities which are directly associated with alterations in cellular morphology. One immediate and major physiological effect is a decline in photosynthesis at 30°C, a phenomenon which is significantly exacerbated at low temperature. This decline is not caused by the inability of the Δ*crhR*mutant to transport or concentrate Ci internally but is caused by the inability to fix carbon photosynthetically from the Ci pool. The resulting lack of photosynthate production would be anticipated to contribute to the decline in growth, which is observed at both temperatures but reduced to the point of the absence of growth at 20°C.

The rate at which photosynthetic oxygen evolution and carbon fixation respond to temperature change in the Δ*crhR* mutant is informative. In WT cells at 20°C or the Δ*crhR* mutant at 30°C, there is sufficient light-harvesting, electron transport and enzymatic capacity to sustain photosynthesis at a rate of 80 μmol mg^{-1} Chl h^{-1}. However, in the Δ*crhR* mutant at 20°C, this rate is reduced 8-fold within minutes, indicating that the pre-existing photosynthetic machinery is

rapidly inactivated at low temperature. Importantly, this defect is rapidly reversed by returning the cells to 30°C. Over the short time span of these experiments, no change in enzymatic activity would be expected (other than that created by Q_{10}) nor would the mutation in *crhR* be capable of dramatically altering gene expression. The results indicate that the photosynthetic defect is not related to photosynthetic capacity but rather to the execution of one or more vital steps in the overall process.

The photosynthetic data also suggest that the defect is unlikely to originate solely in the ability to produce or utilize ATP and NADPH since both energy sources are required for Ci uptake (Price *et al*., 2008). The *crhR* mutant exhibited both active HCO_3^- and CO_2 uptake activity at 20 and 30°C that lead to intracellular Ci accumulation and, therefore, an available supply of Ci for photosynthetic fixation. However, although the *crhR* mutant is able to create an intracellular Ci pool at 20°C, in excess of that observed in WT cells, it is unable to utilize the pool for photosynthetic carbon fixation. Therefore, the mutant possesses sufficient electron transport capacity to generate ATP and NADPH at levels required to energize Ci transport and accumulation at 20°C. This result suggests that the photosynthetic defect is not derived from a complete lack of electron transport and thus generation of NADPH or ATP. We cannot, however, unambiguously exclude these pathways as concurrent contributors to the photosynthetic defect since the lower rate of energy utilization for carbon fixation in the Δ*crhR* mutant potentially allows allocation of available energy to support enhanced Ci transport and accumulation, as observed in the Δ*crhR* mutant at 20°C.

The contribution of a reduction in electron transport was confirmed by an MV-induced decrease in the ratio of photosynthetic oxygen evolution to oxygen consumption in the Δ*crhR* mutant. MV enhancement of oxygen consumption indicated that electron flow does not function at maximal efficiency in the mutant, at either 30 or 20°C. This reduction of electron flow through the electron transport chain could be created either by a defect in one of the carriers or by over-reduction caused by the lack of carbon fixation. The latter scenario is preferred as electron transport supports WT levels of Ci transport and accumulation but not

photosynthetic carbon fixation in the Δ*crhR* mutant. The potential electron transport defect, however, would not appear to explain completely the rapid decrease in photosynthetic oxygen evolution or the reduction in carbon fixation which occurs in response to short-term exposure to 20°C. Thus, an additional defect(s) probably resides in a temperature-sensitive component of the photosynthetic apparatus.

In response to low temperature stress for longer periods, of the order of hours to days, the inability to photosynthesize may additionally be related to the observed morphological abnormalities. For example, prolonged exposure to low temperature resulted in the appearance of abnormal carboxysomes that frequently formed aggregates. Mutations affecting carboxysome structure result in a high Ci requiring phenotype (So *et al*., 2002; Price *et al*., 2008). However, growth of the Δ*crhR* mutant was not restored at low temperature by glucose, again suggesting that the growth defect involved additional lesions in the photosynthetic apparatus and possibly in respiratory electron transport. An additional contributor could be the deterioration of thylakoid structure in the Δ*crhR* mutant potentially leading to decreased rates of photosynthetic electron transport coupled with lower light-harvesting capacity. Evidence for reduced light harvesting is indicated by the observed decrease in both Chl *a* and phycocyanin levels in the Δ*crhR* mutant at 30°C, an effect which is intensified at 20°C. The increase in excitation pressure on the photosynthetic apparatus at low temperature is relieved in part by a decrease in light-harvesting pigments in WT cells as the cells acclimate to the new environmental conditions (Miskiewicz *et al*., 2000; Miskiewicz *et al*., 2002). This same response is observed in the Δ*crhR* mutant, indicating that it still possesses the ability to sense and genetically alter its light-harvesting capacity to reduce the potential for reactive oxygen species (ROS) formation. However, although this regulatory response remains intact, there is also a direct effect of the *crhR* mutation on light harvesting as Chl *a* and phycocyanin levels are decreased below those observed in WT cells at both temperatures.

The source of the progressive accumulation of ultrastructural abnormalities in the Δ*crhR* mutant may be consistent with photooxidative

damage, resulting from *crhR* mutation. A decrease in photosynthetic carbon fixation at constant light is known to increase reduction of the photosynthetic electron transport chain leading to enhanced formation of ROS and associated photooxidative damage. The morphological changes observed in the cellular ultrastructure in the Δ*crhR* mutant may be indicative of this damage. Accumulated ROS damage would also be expected to lead to progressive cell death, an outcome that is observed in the Δ*crhR* mutant at 20°C. This implies that ROS damage contributes to the cellular deterioration in carboxysome and thylakoid structure. The rapidity with which these effects are manifested suggests they originate from pre-existing defects in the Δ*crhR* mutant that are amplified over time and/or are secondary effects related to a general deterioration of the cell due to the lack of photosynthesis at 20°C.

The inability of the *crhR* mutant to grow and photosynthesize was also reflected in morphological changes. Irrespective of temperature, the Δ*crhR* mutant cells are smaller than WT cells, presumably resulting from the fact that the majority of Δ*crhR* mutant cells are present as single cells. These changes suggest that the *crhR* mutant is not entering cell division, as also indicated by a reduced DNA content present in the Δ*crhR* mutant cells at both temperatures. The morphological changes also extend to the cell surface as the Δ*crhR* mutant does not exhibit undulated furrows at 20°C present in the WT or the Δ*crhR* mutant grown at 30°C. Undulated cell surfaces are common in Gram-negative bacteria and indicative of normal development of the outer surface layers (Nogami and Mizushima 1983).

While the exact mechanism by which *crhR* inactivation generates the observed pleiotropic phenotype is not known, it is entirely possible that the unregulated expression of the truncated CrhR protein plays a role. This polypeptide may potentially sequester target RNA or protein factors, reducing their ability to participate in cellular metabolism and thus contributing to the observed phenotype. A truncated polypeptide is also observed in the 6AO6 mutant, a Δ*crhR* mutant that exhibits the same phenotypic traits observed in the 2-76 Δ*crhR* mutant. CrhR may also regulate expression of other gene products, the

over- or underexpression of which may generate the primary defect in photosynthetic electron flow associated with a reduction in carbon fixation. Overall, the data indicate that the observed morphological and physiological defects observed at both temperatures are intimately related to the *crhR* mutation. Furthermore, the results suggest that the lack of CrhR RNA unwinding and/or annealing activity results in the deficiency of a component of the photosynthetic apparatus which is required at all temperatures but is crucial in response to low temperature stress. Identification of this component will contribute to the elucidation of the novel role performed by this RNA helicase in photosynthetic metabolism.

2.5 Reference

Barral, P.M., Sarkar, D., Su, Z., Barber, G.N., DeSalle, R., Racaniello, V.R., and Fisher, P.B. 2009. Functions of the cytoplasmic RNA sensors RIG-I and MDA-5: key regulators of innate immunity. Pharmacol. Ther. **124**(2): 219-234.

Battchikova, N., and Aro, E.M. 2007. Cyanobacterial NDH-1 complexes: multiplicity in function and subunit composition. Physiol. Plantarum **131**(1): 22-32.

Bennett, A., and Bogorad, L. 1973. Complementary chromatic adaptation in a filamentous blue-green alga. J. Cell Biol. **58**(2): 419-435.

Chamot, D., and Owttrim, G.W. 2000. Regulation of cold shock-induced RNA helicase gene expression in the cyanobacterium *Anabaena* sp. strain PCC 7120. J. Bacteriol. **182**(5): 1251-1256.

Chamot, D., Colvin, K.R., Kujat-Choy, S.L., and Owttrim, G.W. 2005. RNA structural rearrangement via unwinding and annealing by the cyanobacterial RNA helicase, CrhR. J. Biol. Chem. **280**(3): 2036-2044.

Chamot, D., Magee, W.C., Yu, E., and Owttrim, G.W. 1999. A cold shock-induced cyanobacterial RNA helicase. J. Bacteriol. **181**(6): 1728-1732.

Charollais, J., Dreyfus, M., and Iost, I. 2004. CsdA, a cold-shock RNA helicase from *Escherichia coli*, is involved in the biogenesis of 50S ribosomal subunit. Nucleic Acids Res. **32**(9): 2751-2759.

Charollais, J., Pflieger, D., Vinh, J., Dreyfus, M., and Iost, I. 2003. The DEAD-box RNA helicase SrmB is involved in the assembly of 50S ribosomal subunits in *Escherichia coli*. Mol. Microbiol. **48**(5): 1253-1265.

Cordin, O., Banroques, J., Tanner, N.K., and Linder, P. 2006. The DEAD-box protein family of RNA helicases. Gene **367**: 17-37.

El-Fahmawi, B., and Owttrim, G.W. 2003. Polar-biased localization of the cold stress-induced RNA helicase, CrhC, in the cyanobacterium *Anabaena* sp. strain PCC 7120. Mol. Microbiol. **50**(4): 1439-1448.

Ensminger, I., Busch, F., and Huner, N. 2006. Photostasis and cold acclimation: sensing low temperature through photosynthesis. Physiol. Plantarum **126**(1): 28-44.

Espie, G.S., Miller, A.G., and Canvin, D.T. 1988. Characterization of the Na-requirement in cyanobacterial photosynthesis. Plant Physiol. **88**(3): 757-763.

Espie, G.S., Miller, A.G., Birch, D.G., and Canvin, D.T. 1988. Simultaneoust transport of CO_2 and HCO_3^- by the cyanobacterium *Synechococcus* UTEX 625. Plant Physiol. **87**(3): 551-554.

Ewen-Campen, B., Schwager, E.E., and Extavour, C.G.M. 2010. The molecular machinery of germ line specification. Mol. Reprod. Dev. **77**(1): 3-18.

Fairman-Williams, M.E., Guenther, U.P., and Jankowsky, E. 2010. SF1 and SF2 helicases: family matters. Curr. Opin. Struct. Biol. **20**(3): 313-324.

Floriano, B., Herrero, A., and Flores, E. 1992. Isolation of arginine auxotrophs, cloning by mutant complementation, and sequence analysis of the *argC* gene from the cyanobacterium *Anabaena* species PCC 7120. Mol. Microbiol. **6**(15): 2085-2094.

Hunger, K., Beckering, C.L., Wiegeshoff, F., Graumann, P.L., and Marahiel, M.A. 2006. Cold-induced putative DEAD box RNA helicases CshA and CshB are essential for cold adaptation and interact with cold shock protein B in *Bacillus subtilis*. J. Bacteriol. **188**(1): 240-248.

Jagessar, K.L., and Jain, C. 2010. Functional and molecular analysis of *Escherichia coli* strains lacking multiple DEAD-box helicases. RNA **16**(7): 1386-1392.

Jankowsky, E. 2011. RNA helicases at work: binding and rearranging. Trends Biochem. Sci. **36**(1): 19-29.

Jones, P.G., Mitta, M., Kim, Y., Jiang, W., and Inouye, M. 1996. Cold shock induces a major ribosomal-associated protein that unwinds double-stranded RNA in *Escherichia coli*. Proceedings of the National Academy of Sciences **93**(1): 76-80.

Kujat, S.L., and Owttrim, G.W. 2000. Redox-regulated RNA helicase expression. Plant Physiol. **124**(2): 703-714.

Li, H., and Sherman, L.A. 2002. Characterization of *Synechocystis* sp. strain PCC 6803 and nbl mutants under nitrogen-deficient conditions. Arch. Microbiol. **178**(4): 256-266.

Linder, P. and Owttrim, G.W. 2009. Plant RNA helicases: linking aberrant and silencing RNA. Trends Plant Sci. **14**: 344–352.

Miller, A.G., Espie, G.S., and Canvin, D.T. 1988. Active transport of CO_2 by the cyanobacterium *Synechococcus* UTEX 625 measurement by mass spectrometry. Plant Physiol. **86**(3): 677-683.

Miskiewicz, E., Ivanov, A.G., and Huner, N.P.A. 2002. Stoichiometry of the photosynthetic apparatus and phycobilisome structure of the cyanobacterium *Plectonema boryanum* UTEX 485 are regulated by both light and temperature. Plant Physiol. **130**(3): 1414-1425.

Nogami, T., and Mizushima, S. 1983. Outer membrane porins are important in maintenance of the surface structure of *Escherichia coli* cells. J. Bacteriol. **156**(1): 402-408.

Ogawa, T., and Mi, H. 2007. Cyanobacterial NADPH dehydrogenase complexes. Photosynthesis Res. **93**(1): 69-77.

Owttrim, G.W. 2006. RNA helicases and abiotic stress. Nucleic Acids Res. **34**(11): 3220-3230.

Patterson-Fortin, L.M., and Owttrim, G.W. 2008. A *Synechocystis* LexA-orthologue binds direct repeats in target genes. FEBS Lett. **582**(16): 2424-2430.

Patterson-Fortin, L.M., Colvin, K.R., and Owttrim, G.W. 2006. A LexA-related protein regulates redox-sensitive expression of the cyanobacterial RNA helicase, *crhR*. Nucleic Acids Res. **34**(12): 3446-3454.

Peil, L., Virumäe, K., and Remme, J. 2008. Ribosome assembly in *Escherichia coli* strains lacking the RNA helicase DeaD/CsdA or DbpA. FEBS Journal **275**(15): 3772-3782.

Porra, R., Thompson, W., and Kriedemann, P. 1989. Determination of accurate extinction coefficients and simultaneous equations for assaying chlorophylls *a* and *b* extracted with four different solvents: verification of the concentration of chlorophyll standards by atomic absorption spectroscopy. Biochim Biophysica Acta (BBA)-Bioenergetics **975**(3): 384-394.

Prentki, P., and Krisch, H.M. 1984. *In vitro* insertional mutagenesis with a selectable DNA fragment. Gene **29**(3): 303-313.

Price, G.D., Badger, M.R., Woodger, F.J., and Long, B.M. 2008. Advances in understanding the cyanobacterial CO_2-concentrating-mechanism (CCM): functional components, Ci transporters, diversity, genetic regulation and prospects for engineering into plants. J. Exp. Bot. **59**(7): 1441-1461.

Rocak, S., and Linder, P. 2004. DEAD-box proteins: the driving forces behind RNA metabolism. Nat Rev Mol Cell Biol **5**(3): 232-241.

Santiago-Santos, M.C., Ponce-Noyola, T., Olvera-Ramírez, R., Ortega-López, J., and Cañizares-Villanueva, R.O. 2004. Extraction and purification of phycocyanin from *Calothrix* sp. Process Biochemistry **39**(12): 2047-2052.

Shivaji, S., and Prakash, J.S.S. 2010. How do bacteria sense and respond to low temperature? Arch. Microbiol. **192**(2): 85-95.

So, A.K., John-McKay, M., and Espie, G.S. 2002. Characterization of a mutant lacking carboxysomal carbonic anhydrase from the cyanobacterium *Synechocystis* PCC6803. Planta **214**(3): 456-467.

Suzuki, I., Los, D.A., Kanesaki, Y., Mikami, K., and Murata, N. 2000. The pathway for perception and transduction of low-temperature signals in *Synechocystis*. Science Signalling **19**(6): 1327.

Trubetskoy, D., Proux, F., Allemand, F., Dreyfus, M., and Iost, I. 2009. SrmB, a DEAD-box helicase involved in *Escherichia coli* ribosome assembly, is specifically targeted to 23S rRNA *in vivo*. Nucleic Acids Res.**37**(19): 6540-6549.

Yu, E., and Owttrim, G.W. 2000. Characterization of the cold stress-induced cyanobacterial DEAD-box protein CrhC as an RNA helicase. Nucleic Acids Res. **28**(20): 3926-3934.

Zhang, P., Battchikova, N., Jansen, T., Appel, J., Ogawa, T., and Aro, E.M. 2004. Expression and functional roles of the two distinct NDH-1 complexes and the carbon acquisition complex NdhD3/NdhF3/CupA/Sll1735 in *Synechocystis* sp PCC 6803. The Plant Cell Online **16**(12): 3326-3340.tection Plan

Chapter 3: Autoregulation of RNA helicase expression in response to temperature stress in *Synechocystis* sp. PCC 6803

A version of this chapter has been published.
Albert Remus R. Rosana, Danuta Chamot, George W. Owttrim.
2012. PLoS ONE. 7(10): e48683.

3.1 Introduction

The rearrangement of RNA secondary structure, required for numerous crucial cellular functions, is catalyzed by a variety of enzymes including RNA helicases. RNA helicases belong to a gene superfamily, SF2, members of which are encoded in essentially every organism from a variety of viruses to humans. SF2 is comprised of a number of protein families, with the DEAD-box proteins comprising the largest family (Fairman-Williams *et al*., 2010). RNA helicases function as molecular motors utilizing ATP hydrolysis to catalyze rearrangement of RNA and RNP structure with individual helicases performing specific functions potentially affecting all aspects of RNA metabolism (Fairman *et al*., 2004; Bowers *et al*., 2006; Linder and Jankowsky, 2011). Cellular pathways requiring RNA helicase activity include not only housekeeping functions such as translation initiation, ribosome biogenesis and RNA splicing and turnover but also developmental and stress pathways and small RNA metabolism (Rocak and Linder, 2004; Owttrim, 2006; Linder and Owttrim, 2006). Once RNA helicase expression is induced, the resulting RNA helicase activity has the potential to regulate expression of downstream genes required for the developmental or stress response.

Organisms utilize a variety of pathways to respond to temperature shift, the best characterized is heat shock while the mechanisms regulating the cold shock response are less defined. Cold stress induces expression of a limited number of genes, however, unlike heat stress, a sigma factor or two-component signal transduction system functioning as a global regulator of the response has not been identified (Guiliodori *et al*., 2007). This indicates that alternative mechanism(s) regulate gene expression in response to a temperature downshift in bacteria.

Frequently, RNA helicases are associated with the cold stress response in bacteria and higher organisms (Lim *et al*., 2000; Gong *et al*., 2002; Charollais *et al*., 2003; Charollais *et al*., 2004; Hunger *et al*., 2006; Kim *et al*., 2008; Pandiani *et al*., 2011). In prokaryotes, extensive analysis associates RNA helicase activity

with ribosome biogenesis, RNA turnover and cold stress. Of the five *Escherichia coli* DEAD-box RNA helicases, *srmB* and *dbpA* are required for ribosome biogenesis, *rhlB* and *rhlE* with RNA degradation as a component of the degradosome and csdA is associated with both functions (Charollais *et al*., 2003; Charollais *et al*., 2004; Khemici *et al*., 2004; Prud'homme-Genereux *et al*., 2004; Purusharth *et al*., 2005; Iost and Dreyfus, 2006). Frequently, these functions are observed in response to cold stress, for example, at low temperature *csdA* and *rhlE* are degradosome-associated (Prud'homme-Genereux *et al*., 2004; Purusharth *et al*., 2005). The association of RNA helicase expression and function with low temperature is also observed in photosynthetic Gram-negative cyanobacteria in which two DEAD-box RNA helicases have been studied, *crhC* and *crhR* (Chamot *et al*., 1999; Chamot and Owttrim, 2000; Kujat and Owttrim, 2000; Yu and Owttrim, 2000; El-Fahmawi and Owttrim, 2003; Chamot *et al*., 2005). *crhC* is expressed solely in response to low temperature (Chamot *et al*., 1999; Chamot and Owttrim, 2000) while *crhR* is regulated by the redox status of the electron transport chain, with expression increased by conditions that enhance reduction of the chain, for example low temperature or salt stress and dark-light transition (Kujat and Owttrim, 2000; Vinnemeier and Hagemann, 1999). Despite the presence of numerous cold-induced RNA helicases in prokaryotes, the mechanism(s) by which their expression is regulated by temperature shift is not well defined.

At the physiological and morphological levels, *crhR* inactivation has profound effects on cellular metabolism at 30^{o}C which are exacerbated at 20^{o}C (Rosana *et al*., 2012). *crhR* mutants are cold sensitive with respect to both growth and photosynthetic activity, a phenotype resulting primarily from a defect in photosynthetic carbon fixation. These physiological effects are manifested morphologically by the *crhR* mutant progressively accumulating cellular damage at 20^{o}C, including a reduction in the level and organization of carboxysomes and thylakoid membranes with the concomitant accumulation of membrane vesicles within the cells (Rosana *et al*., 2012).

Here, we comprehensively investigate the molecular regulation of *crhR* expression in response to abiotic stress. In particular, we identify that temperature regulation of transcript and protein stability contributes significantly to *crhR* expression involving a unique combination of CrhR-dependent and CrhR-independent pathways. The results provide evidence that CrhR RNA helicase activity is required for transcriptional and post-transcriptional mechanisms that result in autoregulated expression.

3.2 Materials and Methods

3.2.1 Bacterial strains and growth conditions

Wild type *Synechocystis* sp. strain PCC 6803 and the partial deletion mutant, Δ*crhR* (Rosana *et al*., 2012), were maintained on BG11-agar plates containing 10 mM Tricine pH 8.0 and 0.3% sodium thiosulphate at a light intensity of 50 µmol photons m^{-2} s^{-1}. For liquid cultures, 50 mL BG-11 cultures were grown with shaking and used to inoculate 300 mL cultures that were aerated by continuous shaking and bubbling with humidified air (Chamot *et al*., 1999; Chamot and Owttrim, 2000; Owttrim, 2012). Media for *crhR* mutant growth was supplemented with spectinomycin and streptomycin, both at 50 mg/mL (Rosana *et al*., 2012). Temperature and dark stress were induced by transferring aliquots of cultures grown at 30^{o}C to the indicated condition for 1 h. Cells for protein analysis were harvested at the stated growth temperature and cell pellets flash frozen in liquid nitrogen. For RNA extraction, cells and RNases were rapidly inactivated by addition of an equal volume of ice-cold ethanol-phenol buffer (ethanol-5% buffer saturated phenol) directly to the cell culture at the stated growth temperature. For temperature and half-life time course experiments, 400 mL cultures grown at 30^{o}C were transferred to the indicated conditions and 50 mL aliquots removed at the indicated times for RNA and protein extraction. All experiments were repeated a minimum of two times with representative data shown.

3.2.2 RNA manipulation

RNA was extracted using glass bead lysis in the presence of phenol followed by extensive phenol-chloroform extraction and lithium chloride precipitation. Northern analysis, using a 32^{P}-labelled riboprobe corresponding to a 93 bp *Hinc*II-*Sac*II internal fragment of the *crhR* ORF, was performed in formamide buffer at 65^{o}C, as described previously (Chamot *et al*., 1999; Chamot and Owttrim, 2000; Owttrim, 2012). Transcript half-life was estimated in the presence of rifampicin (400 mg/mL), added to cultures immediately prior to transfer to the new temperature. Accumulation of the *Synechocystis rnpB* transcript was utilized as a control for RNA loading. The *rnpB* transcript abundance is extensively utilized for this purpose in cyanobacteria (Lopez-Maury *et al*., 2002; Mitschke *et al*., 2011; Shimura *et al*., 2012). Transcript size was estimated using Fermentas RiboRuler^{TM} RNA markers. Transcript levels were quantified using the Image J software Version 1.45 S (NIH, USA) (Schneider *et al*., 2012).

3.2.3 Protein manipulation

Protein extraction and immunoblot analysis were performed essentially as described previously (Chamot and Owttrim, 2000, Owttrim, 2012). Soluble protein was extracted using glass bead lysis, 25 mg resolved by 10% SDS-PAGE, electro-transferred to Hybond ECL membrane and probed with the indicated antibody. Antibody complexes were detected on X-ray film using the Amersham ECL Western Blotting Detection kit. Polyclonal antiserum against *Synechocystis* CrhR or *E. coli* Rps1 was used at a dilution of 1:5000. Rps1 levels were used as an internal control for protein loading. Protein half-life was determined in cells grown to mid-log phase at 30^{o}C, transferred to 20^{o}C for 2 h to achieve maximum accumulation of CrhR at which time chloramphenicol (250 mg/ml) was added to inhibit *de novo* protein synthesis and half of each culture transferred to 30^{o}C. Protein concentration was quantified using the Bradford assay (Bio-Rad) with

BSA as the standard. Protein levels were quantified using Image J software Version 1.45 S (NIH, USA) (Schneider *et al*., 2012).

3.2.4 ImageJ analysis

X-ray films were scanned using a UMAX PowerLook 2100XL scanner with the resolution set to 800 dpi. Scans were saved as tif files and imported into the ImageJ software package, available from http://imagej.nih.gov/ij/ (Schneider *et al*., 2012). The density of transcript and protein signals were plotted, corrected for background and integrated to give area values. Calculations normalizing for loading, correction of detected signals and determination of accumulation and abundance to quantify transcript and protein levels are described in Methods S1.

3.2.5 Supplementary Methods

3.2.5.1 RNA Quantitation

Transcript levels were quantified using the Image J software Version 1.45S (NIH, USA) available from http://imagej.nih.gov/ij/ (Schneider *et al*., 2012) with *rnpB* as loading control (Lopez-Maury *et al*., 2002; Mitschke *et al*., 2011; Shimura *et al*., 2012). Analysis was performed by normalizing *rnpB* in each lane with wild type 30^{o}C *rnpB* levels set to 1.0. The normalized *rnpB* ratios were used to correct the abundance in the corresponding *crhR* lane. Corrected *crhR* values determined the fold change in each lane based on the basal accumulation observed in wild type cells grown at 30^{o}C in the light which is set to 1.0 or maximum abundance (100%), as indicated. Corrected values were reported as either relative accumulation for time course analyses or relative abundance for half-life analysis.

Calculation of *crhR* transcript accumulation/abundance is provided below:

Formula 1: Normalizing rnpB

$$\textbf{Normalized } \textit{rnpB} \textbf{ ratio } E_x = \frac{\textit{rnpB} \textbf{ value } E_x}{\textit{rnpB} \textbf{ value in WT at } 30^{o}\textbf{C}}$$

where;

rnpB value E_x = signal from experimental lane X

rnpB value of WT at 30°C = signal from wild type, 30°C grown cells, illuminated

Formula 2: Correcting crhR transcript level

$$\textbf{Normalized } \textit{crhR} \textbf{ level } E_x = \frac{\textit{crhR} \textbf{ value } E_x}{\textbf{Normalized } \textit{rnpB} \textbf{ ratio } E_x}$$ *from formula 1*

where;

crhR value E_x = *crhR* signal from experimental lane X

normalized *rnpB* ratio E_x = ratio of normalized *rnpB* in experimental lane X, value obtained from *Formula 1*

Formula 3: Relative crhR Accumulation or Abundance

$$\textbf{Relative } \textit{crhR} \textbf{ Accumulation } E_x = \frac{\textbf{Normalized } \textit{crhR} \textbf{ value } E_x}{\textbf{Normalized } \textit{crhR} \textbf{ levels in WT at } 30^{\circ}\textbf{C}}$$ *from formula 2*

where;

normalized *crhR* value E_x = corrected *crhR* signal from experimental lane X

normalized *crhR* levels at WT 30°C = corrected *crhR* signal from experimental lane WT 30°C, illuminated cell, value obtained from *Formula 2*

Note:

for Relative *crhR abundance* calculation, multiply the Relative *crhR* Accumulation E_x value by 100%

3.2.5.2 Protein quantitation

Protein levels were quantified using Image J software Version 1.45S (NIH, USA) available from http://imagej.nih.gov/ij/ (Schneider *et al*., 2012) with Rps1 as loading control (Owttrim, 2012). Normalization, correction and determination of relative CrhR protein levels were calculated essentially as described above for *crhR* transcript abundance, except that the abundance of ribosomal protein S1 (Rps1) was used as loading control. Rps1 levels were normalized for each lane using the abundance detected in wild type cells grown at 30^{o}C in the light, set to 1.0 and used to normalize Rps1 levels in all lanes. The normalized Rps1 levels were used to correct for protein loading in each lane generating corrected CrhR abundances with the level observed in illuminated wild type cells grown at 30^{o}C set to 1.0 or 100%. Corrected values were reported as either relative accumulation for time course analyses or relative abundance for half-life analysis.

Calculation of CrhR protein accumulation/abundance is provided below:

Formula 1: Normalizing Rps1

$$\textbf{Normalized Rps1 ratio } E_x = \frac{\textbf{Rps1 value } E_X}{\textbf{Rps1 value in WT at } 30^{o}\textbf{C}}$$

where;

Rps1 value E_x = signal from experimental lane X

Rps1 value of WT at 30^{o}C = signal from wild type, 30^{o}C grown cells, illuminated

Formula 2: Correcting CrhR protein level

$$\textbf{Normalized CrhR level } E_x = \frac{\textbf{CrhR value } E_x}{\textbf{Normalized Rps1 ratio } E_x}$$ *from formula 1*

where;

CrhR value E_x = CrhR signal from experimental lane X

normalized Rps1 ratio E_x = ratio of normalized Rps1 in experimental lane X, value obtained from *Formula 1*

Formula 3: Relative crhR Accumulation or Abundance

$$\textbf{Relative CrhR Accumulation } E_x = \frac{\textbf{Normalized CrhR value } E_x}{\textbf{Normalized CrhR levels at WT } 30^{o}\textbf{C}}$$ *from formula 2*

where;

normalized CrhR value E_x = corrected CrhR signal from experimental lane X

normalized CrhR levels at WT 30^{o}C = corrected CrhR signal from experimental lane WT 30^{o}C, illuminated cell, value obtained from *Formula 2*

Note:

for Relative CrhR Abundance calculation, multiply the Relative CrhR Accumulation E_x value by 100%

3.3 Results

3.3.1 Induction of *crhR* expression in response to temperature and light-dark stress

We have extended our previous observations indicating that *crhR* expression is regulated in response to light-induced alteration of the redox poise of the electron transport chain (Kujat and Owttrim, 2000) by investigating expression in response to temperature and light-dark transitions in wild type and *crhR* mutant Synechocystis (Fig. 3.1). In the *crhR* mutant, the ΔCrhR peptide is biochemically inactive, as it does not unwind dsRNA or anneal complementary ssRNAs (Chamot and Owttrim, unpublished). The fate of the truncated mRNA and protein products can therefore be investigated in the absence of biochemically active CrhR. In wild type cells grown at 30^{o}C, a basal level of *crhR* transcript accumulation is observed, a level which decreases significantly in response to dark treatment for 1 h (Fig. 3.1A). *crhR* mutation altered this basal level as crhR transcript accumulation is enhanced 2.6-fold under standard growth conditions at 30^{o}C in illuminated cells (Fig. 3.1A). However, regulation of transcript accumulation at 30^{o}C was not completely lost in the Δ*crhR* mutant as transcript abundance, while elevated, was not increased to the levels observed under cold stress (Fig. 3.1A). While a predominant, 1.5 knt *crhR* transcript was observed in wild type cells other stable, low abundance transcripts are also detected. *crhR* inactivation altered the transcript pattern, with four prominent stable transcripts of 2.3, 1.5, 1.3 and 0.75 knt accumulating in mutant cells. Although in wild type cells, the *crhR* probe detects multiple transcripts, they do not accumulate to the levels observed in the mutant. In response to temperature stress at 20^{o}C for 1 h, *crhR* transcript levels increase and decrease substantially in the light and dark, respectively (Fig. 3.1A). However, similar responses to low temperature in both wild type and Δ*crhR* cells were observed, increasing significantly and, importantly, to approximately the same degree with respect to the basal levels observed at 30^{o}C (Fig. 3.1A). Thus, *crhR* mutation altered the basal transcript abundance at 30^{o}C but not the magnitude of the initial response to low temperature stress. Unexpectedly, accumulation of the *rnpB* transcript, coding for

the functional RNA, RNase P, and used as a control for RNA loading, is marginally (8–10%) but consistently reduced in the Δ*crhR* mutant under all conditions tested (Fig. 3.1A). CrhR protein abundance corresponds with transcript accumulation in wild type cells with a basal level observed in the light at 30^{o}C increasing significantly at 20^{o}C and decreasing in response to dark treatment (Fig. 3.1B). In contrast, temperature regulation of protein accumulation was significantly altered in the Δ*crhR* mutant, in which the 27 kDa truncated CrhR polypeptide (ΔCrhR) was constitutively present at an elevated level, irrespective of temperature or light-dark stress (Fig. 3.1B). Interestingly, the enhanced abundance of the ΔCrhR peptide observed under all conditions was essentially identical to that observed in wild type cells at 20^{o}C. Thus, in wild type and Δ*crhR* cells, CrhR protein levels do not correspond to transcript abundance and CrhR protein accumulates to a maximal level, irrespective of either transcript abundance or temperature.

3.3.2 Time course of *crhR* transcript accumulation

Alteration of the cellular response to temperature and light-dark stresses associated with *crhR* inactivation prompted investigation of the kinetics of transcript accumulation. An essentially identical initial response in transcript accumulation is observed in both wild type and Δ*crhR* cells exposed to 20^{o}C, transcript increasing in a linear fashion from a basal level at 30^{o}C to a maximal level within 20 min (Fig. 3.2A and 3.2B). *crhR* transcript accumulation occurs transiently in wild type cells, decreasing to the basal level observed at 30^{o}C within 6 h of exposure to cold stress (Fig. 3.2A and 3.2C). The transient expression occurring in wild type cells is not observed in the absence of functional CrhR, maximal *crhR* transcript levels accumulate after 20 min and remain consistently elevated for the duration of the experiment (Fig. 3.2B and 3.2C). Again, differential accumulation of four stable *crhR* transcripts was observed between wild type and mutant cells. This suggests that there is a defect in *crhR* transcript processing and/or degradation of the processed transcripts in the absence of CrhR activity (Fig. 3.2A and 3.2B).

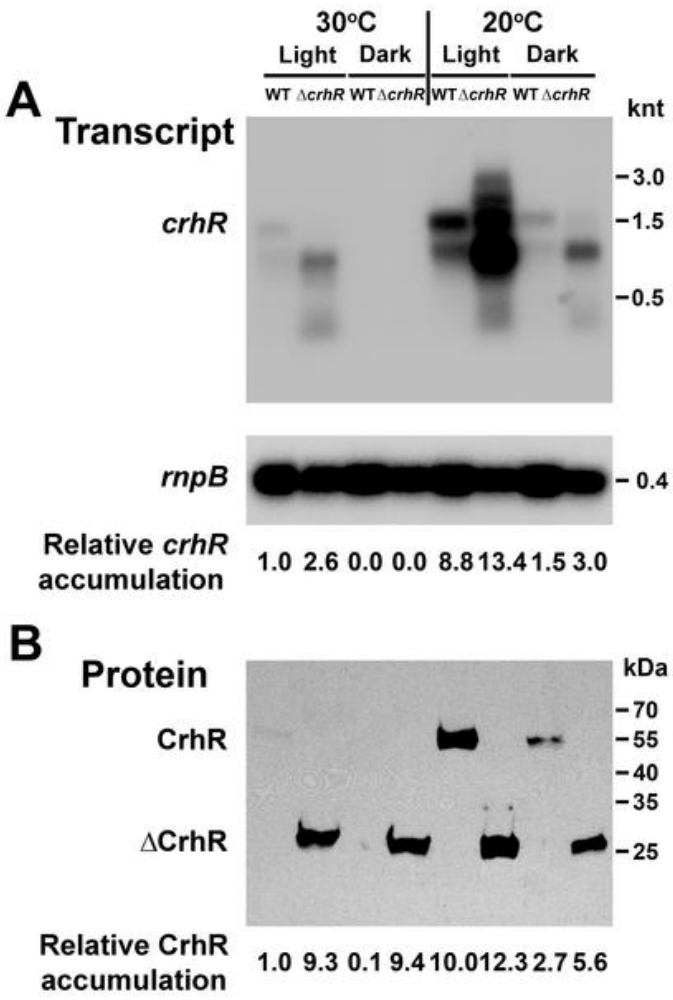

Figure 3.1 *crhR* expression in response to abiotic stress.

(A) Northern analysis. Total RNA (5 mg) was probed with a 93 bp *Hinc*II-*Sac*II internal fragment of *crhR*. *Synechocystis* cells were grown at 30^{o}C and stressed by transfer to the dark or 20^{o}C for 1 h before harvesting at the indicated temperature. Shown below is the stripped blot probed with the *Synechocystis rnpB* as a control for RNA loading. Transcript abundance was quantified using Image J software Version 1.45 S (NIH, USA) (Schneider *et al*., 2012), *crhR* transcript abundance was normalized using corrected *rnpB* levels with basal transcript abundance observed in illuminated wild type cells grown at 30^{o}C set to 1.0 serving as a reference for the fold-change values shown (Methods S1, Section 3.2.5.1).

(B) Western analysis. Soluble protein (25 mg) isolated from the cells used for Northern analysis above was probed with anti-CrhR antibody. The anti-CrhR antibody detects a 55 kDa polypeptide in wild type cells and a, 27 kDa truncated polypeptide in the Δ*crhR* mutant. Relative protein abundance is provided below each lane, in comparison with the abundance detected in illuminated wild type cells grown at 30^{o}C set to 1.0.

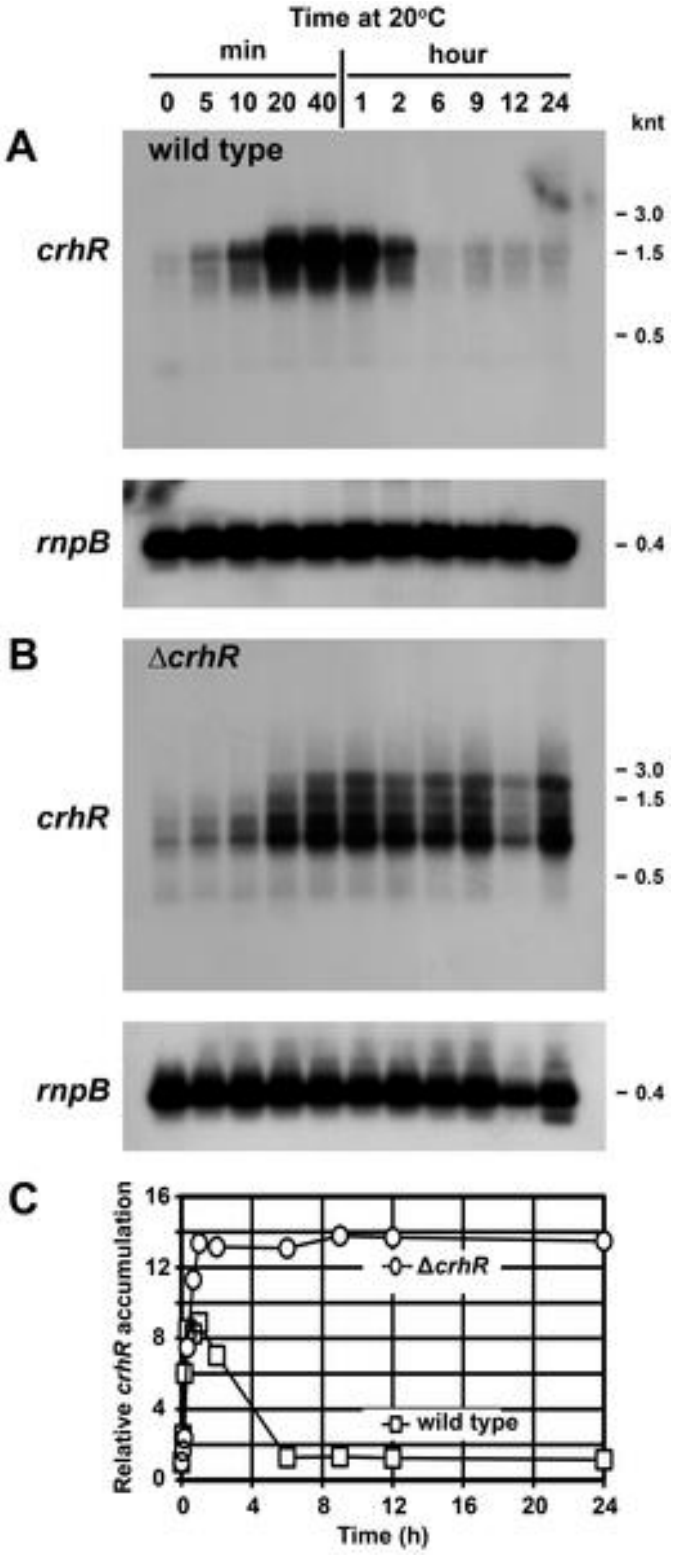
Time at 20°C
min
hour
0 5 10 20 40 1 2 6 9 12 24
knt
A
wild type
crhR
3.0
1.5
0.5
rnpB
0.4
B
ΔcrhR
crhR
3.0
1.5
0.5
rnpB
0.4
C
Relative crhR accumulation
16
12
8
4
0
ΔcrhR
wild type
0 4 8 12 16 20 24
Time (h)

Figure 3.2 Time course of *crhR* transcript accumulation.
Wild type **(A)** or Δ*crhR* mutant **(B)** *Synechocystis* were grown to mid-log phase at 30^{o}C at which time the cultures were transferred to 20^{o}C for the indicated times before harvesting. *crhR* transcript was detected in total RNA probed with a 93 bp *Hinc*II-*Sac*II internal fragment of *crhR*. The blots were stripped and probed with the *Synechocystis rnpB* gene as a control for RNA loading.
C) Quantification of *crhR* transcript levels. Transcript levels were quantified as described in Figure 3.1 and expressed as accumulation relative to *crhR* abundance observed in illuminated wild type cells grown at 30^{o}C (set to 1.0) serving as a reference for the fold-change values shown (Method S1, Section 3.2.5.1). Open circles, Δ*crhR*; open boxes, wild type.

3.3.3 Time course of CrhR protein accumulation

CrhR protein accumulation in response to growth at 20^{o}C also did not reflect the kinetics of *crhR* transcript accumulation in either cell type. In wild type cells, CrhR protein abundance corresponded with transcript levels during the early stages of the low temperature response but with delayed kinetics, reaching a maximum within 2 h of exposure. This correspondence did not hold at longer exposure times, with protein levels remaining elevated for the course of the experiment while transcript decreased significantly (compare Fig. 3.2A and Fig. 3.3A). As observed in Figure 3.1, temperature-regulated expression of the ΔCrhR polypeptide was absent in the Δ*crhR* mutant. ΔCrhR protein was expressed at relatively constant levels at all time points, with only a slight increase observed with extended low temperature exposure (Fig. 3.3B and 3.3C). Thus, again, *crhR* mutation resulted in a constant level of CrhR protein accumulation irrespective of transcript level or temperature.

3.3.4 *crhR* transcript and CrhR protein half-life

The observed alterations in transcript and protein accumulation may reflect changes in macromolecular half-life. Indeed, *crhR* transcript abundance was regulated by temperature, but in a similar manner in both wild type and Δ*crhR* cells. Transcript stability was significantly enhanced at low temperature in wild type *Synechocystis* with half-lives of >30 and ~10 min at 20^{o}C and 30^{o}C, respectively (Fig. 3.4A). Half-life was not altered by *crhR* mutation as similar values are observed in the Δ*crhR* cells, >30 min at 20°C and ~13 min at 30°C (Fig. 3.4B). These results suggest that the enhanced accumulation of *crhR* transcript or the lack of transient accumulation observed in Δ*crhR* cells in response to low temperature do not result from a defect in CrhR-dependent degradation of the *crhR* transcript.

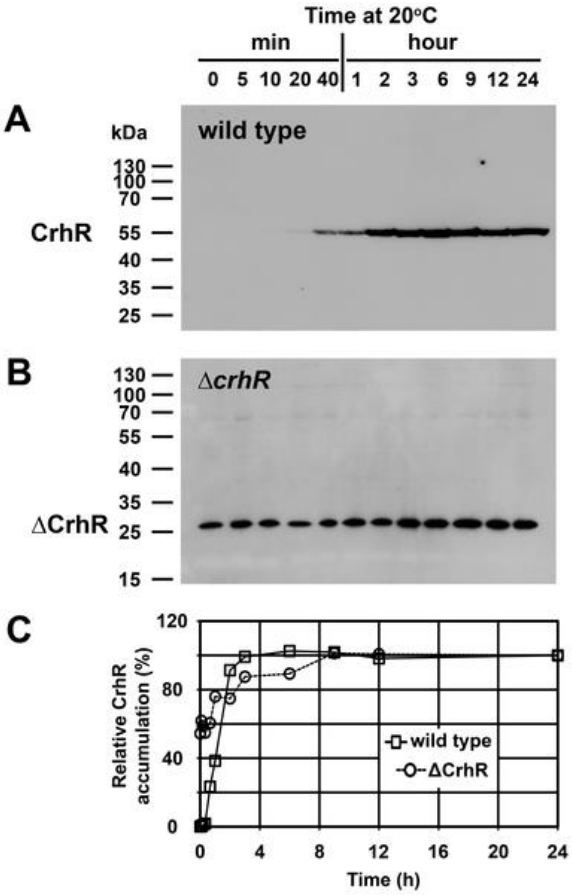

Figure 3.3 Time course of CrhR protein accumulation.

CrhR in soluble proteins extracted from an aliquot of the cells used in Figure 3.2 was detected with an anti-CrhR antibody. **(A)** Wild type *Synechocystis*. **(B)** Δ*crhR* mutant. **(C)** Quantification of CrhR protein levels. Relative CrhR and ΔCrhR protein levels are indicated, normalized with respect to those present at 24 h, as described in Figure 3.1. Open circles, ΔCrhR; open boxes, wild type.

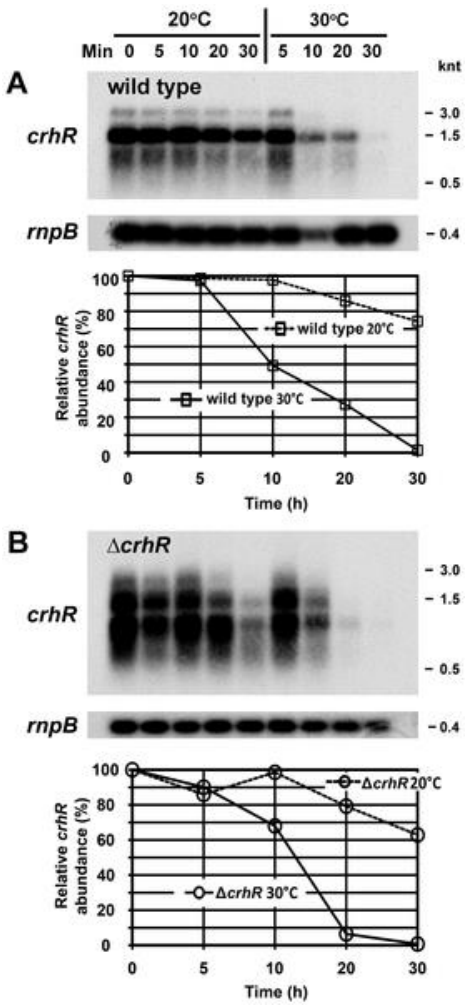

Figure 3.4 *crhR* transcript half-life.

Wild type **(A)** and Δ*crhR* **(B)** *Synechocystis* were grown at 30^{o}C to mid-log phase (0 min) at which time the cultures were cold stressed at 20^{o}C for 1 h to induce maximal *crhR* transcript abundance. *de novo* RNA synthesis was subsequently inhibited by the addition of rifampicin (400 mg/ml) and one-half of the culture transferred back to 30^{o}C. Aliquots for RNA extraction were harvested at the indicated times. *crhR* transcript was detected in total RNA probed with a 93 bp *Hinc*II-*Sac*II internal fragment of *crhR*. The blots were stripped and probed with the *Synechocystis rnpB* gene as a control for RNA loading. Quantification of relative transcript abundance (%) at each time point is provided below each lane, normalized for the level of *rnpB* detected in each lane as described in Methods S1 (Section 3.2.5.1). Open circles, Δ*crhR*; open boxes, wild type.

Temperature regulation of protein half-life similarly controls CrhR accumulation in wild type cells (Fig. 3.5A). At 30^{o}C, CrhR exhibited a relatively short half-life of <3 h which was increased significantly to >48 h at 20°C. In the Δ*crhR* mutant, ΔCrhR peptide levels remained elevated over the entire time course, not altering significantly in response to either chloramphenicol or temperature (Fig. 3.5B). Thus, while transcript half-life is not affected by *crhR* mutation, peptide half-life is significantly altered at both temperatures but more dramatically at 30^{o}C, a response that is CrhR-dependent. The results indicate that *crhR* inactivation does not affect *crhR* transcript turnover but significantly affects CrhR protein turnover.

3.3.5 Temperature gradient induction of *crhR* transcript and protein accumulation

It was of interest to determine if the temperature induction was a gradual or an all-or-none process. This was investigated byanalyzing steady-state transcript and protein levels in *Synechocystis* exposed to temperatures ranging from 35^{o}C to 10^{o}C for 1 h (Fig. 3.6). At the transcript level, a basal level of *crhR* transcript accumulated at 35 and 30^{o}C, which progressively increased to a maximum at 15^{o}C (Fig. 3.6A). At 10^{o}C, transcript accumulation was enhanced marginally, *crhR* transcript levels increasing 1.7-fold in comparison with the basal level detected at 30^{o}C (Fig. 3.6A). CrhR protein expression in wild type cells mimicked transcript levels with the basal level of CrhR protein expression observed at 35 and 30^{o}C increasing to a maximum at 20^{o}C and subsequently decreasing to the basal level at 10^{o}C (Fig. 3.6B). In the Δ*crhR* mutant, transcript abundance increases in response to decreasing temperature but reaches a maximum more rapidly and accumulates above basal levels at 10^{o}C compared to wild type (Fig. 3.6A). As observed in Figure 3.3B, ΔCrhR protein levels in the *crhR* mutant remain essentially constant over the entire temperature gradient, increasing marginally in response to a 1 h exposure to temperatures ≤20^{o}C (Fig. 3.6B).

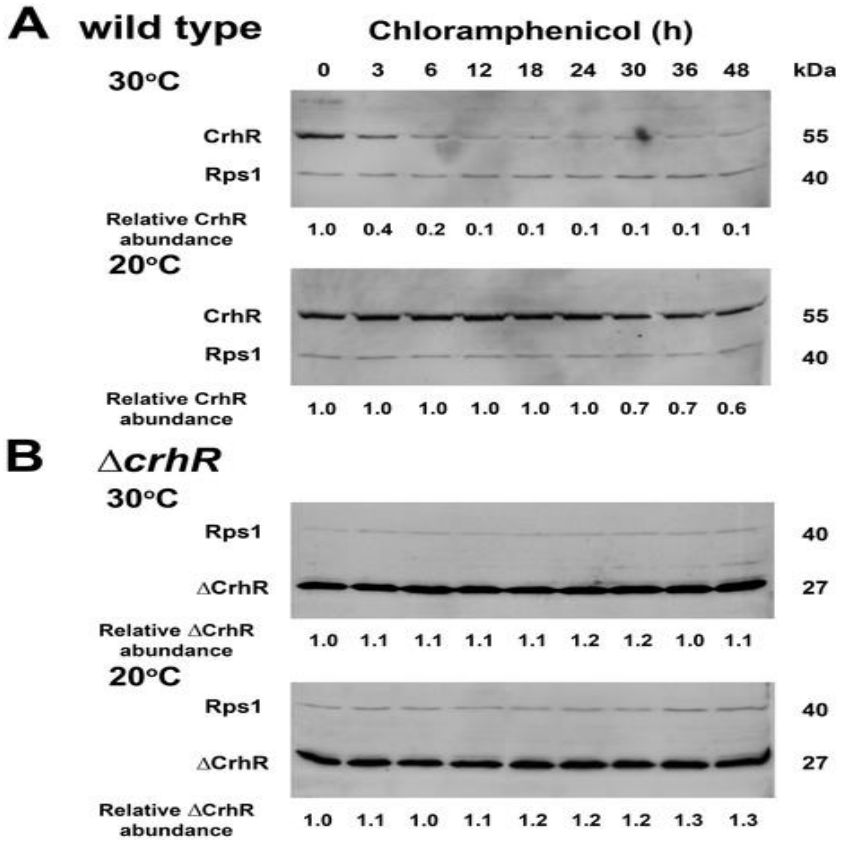

Figure 3.5 CrhR protein half-life.

Wild type **(A)** and Δ*crhR* **(B)** *Synechocystis* were grown to mid-log phase at 30^{o}C (0 min) at which time the cultures were transferred to 20^{o}C for 2 h to achieve maximum CrhR and ΔCrhR abundance. Chloramphenicol (250 mg/ml) was added to inhibit *de novo* protein synthesis and one-half of each culture was transferred back to 30^{o}C. Samples for soluble protein extraction were harvested at the indicated times. Blots were simultaneously probed with antibodies against CrhR and *E. coli* ribosomal protein S1 (Rps1), used as a control for protein loading. Quantification of relative CrhR and ΔCrhR protein abundance at each time point is provided, below each lane, normalized for the level of Rps1, as described in Methods S1 (Section 3.2.5.2)

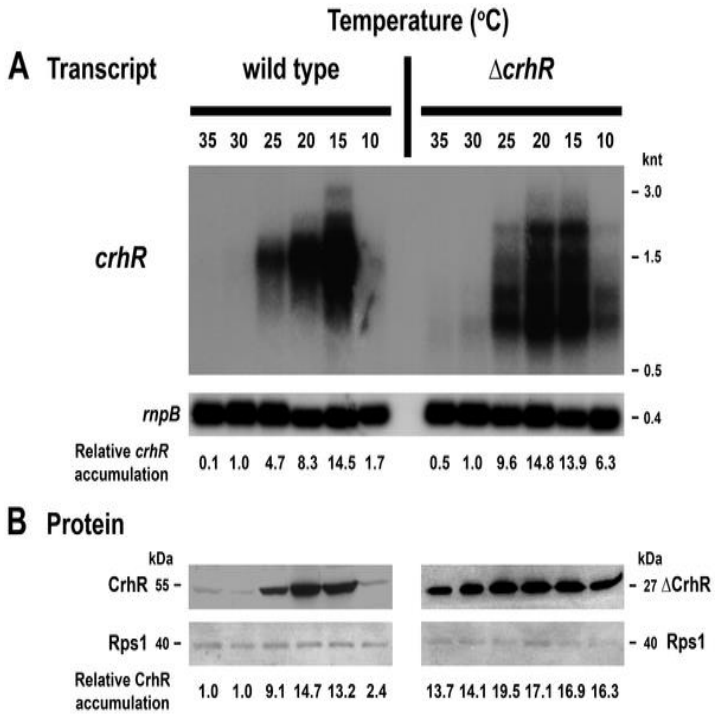

Figure 3.6 Temperature gradient of *crhR* expression.

Wild type and Δ*crhR Synechocystis* were grown to mid-log phase at 30°C and divided into 6 aliquots, each of which was incubated at the indicated temperature for 1 h and samples were harvested for RNA and protein extraction. (**A**) Total RNA on a northern blot was probed with a 93 bp *Hinc*II-*Sac*II internal fragment of *crhR*, stripped and probed with the*Synechocystis rnpB* gene as a control for RNA loading. *crhR* transcript levels were quantified at each temperature as described in Methods S1 (Section 3.2.5.1) and the fold change in *crhR* accumulation compared to the abundance in illuminated, wild type cells grown at 30°C (set to 1.0) is provided below each lane. (**B**) Western blots were probed with anti-CrhR antiserum and subsequently probed with antibodies against *E. coli* Rps1 as a control for protein loading. Protein levels were quantified at each temperature and the fold change in CrhR or ΔCrhR compared to the abundance in illuminated, wild type cells grown at 30°C (set to 1.0) is provided below each lane, as described in Methods S1 (Section 3.2.5.2).

3.3.6 Time course of *crhR* transcript and protein accumulation at 10^{o}C

The observation that *crhR* transcript levels were not enhanced in response to growth at 10^{o}C indicates that a 5^{o}C downshift in temperature dramatically affected cellular ability to respond to low temperature. This could result from either an inability to sense and/or respond at the transcriptional level or simply reflect a temperature-induced reduction in overall transcriptional activity. To further investigate this phenomenon, *crhR* transcript and protein levels were analyzed in response to prolonged exposure to 10^{o}C. Overall, the time course of both *crhR* transcript and protein accumulation in wild type cells resembled that observed at 20^{o}C (Fig. 3.2 and 3.3) however the kinetics were delayed at 10^{o}C. In wild type cells, maximal transcript accumulation occurred within 3 h, plateauing and then decreasing up to 24 h (Fig. 3.7A). Conversely, CrhR protein accumulated progressively over the course of the experiment, even subsequent to *crhR* transcript decline (Fig. 3.7A), as also observed in Figures 3.2 and 3.3. In contrast, *crhR* transcript in the Δ*crhR* mutant was constitutively observed at all time points at 10^{o}C (Fig. 3.7B, Table S1). The pattern of transcript accumulation differed from that observed at 20^{o}C (Fig. 3.6A) with the 2.3 and 0.75 knt transcripts predominating at 10^{o}C (Table S1). In addition, although the total accumulation of the four detected transcripts was not altered (Table S1), the relative accumulation of the two transcripts shifted in response to extended exposure to 10^{o}C, with the 0.75 knt predominating at shorter and the 2.3 knt predominating at longer exposures, respectively (Fig. 3.7B, Table S1). This was not a result of alteration in total transcript, as quantification indicates that abundance of all four transcripts was constant over the experiment (Table S1). This is reflective of the results shown in Figures 3.2B and 3.2C, in both cases *crhR* transcript accumulation in the mutant is maximal within 1 h of exposure to 20^{o}C and remains constant thereafter. These results imply that there is a defect in *crhR* transcript

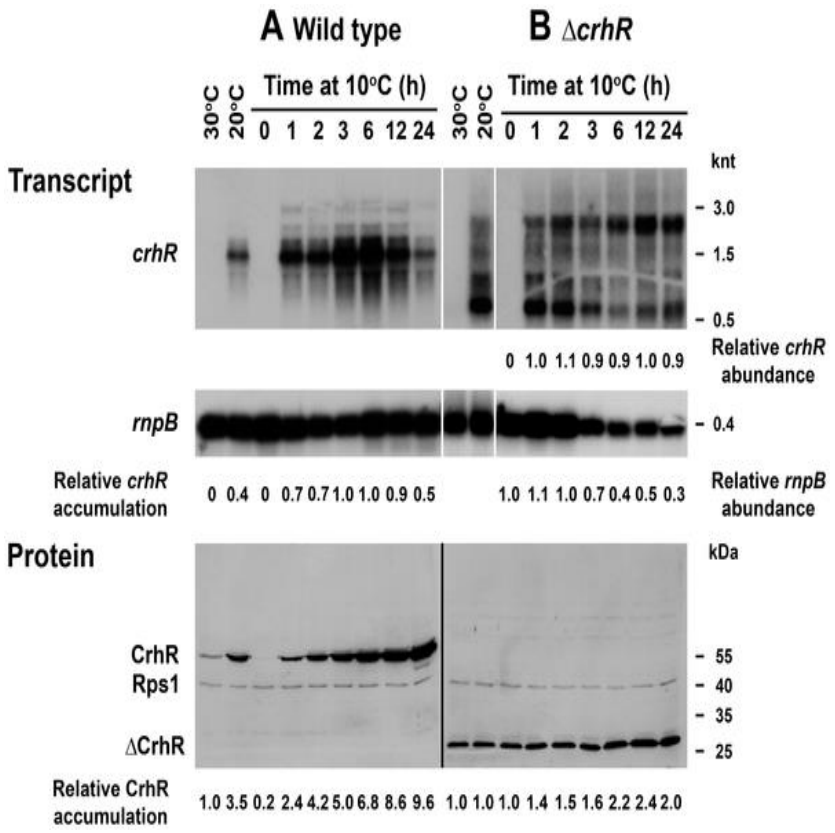

Figure 3.7 Time course of *crhR* expression at 10°C.

Wild type **(A)** and Δ*crhR* **(B)** *Synechocystis* were grown to mid-log phase at 30°C and transferred to 10°C for the indicated times. Samples were harvested for RNA and soluble protein extraction at the indicated time points. Cells grown at 30°C and 20°C are included as references. **(A)** The relative *crhR* accumulation in comparison with the abundance in illuminated, wild type cells grown at 30°C corrected for *rnpB* levels (set to 1.0), is given below each lane for wild type cells. For Δ*crhR* cells, decreasing *rnpB* accumulation necessitated calculation of the relative abundance of *crhR* and *rnpB* independently. Transcript levels at 1 h of exposure to 10°C and 0 time were set to 1.0 for *crhR* and *rnpB*, respectively. Quantification of the 2.3 and 0.75 knt transcripts is shown in Table 3.S1. Ethidium bromide staining of the RNA present on the Northern blot indicates that essentially equal quantities of RNA were loaded in each lane (Figure 3.S1) **(B)** Western blots were simultaneously probed with antibodies against CrhR and *E. coli* Rps1 that served as a control for protein loading. The relative fold change in

CrhR and ΔCrhR accumulation, corrected for Rps1 levels, as described in Method 3.S1 (Section 3.2.5.1), is given below each lane. Protein samples were resolved on separate gels, hence normalization was performed independently for the wild type and mutant, with abundance observed in wild type and mutant at 30°C set to 1.0.

processing in the absence of CrhR RNA helicase activity. Again, ΔCrhR peptide levels remain relatively constant under all conditions tested, with only a marginal increase observed after prolonged exposure to 10^{o}C, irrespective of RNA abundance (Fig. 3.7B). Similar to the results shown in Fig. 3.1A were *rnpB* transcript levels are consistently reduced under all conditions at 20^{o}C, *rnpB* levels decreased progressively in response to extended growth at 10^{o}C in the Δ*crhR* mutant (Fig. 3.7B). The observed decrease in *rnpB* accumulation would normally be an indication of unequal RNA loading, however analysis of total RNA in each lane, visualized by ethidium bromide staining, indicated that RNA loading was approximately equal in each lane (Fig. 3.S1). *crhR* expression was also evaluated in response to exposure of a single culture to a 5^{o}C decrease in growth temperature for one hour, progressively from 35 to 10^{o}C. In this scenario, a significant increase in *crhR* transcript level was detected in wild type cells in response to the temperature decrease from 15 to 10^{o}C. This implies that wild type cells possess the capacity to respond to 10^{o}C if they are cold adapted for one hour (data not shown). In agreement, CrhR protein levels also increase at 10^{o}C in response to this temperature regime. As expected from experiments presented above, the level of the ΔCrhR polypeptide detected in mutant cells remained relatively constant, increasing slightly at temperatures below 20^{o}C. Again, *rnpB* levels were observed to decrease at 10^{o}C in the single culture exposed to the progressive 5^{o}C decreases in temperature for 1 h intervals (data not shown).

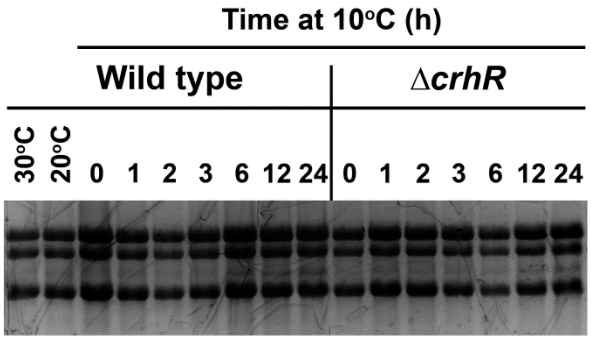

Figure 3.S1. Ethidium bromide stained gel corresponding to the crhR induction time course at 10°C.

Total RNA (5 µg) extracted from wild type and Δ*crhR Synechocystis* cells was separated on a 1.2% formalydehyde agarose gel at 100V for 2.5 h. The gel was stained with ethidium bromide and imaged using a LKB 2011 Macrovue UV transilluminator equipped with a Kodak EDAS DC 290 camera and processed using Kodak 1D 3.6 imaging software. The ethidium fluorescence indicates that essentially equal amounts of RNA were loaded in each lane. Therefore, variations in *rnpB* transcript levels are not related to unequal RNA present in each lane.

Table 3-S1 Quantification of *crhR* transcript hybridization detected in the Δ*crhR* mutant shown in Figure 3.7B

ΔcrhR	**Relative transcript level***		
	2300 nt*	**750 nt***	**Total *crhR*****
10°C – 0 h	0.00	0.00	0.00
10°C – 1 h	1.00	1.00	1.00
10°C – 2 h	2.16	0.92	1.10
10°C – 3 h	1.09	0.65	0.90
10°C – 6 h	2.34	0.30	0.90
10°C – 12 h	3.57	0.56	1.00
10°C – 24 h	3.23	0.65	0.90

*Individual transcript abundance was calculated by setting the level observed at 10°C for 1 h as 1.0.

**Total *crhR* abundance was quantitated using Image J analysis performed on the total area of hybridization in each lane.

3.4 Discussion

The lack of a common global regulator of cold stress indicates that a variety of transcriptional and post-transcriptional mechanisms control gene expression in response to a temperature downshift (Guiliodori *et al*., 2007). The data presented here provide evidence that expression of the cyanobacterial RNA helicase, *crhR*, is controlled by a complex network of regulatory checkpoints involving both CrhR-dependent and CrhR-independent pathways, as outlined in Figure 3.8. Determination if CrhR is directly or indirectly involved in the autoregulation process and the mechanism by which the autoregulation functions are crucial questions. RNA helicases have well defined direct roles in translation initiation, RNA turnover and ribosome biogenesis in prokaryotic and eukaryotic systems (Linder and Jankowsky, 2011; Iost and Dreyfus, 2006). An indirect role for CrhR in autoregulatory mechanisms may be associated with one of these cellular pathways. For example, transient expression and proteolysis may originate indirectly from CrhR-regulated translation of transcripts whose protein products are required for these processes. An indirect role for CrhR in the observed regulation involving small RNA metabolism, as observed for RNA helicases in abiotic stress responses in eukaryotic systems (Owttrim, 2006) or on transcription cannot be ruled out. These may not reflect an indirect effect as p68 and p72 RNA helicases that catalyze similar biochemical reactions as CrhR (Chamot *et al*., 2005), function as transcriptional co-regulators (Fuller-Pace and Ali, 2008).

Temperature plays a profound role in *crhR* expression, enhancing both *crhR* transcript and protein half-life, although CrhR performs divergent roles in both mechanisms. CrhR-independent pathways are associated with temperature sensing, signal transduction and subsequent molecular response at the initial stages of cellular response to low temperature. The CrhR-independence of the initial response generating *crhR* transcript accumulation is related to

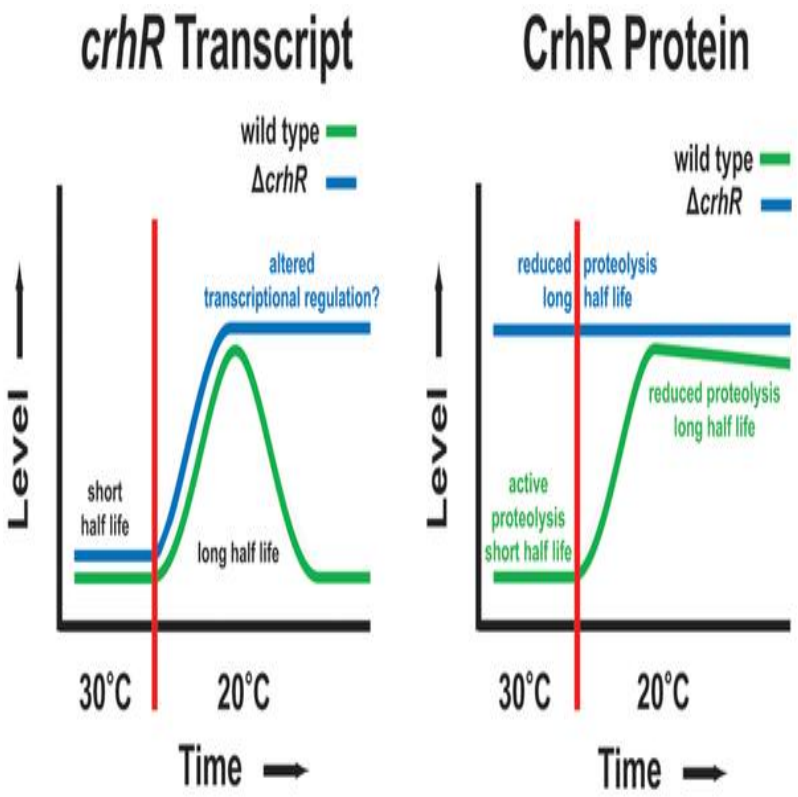

Figure 3.8 Schematic summary of *crhR* expression and regulation.
crhR expression is controlled by a complex interaction between temperature-regulation of both transcript accumulation and protein degradation. *crhR* **transcript.** *crhR* transcript half-lives are equal and short in both wild type and Δ*crhR Synechocystis* cells which contributes to a basal level of transcript accumulation at 30°C. A temperature downshift to 20°C rapidly induces *crhR* transcript accumulation associated with enhanced half-life and with similar kinetics in both cell types, suggesting that CrhR is not required for temperature sensing or induction of its own transcript accumulation. At low temperature, *crhR* is transiently accumulated in wild type cells whereas conversely, transcript remains elevated at 20°C in the Δ*crhR* mutant, suggesting that CrhR activity is required for the transient expression. Although *crhR* half-life is influenced by temperature, being significantly longer at 20°C, it is identical in both cell types. This suggests that CrhR is not directly involved in degradation of

its own transcript but functional CrhR is directly associated with repression of *crhR* transcript accumulation, most likely through another mechanism, possibly altered regulation of transcription. **CrhR protein.** CrhR protein levels correspond to transcript levels in wild type *Synechocystis*, accumulating to a basal level at 30°C and increasing significantly at 20°C. This is distinctly not the case in the Δ*crhR* mutant in which CrhR protein remains elevated and constant at both temperatures. CrhR protein accumulates to the level observed in wild type *Synechocystis* at 20°C, irrespective of transcript accumulation or temperature. Combined, these results suggest that the reduced level of CrhR at 30°C is caused by proteolytic degradation which is temperature- and CrhR-dependent as this process is inactive in the Δ*crhR* mutant. In addition, there appears to be a maximal level of CrhR that can accumulate in cells, irrespective of the transcript level, a process that is CrhR independent. This accumulation appears to be a default level as it was never observed to increase above the level detected in wild type cells at 20°C.

the enhanced reduction of the electron transport chain at low temperature that is required for *crhR* transcription (Kujat and Owttrim, 2000). A major aspect regulating *crhR* transcript abundance is controlled by temperature alteration of *crhR*transcript half-life, unstable at 30°C and significantly stabilized at 20°C, as observed for other cold-regulated bacterial transcripts (Chamot and Owttrim, 2000; Goldenberg *et al*., 1996; Prudhomme-Genereux *et al*., 2004). The level of *crhR* transcript accumulation at different temperatures can potentially be explained by the temperature alteration of transcript stability, although we cannot rule out effects of CrhR regulation of transcription. The pathway conferring transcript stability is CrhR-independent, as *crhR* transcript half-life is not altered by *crhR* mutation. This observation suggests that CrhR is not directly involved in the RNA degradation pathway responsible for turnover of its own transcript. This is an important observation as RNA helicases frequently function in RNA turnover in prokaryotic systems, switching of RNA helicase composition in the RNA degradosome occurring in response to low temperature, resulting in formation of a cold-adapted degradation complex (Regonesi *et al*., 2006; Nickel *et al*., 2004; Arraiano *et al*., 2010). It is possible that CrhR is indirectly involved in degradation of its own transcript through regulation of translation initiation or another aspect of RNA metabolism associated with expression of the required RNase.

Transient accumulation of *crhR* transcript at 20°C and CrhR protein stability at all temperatures is CrhR-dependent. Transient transcript accumulation is a common characteristic of cold-induced genes in prokaryotic systems, although the mechanism is not well characterized (Goldenberg *et al*., 1999; Sato, 1995; Aguilar *et al*., 1999). While transient accumulation in the absence of functional CrhR can also be interpreted as evidence that CrhR functions in the degradation of its own transcript, the lack of *crhR* transcript half-life alteration in the *crhR* mutant suggests that this is not the case. The kinetics of *crhR* transcript and protein accumulation more closely fit a scenario in which CrhR binding to the *crhR* transcript directs the CrhR-*crhR* complex to a CrhR-independent RNA degradation pathway. This proposal is similar to the direct mechanism by which

proteolysis of the RNA chaperone CspC at high temperature regulates transient expression of heat shock mRNAs in *E. coli (Shenhar et al., 2009),* except that CrhR protein levels remain elevated continuously during temperature stress. Thus it appears that the CrhR-dependent transient accumulation of *crhR* transcript involves a direct association with RNA helicase activity, a role that does not involve RNA degradation.

CrhR peptide accumulation depends on a complex interplay between temperature regulation of both transcript and protein stability. The CrhR-dependent enhancement of CrhR peptide half-life at low temperature occurs in the absence of a correlation between protein and transcript levels. CrhR protein continues to accumulate in the absence of significant transcript accumulation at low temperature, similar to that observed for Rbp proteins in cyanobacteria (Sato, 1995). This is in contrast to other cold-induced proteins where both transcript and protein transiently accumulate (Goldenberg *et al*., 1999). Changes in CrhR abundance could result from either altered translational efficiency or proteolysis. The increase in CrhR peptide abundance in the absence of functional CrhR at 30°C suggests that CrhR is not required for translation of its own transcript but is more likely indirectly involved to produce a component required for activity of the proteolytic degradation machinery. The mechanism does not appear to involve a general protein degradation pathway, as Rps1 levels are not significantly altered in these experiments. In addition, truncated CrhR polypeptide levels did not exceed those present in wild type cells at 20°C, suggesting that a CrhR-independent mechanism limits CrhR accumulation irrespective of transcript level or temperature. This implies that there is a maximum, default level to which CrhR can accumulate in *Synechocystis*, a process that is CrhR- and temperature-independent.

Proteolysis regulates the level of numerous proteins and regulatory circuits in bacterial systems, a prime example being the heat shock response (Gottesman, 2003; Gur et al., 2011; Mayer and Baker, 2011). In a natural environment, *Synechocystis* would normally experience temperatures below 25°C,

conditions under which *crhR* expression would be constitutively induced. A temperature upshift to 30°C would enhance the proteolytic machinery that degrades CrhR. We therefore suggest that the results presented here resemble the regulation observed in response to heat stress rather than a cold stress specific phenomenon (Meyer and Baker, 2001).

Regulation of prokaryotic gene expression is primarily thought to occur at the transcriptional level, with limited examples of control at the level of transcript or protein stability. The findings reported here, summarized in Figure 3.8, indicate that *crhR* expression is regulated in an unexpectedly complex manner, involving both CrhR-dependent and -independent pathways. CrhR-dependent pathways contribute to *crhR* expression via a novel combination of transcriptional and post-transcriptional mechanisms including autoregulation of the transient expression of *crhR* transcript at low temperature and CrhR protein accumulation at all temperatures. In contrast, aspects of temperature sensing, signal transduction, the initial increase in *crhR* accumulation and temperature-regulation of *crhR* transcript half-life involve CrhR-independent pathways. Frequently, these mechanisms regulate *crhR* expression in the absence of a correlation between protein and transcript levels. CrhR modulation of these divergent pathways coordinates cyanobacterial response to temperature fluctuation.

The data provide unique insights into the complexity of pathways regulating RNA helicase expression associated with bacterial response to temperature stress at the molecular level. Moreover, the research highlights the importance of RNA helicase remodeling of RNA secondary structure on downstream gene expression and the physiological implications for bacterial adaptation to temperature change.

3.5 References

Aguilar, P.S., Lopez, P., and De Mendoza, D. 1999. Transcriptional control of the low-temperature-inducible des gene, encoding the Δ5 desaturase of *Bacillus subtilis*. J. Bacteriol. **181**(22): 7028-7033.

Arraiano, C.M., Andrade, J.M., Domingues, S., Guinote, I.B., Malecki, M., Matos, R.G., Moreira, R.N., Pobre, V., Reis, F.P., and Saramago, M. 2010. The critical role of RNA processing and degradation in the control of gene expression. FEMS Microbiol. Rev. **34**(5): 883-923.

Bowers, H.A., Maroney, P.A., Fairman, M.E., Kastner, B., Lührmann, R., Nilsen, T.W., and Jankowsky, E. 2006. Discriminatory RNP remodeling by the DEAD-box protein DED1. RNA **12**(5): 903-912.

Chamot, D., and Owttrim, G.W. 2000. Regulation of cold shock-induced RNA helicase gene expression in the cyanobacterium *Anabaena* sp. strain PCC 7120. J. Bacteriol. **182**(5): 1251-1256.

Chamot, D., Colvin, K.R., Kujat-Choy, S.L., and Owttrim, G.W. 2005. RNA structural rearrangement via unwinding and annealing by the cyanobacterial RNA helicase, CrhR. J. Biol. Chem. **280**(3): 2036-2044.

Chamot, D., Magee, W.C., Yu, E., and Owttrim, G.W. 1999. A cold shock-induced cyanobacterial RNA helicase. J. Bacteriol. **181**(6): 1728-1732.

Charollais, J., Dreyfus, M., and Iost, I. 2004. CsdA, a cold-shock RNA helicase from *Escherichia coli*, is involved in the biogenesis of 50S ribosomal subunit. Nucleic Acids Res. **32**(9): 2751-2759.

Charollais, J., Pflieger, D., Vinh, J., Dreyfus, M., and Iost, I. 2003. The DEAD-box RNA helicase SrmB is involved in the assembly of 50S ribosomal subunits in *Escherichia coli*. Mol. Microbiol. **48**(5): 1253-1265.

El-Fahmawi, B., and Owttrim, G.W. 2003. Polar-biased localization of the cold stress-induced RNA helicase, CrhC, in the cyanobacterium *Anabaena* sp. strain PCC 7120. Mol. Microbiol. **50**(4): 1439-1448.

Fairman, M.E., Maroney, P.A., Wang, W., Bowers, H.A., Gollnick, P., Nilsen, T.W., and Jankowsky, E. 2004. Protein displacement by DExH/D" RNA helicases" without duplex unwinding. Science **304**(5671): 730-734.

Fairman-Williams, M.E., Guenther, U.P., and Jankowsky, E. 2010. SF1 and SF2 helicases: family matters. Curr. Opin. Struct. Biol. **20**(3): 313-324.

Fuller-Pace, F., and Ali, S. 2008. The DEAD box RNA helicases p68 (Ddx5) and p72 (Ddx17): novel transcriptional co-regulators. Biochem. Soc. Trans. **36**: 609-612.

Giuliodori, A., Gualerzi, C.O., Soto, S., Vila, J., and Tavio, M.M. 2007. Review on bacterial stress topics. Ann. N. Y. Acad. Sci. **1113**(1): 95-104.

Goldenberg, D., Azar, I., and Oppenheim, A.B. 2003. Differential mRNA stability of the *cspA* gene in the cold-shock response of *Escherichia coli*. Mol. Microbiol. **19**(2): 241-248.

Gong, Z., Lee, H., Xiong, L., Jagendorf, A., Stevenson, B., and Zhu, J.K. 2002. RNA helicase-like protein as an early regulator of transcription factors for plant chilling and freezing tolerance. Proceedings of the National Academy of Sciences **99**(17): 11507-11512.

Gottesman, S. 2003. Proteolysis in bacterial regulatory circuits. Annu. Rev. Cell Dev. Biol. **19**(1): 565-587.

Gur, E., Biran, D., and Ron, E.Z. 2011. Regulated proteolysis in Gram-negative bacteria—how and when? Nature Reviews Microbiology **9**: 839–848

Hunger, K., Beckering, C.L., Wiegeshoff, F., Graumann, P.L., and Marahiel, M.A. 2006. Cold-induced putative DEAD box RNA helicases CshA and CshB are essential for cold adaptation and interact with cold shock protein B in *Bacillus subtilis*. J. Bacteriol. **188**(1): 240-248.

Iost, I., and Dreyfus, M. 2006. DEAD-box RNA helicases in *Escherichia coli*. Nucleic Acids Res. **34**(15): 4189-4197.

Khemici, V., Toesca, I., Poljak, L., Vanzo, N.F., and Carpousis, A.J. 2004. The RNase E of *Escherichia coli* has at least two binding sites for DEAD-box RNA helicases: Functional replacement of RhlB by RhlE. Mol. Microbiol. **54**(5): 1422-1430.

Kim, J.S., Kim, K.A., Oh, T.R., Park, C.M., and Kang, H. 2008. Functional characterization of DEAD-box RNA helicases in *Arabidopsis thaliana* under abiotic stress conditions. Plant and cell physiology **49**(10): 1563-1571.

Kujat, S.L., and Owttrim, G.W. 2000. Redox-regulated RNA helicase expression. Plant Physiol. **124**(2): 703-714.

Lim, J., Thomas, T., and Cavicchioli, R. 2000. Low temperature regulated DEAD-box RNA helicase from the antarctic archaeon, *Methanococcoides burtonii*. J. Mol. Biol. **297**(3): 553-567.

Linder, P., and Jankowsky, E. 2011. From unwinding to clamping — the DEAD box RNA helicase family. Nature Reviews Molecular Cell Biology **12**(8): 505-516.

Linder, P., and Owttrim, G.W. 2009. Plant RNA helicases: linking aberrant and silencing RNA. Trends Plant Sci. **14**(6): 344-352.

López-Maury, L., García-Domínguez, M., Florencio, F.J., and Reyes, J.C. 2002. A two-component signal transduction system involved in nickel sensing in the cyanobacterium *Synechocystis* sp. PCC 6803. Mol. Microbiol. **43**(1): 247-256.

Meyer, A.S., and Baker, T.A. 2011. Proteolysis in the *Escherichia coli* heat shock response: a player at many levels. Curr. Opin. Microbiol. **14**(2): 194-199.

Mitschke, J., Vioque, A., Haas, F., Hess, W.R., and Muro-Pastor, A.M. 2011. Dynamics of transcriptional start site selection during nitrogen stress-induced cell differentiation in *Anabaena* sp. PCC7120. Proceedings of the National Academy of Sciences **108**(50): 20130-20135.

Nickel, M., Homuth, G., Böhnisch, C., Mäder, U., and Schweder, T. 2004. Cold induction of the *Bacillus subtilis* bkd operon is mediated by increased mRNA stability. Molecular Genetics and Genomics **272**(1): 98-107.

Owttrim, G.W. 2012. RNA Helicases in cyanobacteria: Biochemical and molecular approaches. Meth. Enzymol. **511**: 385.

Owttrim, G.W. 2006. RNA helicases and abiotic stress. Nucleic Acids Res. **34**(11): 3220-3230.

Pandiani, F., Chamot, S., Brillard, J., Carlin, F., and Broussolle, V. 2011. Role of the five RNA helicases in the adaptive response of *Bacillus cereus* ATCC 14579 cells to temperature, pH, and oxidative stresses. Appl. Environ. Microbiol. **77**(16): 5604-5609.

Prud'homme-Généreux, A., Beran, R.K., Iost, I., Ramey, C.S., Mackie, G.A., and Simons, R.W. 2004. Physical and functional interactions among RNase E, polynucleotide phosphorylase and the cold-shock protein, CsdA: evidence for a 'cold shock degradosome'. Mol. Microbiol. **54**(5): 1409-1421.

Purusharth, R.I., Klein, F., Sulthana, S., Jäger, S., Jagannadham, M.V., Evguenieva-Hackenberg, E., Ray, M.K., and Klug, G. 2005. Exoribonuclease R interacts with endoribonuclease E and an RNA helicase in the psychrotrophic bacterium *Pseudomonas syringae* Lz4W. J. Biol. Chem. **280**(15): 14572-14578.

Regonesi, M.E., Del Favero, M., Basilico, F., Briani, F., Benazzi, L., Tortora, P., Mauri, P., and Deho, G. 2006. Analysis of the *Escherichia coli* RNA degradosome composition by a proteomic approach. Biochimie **88**(2): 151-161.

Rocak, S., and Linder, P. 2004. DEAD-box proteins: the driving forces behind RNA metabolism. Nature Reviews Molecular Cell Biology **5**(3): 232-241.

Rosana, A.R.R., Ventakesh, M., Chamot, D., Patterson-Fortin, L.M., Tarassova, O., Espie, G.S., and Owttrim, G.W. 2012. Inactivation of a low temperature-induced RNA Helicase in *Synechocystis* sp. PCC 6803: Physiological and morphological consequences. Plant and Cell Physiology **53**(4): 646-658.

Sato, N. 1995. A family of cold-regulated RNA-binding protein genes in the cyanobacterium *Anabaena variabilis* M3. Nucleic Acids Res. **23**(12): 2161-2167.

Schneider, C.A., Rasband, W.S., and Eliceiri, K.W. 2012. NIH Image to ImageJ: 25 years of image analysis. Nature Methods **9**(7): 671-675.

Shenhar, Y., Rasouly, A., Biran, D., and Ron, E.Z. 2009. Adaptation of *Escherichia coli* to elevated temperatures involves a change in stability of heat shock gene transcripts. Environ. Microbiol. **11**(12): 2989-2997.

Shimura, Y., Shiraiwa, Y., and Suzuki, I. 2012. Characterization of the subdomains in the N-terminal region of histidine kinase Hik33 in the cyanobacterium *Synechocystis* sp. PCC 6803. Plant and Cell Physiology **53**(7): 1255-1266.

Vinnemeier, J., and Hagemann, M. 1999. Identification of salt-regulated genes in the genome of the cyanobacterium *Synechocystis* sp. strain PCC 6803 by subtractive RNA hybridization. Arch. Microbiol. **172**(6): 377-386.

Yu, E., and Owttrim, G.W. 2000. Characterization of the cold stress-induced cyanobacterial DEAD-box protein CrhC as an RNA helicase. Nucleic Acids Res. **28**(20): 3926-3934.

Chapter 4: CrhR RNA helicase regulates the expression of *slr0082-slr0083* operon in response to temperature stress

A version of this chapter has been submitted for publication

4.1 Introduction

Microorganisms are constantly exposed to different environmental challenges, both biotic and abiotic factors, diminishing cellular fitness (Owttrim, 2006). Fluctuating temperature is a constant stress encountered by free-living cells and deviation from the optimum growth temperature results in a complex cascade of molecular response (Owttrim, 2013). Downshifts in temperature affect the organism's physiology at different levels including alteration of membrane fluidity and stabilization of secondary structures in DNA and RNA, necessitating adjustments in transcription and/or translation to reroute metabolic processes allowing acclimation to the environmental change (Graumann and Marahiel, 1996).

In bacteria, expression of a variety of operons is associated with cellular response to environmental stimuli including temperature downshift (Regnier and Portier, 1986, Cairrão *et al*., 2003, O'Connell and Thomashow, 2000). Expression of individual genes within operons is frequently not coordinated, resulting in differential transcript accumulation of operon members. Differential expression involves a complex combination of post-transcriptional mechanisms including alteration of RNA degradosome components and modification of the translational apparatus. Temperature-dependent transcript half-life stabilization is a major contributor to the preferential expression of cold shock transcripts. Interaction of protein factors with the unusually long 5' untranslated region (UTR) present in cold-shock mRNAs contributes to the preferential enhanced stabilization and thus translation of cold shock transcripts (Gualerzi *et al.*, 2003). Polycistronic transcripts processing involves an initial site-specific endonucleolytic cleavage generating monocistronic transcripts which subsequently undergo maturation by either 3'-5' (Mohanty and Kushner, 2010) or 5'-3' exonuclease trimming (Even *et al*., 2005). This processing contributes to variations in transcript stability, leading to differential expression of operon members (Arraiano *et al*., 2010, Pedersen *et al*., 2011).

A major impact of growth at reduced temperature involves thermodynamic stabilization of RNA secondary structure that inhibits RNA reorganization and thus function. RNA stabilization is reported to be relieved by a variety of RNA binding proteins which function as RNA chaperones. (Jarmoskaite and Russell, 2011). Expression of chaperone encoding genes is frequently temperature regulated in prokaryotes, including proteins belonging to the Csp gene family in *E. coli* (Jones and Inouye, 1994) and *Bacillus* species (Graumann *et al*., 1997) and RNA helicases in numerous bacteria (Owttrim, 2013, Iost *et al*., 2013). RNA helicases rearrange RNA secondary structure via duplex unwinding and/or annealing (Chamot *et al*., 2005) and therefore are potentially involved with all aspects of RNA metabolism (Cordin *et al*., 2006). The ability to relive temperature-stabilized RNA secondary structure is frequently ascribed to require RNA helicase activity that actively rearranges structured RNA at the expense of ATP hydrolysis (Linder, 2006).

Cyanobacteria are a ubiquitous group of Gram-negative photosynthetic bacteria that enhance expression of typical cold stress genes (Sakamoto and Bryant, 1997; Sato, 1994). In cyanobacteria, DEAD-box RNA helicases are one of most highly induced genes in response to temperature downshift including *crhC* in *Anabaena* sp. PCC 7120 and *crhR* (*slr0083*) in *Synechocystis* sp. PCC 6803 (Chamot *et al*., 1999; Yu and Owttrim, 1999; Kujat and Owttrim, 2000; Chamot and Owttrim, 2000; Rosana *et al*., 2012a). Expression of *crhR* is controlled by the light-driven redox status of the electron transport chain, a level that is enhanced by environmental stresses that reduce the chain (Vinnemeier and Hagemann, 1998; Kujat and Owttrim, 2000; Mikami *et al*., 2002; Rosana *et al*., 2012b). In response to a downshift in temperature from 30 to 20^{o}C, *crhR* transcript and protein accumulation is enhanced 8-10 fold (Rosana *et al*., 2012b). Previous reports indicated that a monocistronic *crhR* transcript is generated from its own promoter (Vinnemeier and Hagemann, 1999; Kujat and Owttrim, 2000), although recent deep sequencing analysis (Hess and Owttrim, unpublished data, Mistchke *et al*., 2011) and gene specific riboprobing suggests that *crhR* is also

possibly co-transcribed as a dicistronic message from a promoter upstream of the adjacent gene, *slr0082* (Rosana *et al.*, 2012b).

We have recently investigated the temperature-regulated expression of *slr0083* showing that CrhR autoregulates its own expression involving a complex network of interactions at both the transcriptional and post-transcriptional levels involving temperature induced alteration of transcript and protein stability (Rosana *et al.*, 2012b). Here, we extend our analysis to the upstream gene, *slr0082* that encodes a hypothetical protein having significant identity with the related proteins, RimO, a ribosomal protein S12 methylthiotransferase (Anton *et al.*, 2008) and MiaB, a tRNA methylthiolase (Hernandez *et al*., 2007). Transcript analysis confirmed that both genes are transcribed as a dicistronic message that is processed into four transcripts, each of which exhibits differential RNA stability. The differential accumulation and stabilization of multiple transcripts from the operon suggest a complex interplay of operon processing, transcript maturation and RNA degradation that are dependent on a functional CrhR RNA helicase. The mechanisms by which expression of the *slr0082-slr0083* operon is self-regulated in response to cold stress and the implication of processing operons mediated by CrhR is discussed.

4.2 Materials and Methods

4.2.1 Strains and Growth Conditions

Synechocystis sp. strain PCC 6803 was maintained on BG-11 agar supplemented with 10 mM Tricine pH 8.0 and 0.3 % sodium thiosulfate (Rosana *et al.*, 2012a). Two *crhR* mutant strains, a partial deletion *crhR* mutant (2-76) created by insertion of spectinomycin cassette (*crhR*::spec) (Rosana *et al.*, 2012a) and a *crhR* complete deletion mutant (*crhR*::kan) (Tarassova and Owttrim, unpublished) were grown as describe above. The previously reported Δ*crhR* strain 2-76 was redesignated/renamed as Δ*crhR*^{TR} to differentiate it from the complete deletion mutant, Δ*crhR*. Corresponding antibiotics were included as required,

spectinomycin-streptomycin (50 µg/ml of each) for Δ*crhR*^{TR} and kanamycin (50 µg/ml) for complete deletion mutant. Liquid cultures were grown at 30^{o}C with continuous shaking (150 rpm) and bubbling with humidified air at an illumination of 50 µmol photons m^{-2} s^{-1} (Chamot and Owttrim, 2000). Cold stress was induced in mid-log phase cells at 20^{o}C for the indicated times. RNA was extracted from cells treated with an equal volume of 5% phenol-alcohol at the stated growth temperature (Rosana *et al*., 2012b). For temperature gradient and transcript half-life analyses, liquid cultures grown at 30^{o}C were subjected to the indicated condition and aliquots harvested at the designated times for RNA and protein isolation. Representative data is shown from a minimum of two biological replicates.

4.2.2 RNA Manipulation

Total RNA was extracted from *Synechocystis* cells as defined previously using glass bead lysis and extensive phenol-chloroform extraction (Rosana *et al.*, 2012b). Total RNA was resolved in either formaldehyde 1.2% agarose gels for *slr0082* transcript analysis or urea-8% polyacrylamide gels for detecting the *slr0082* 5'UTR. Resolved RNA was either capillary blotted from agarose gels or electro-transferred from polyacrylamide gels to nylon membranes (Amersham) using semi-dry transfer (Tyler). Transferred RNA was UV-crosslinked to the membrane using the autocrosslink mode (StrataLink UV 4000). Northern analysis was performed as previously described (Chamot *et al.*, 1999; Owttrim, 2012) using a ^{32}P-labelled riboprobe corresponding to a 220 nt fragment (*Synechocystis* genomic position: 2886403-2886603) internal to the *slr0082* ORF or a 110 nt segment (2886040-2886129) for the detection of the *slr0082* 5'UTR transcript (Fig. 4.1A). Oligonucleotides used to create the riboprobes are indicated in Table 4.1. Transcript half-life was determined in the presence of 400 µg/ml rifampicin to inhibit *de novo* mRNA synthesis. The constitutively expressed transcript, *rnpB*, was utilized as a control for RNA loading. Transcript size was estimated using either the high range or low range RiboRuler^{TM} RNA ladders (Thermo Scientific). Hybridized membranes were exposed to X-ray film and quantitation of transcript

level was performed using Image J software ver. 1.45 S (NIH, USA) (Schneider *et al.*, 2012; Rosana *et al.*, 2012b).

4.2.3 Protein Manipulation

Soluble protein was extracted from *Synechocystis* cells by vortexing in the presence of glass beads as described previously (Rosana *et al.,* 2012b, Owttrim, 2012). Aliquots of this soluble fraction (25 µg) were separated on a 10% SDS-PAG. Immunoblotting analysis was performed using the indicated anti-sera and secondary antibody (anti-rabbit IgG at 1:20000 dilution, Sigma) combinations detected by chemiluminescence (Amersham). Polyclonal antibodies against the *Synechocystis* CrhR or the *E. coli* Rps1 were utilized simultaneously at 1:5000 dilution for the parallel detection of both polypeptides. Protein loading was normalized using Bradford reagent (BioRad) and detection of ribosomal protein Rps1 (Rosana *et al.,* 2012b).

4.2.4 5'RACE-RCA, Inverse PCR and DNA Sequencing

The 5' ends of the transcripts were determined using 5'RACE-RCA analysis as described by Polidoros *et al.,* 2006. Extracted total RNA was treated with RNase-free DNase I (0.2 U per 1 µg RNA) (Invitrogen) for 15 min at 37^{o}C. Treated RNA was purified by extensive phenol-chloroform extraction, LiCl (2 M) precipitation and finally ethanol precipitation and dissolved in RNase-free water (Invitrogen). RNA was tested for DNA contamination using PCR by amplifying the universal bacterial *16s rDNA* gene (primer 27F and 1492R) and the *Synechocystis rnpB* gene (primer *rnpB*f and *rnpB*r) (Table 4.1). *crhR* gene specific cDNA synthesis was directed using a 5' phosphorylated primer ARRR1 (Table 1) targeting transcripts with *crhR* containing mRNA sequences starting 3 bp upstream of the internal *Pml*I site, the site used to generate the Δ*crhR*^{TR} (Fig. 4.1A). First strand cDNA synthesis was performed in a final volume of 20 µl containing 1.0 µg DNA-free RNA ; 0.025 µg/µl phosphorylated ARRR1 primer; 0.5 mM dNTP (Fermentas); 40 U RNase-OUT (Ambion) and 200 U M-MLV reverse transcriptase (Superscript III, Invitrogen). Reverse transcription was

performed in a Techgene Thermal Cycler (Life Sciences) using the following conditions: 37^{o}C for 60 min, 42^{o}C for 60 min, 70^{o}C for 15 min. First strand cDNA was treated with 2 U RNase H (Invitrogen) for 15 min at 37^{o}C and purified on a QiaQuick PCR purification column (Qiagen).

Purified 5' phosphorylated first strand cDNA products were circle ligated using CircLigase I (Epicentre). Ligation reactions contained 25 µl purified cDNA, 1X CircLigase buffer, 0.05 mM ATP and 150 U CirCLigase I. The reaction mixture was incubated at 60^{o}C for 1 h, heat inactivated at 80^{o}C for 10 min and the final volume adjusted to 36.5 µl. Ligated cDNA was amplified using rolling circle amplification (RCA). The reaction mixture consisted of 36.5 µl cDNA, 11 µM modified random heptaprimer (phosphothioate blocked 3'n-1, n-2) (IDT DNA Technologies), 1.2 mM dNTP and 10 U Φ29 DNA polymerase (New England Biolabs) and incubated in a Techgene Thermal Cycler (Life Sciences) for 20 h at 30^{o}C.

Inverse PCR was performed on RCA products using primers GWO39 and LPF46 (Table 4.1) to amplify cDNA sequencing containing *crhR* sequences. Amplified products were gel purified (QiaQuick gel purification kit, Qiagen) according to manufacturer's instructions. Gel-purified PCR products were sequenced using primer GWO39 and BigDye Terminator v3.1 cycle sequencing kit (Applied Biosystems).

4.2.5 His-CrhR Expressing Strains

The 2.1 kbp *Xba* I-*Eco* RI restriction fragment from pRSETA-*crhR* , containing the His-CrhR sequence (Chamot *et al*., 2005), was cloned into pMon 36546 under the control of the *nirA* promoter (Qi *et al.*, 2005, Monsanto USA,). Both Δ*crhR* strains and wild type cells were transformed with the plasmid as described previously (Zang *et al*., 2007, Owttrim, 2012). Transformants were selected with increasing gentamycin to a final concentration of 10 µg/mL. Cellular growth rates and cold sensitivity were analyzed by establishing growth curves over 7 days at normal (30^{o}C) and cold stress (20^{o}C) temperatures. An aliquot was removed at the indicated time for northern and western analyses.

Photosynthetic pigment composition (chl *a* and phycocyanin) were determined spectrophotometrically on 2 h cold stressed cultures as described previously (Rosana *et al.*, 2012a).

Table 4.1 Bacterial strains, plasmids and oligonucleotides utilized in this study

Strains, plasmid or oligonucleotide	Relevant characteristic (s) or sequence*	Source, reference or application
***Synechocystis* strains**		
Wild type	glucose-tolerant strain	Kujat and Owttrim, 2000
Δ*crhR*^{TR}	*crhR*:: spectinomycin cassette	Rosana *et al*., 2012
Δ*crhR* CD	replacement of the complete *crhR* ORF with a kanamycin resistant cassette	This study
***E. coli* strains**		
DH5α	F-Φ80lacZΔM15 Δ(lacZYA-argF) U169recA1 endA1 hsdR17 (rK-, mK+) phoA supE44 λ-thi-1 gyrA96 relA1	Laboratory collection
Plasmids		
pMon 36546	*E. coli – Synechocystis* hybrid cloning vector, Gen^{R}	Qi *et al.*, 2005 Monsanto, USA
pRSET-CrhR	*Synechocystis* 6-his-*crhR* fragment in pRSET	Chamot *et al*., 2005
pMon-His-CrhR	*Synechocystis* 6-his-*crhR* fragment in pMon	This study
Oligonucleotide		
rnpBf	**TAA TAC GAC TCA CTA TAG GG**G GGC AGG AAA AAG ACC AAC C	*rnpB* RNA probe
rnpBr	TAA CTG ACC ACT GAA AAG G	*rnpB* RNA probe
DCsr21f	**TAA TAC GAC TCA CTA TAG GG**T GTA GGG TAG GGA CTA AAC	5’ UTR RNA probe
DCsr21r	CAA ATA AAA AGG GTC TGA CC	5’ UTR RNA probe
DCsr20f	**TAA TAC GAC TCA CTA TAG GG**G TGG TGC GAT AAC GTG G	*slr0082* RNA probe
DCsr20r	CGT TAT TTC CGG TTG CC	*slr0082* RNA probe
ARRR1	ATA AAG CTG CTG CTC AAT GCG	5’ RACE-RCA
GWO39	TGA CGA TGT GAA AAC C	Inverse PCR, Sequencing
LPF46	CAG TTT GAA TTT GGG TGG GA	Inverse PCR, Sequencing
27F	GAG TTT GMT CCT GGC TCA G	Stubner, 2002
1492R	ACG GYT ACC TTG TTA CGA CTT	Stubner, 2002

*T7 RNA polymerase promoter sequence in bold letters

4.3 Results

4.3.1 The *slr0082-slr0083* operon in *Synechocystis* sp. PCC 6803

The gene *slr0083* in *Synechocystis* sp. PCC 6803 encodes the DEAD-box RNA helicase, *crhR*, whose expression is regulated by the redox status of the electron transport chain (Kujat and Owttrim, 2000). Two *crhR* deletion mutants were analyzed by disruption of the *slr0083* open reading frame. The genomic organization of wild type, the partial deletion mutant, Δ*crhR*^{TR} (Rosana *et al.*, 2012a) and a complete deletion mutant, Δ*crhR* (Tarassova and Owttrim, unpublished) is shown in **Fig. 4.1A.** Upstream of *slr0083* is a hypothetical gene, *slr0082*, whose putative protein product has 46% identity with the related proteins, RimO, a ribosomal protein S12 methylthiotransferase and MiaB, a tRNA methylthiolase. The effect of temperature shift on CrhR protein accumulation in the three strains is shown in **Fig. 4.1B**. The 55 kDa wild type CrhR polypeptide accumulated in response to a temperature downshift from 30 to 20oC while the 27 kDa truncated form of the polypeptide accumulated to maximal levels irrespective of temperature shift, confirming previous results (Rosana *et al*., 2012b). CrhR protein was not detected at either temperature in the Δ*crhR* mutant, indicating complete segregation of the Δ*crhR* strain (**Fig. 4.1B**). Segregation in the Δ*crhR* mutant was also confirmed by PCR amplification (data not shown).

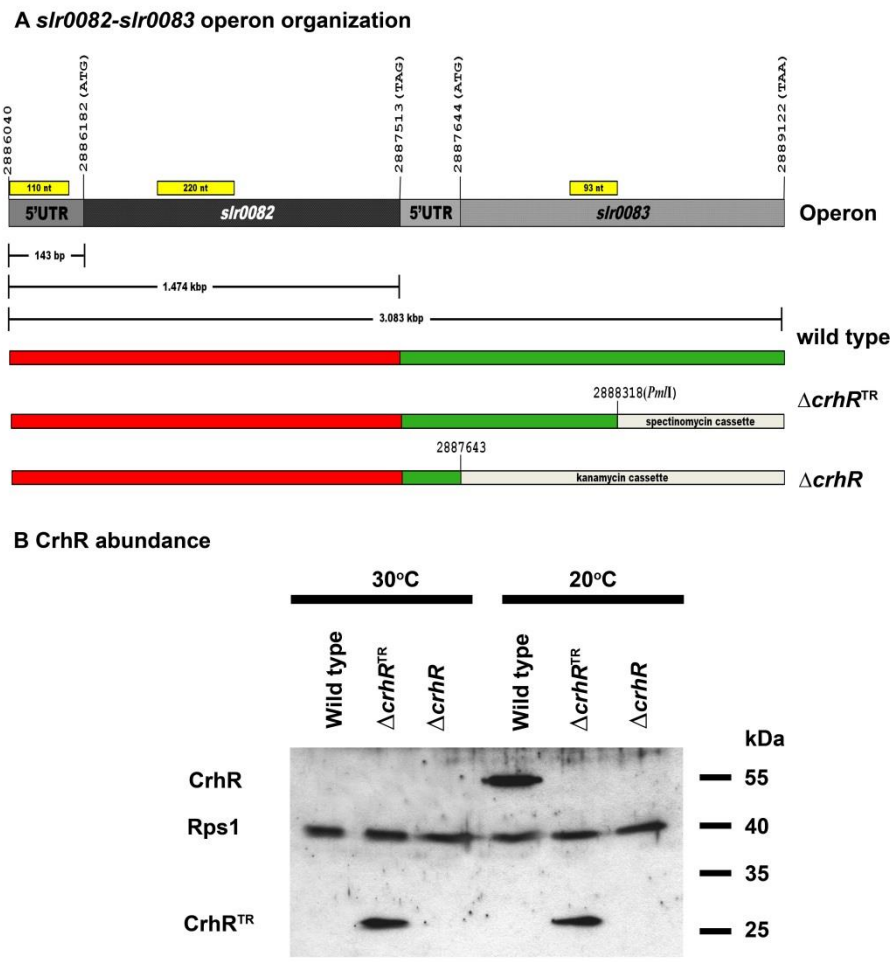

Figure 4.1 Genomic organization of the *slr00082-slr0083* operon in *Synechocystis* sp. PCC 6803 and CrhR protein accumulation in wild type and *crhR* mutant strains**.**

(A) Genomic organization of *slr0082* and *slr0083* together with their respective 5' untranslated regions (UTR) in wild type, Δ*crhR*^{TR}, a partial deletion mutant (Rosana *et al*., 2012a) which expresses a truncated *crhR* transcript and a 27 kDa polypeptide (Rosana et al, 2012b) and a Δ*crhR* mutant in which the complete *crhR* ORF is deleted from the start to stop codons (Tarassova and Owttrim, unpublished). The numbering refers to nucleotide (nt) position in the genome (Nakao *et al.*, 2010). The relative positions of the riboprobes used for transcript analysis are indicated on top of the operon. The predicted transcript lengths

corresponding to the 5' UTR, *slr0082* alone and the entire operon are indicated. The diagram is not to scale.

(B) CrhR polypeptide accumulation in wild type and *crhR* mutant strains. Western analysis of soluble protein (25 µg) from wild type and the two *crhR* mutants grown at 30^{o}C and cold stressed at 20^{o}C for 1 h, simultaneously immunodecorated with anti-CrhR and anti-Rps1 antibodies and detected using enhanced chemiluminesence. A 55 kDa native CrhR protein was overexpressed in wild type cells at 20^{o}C while a 27 kDa truncated CrhR polypeptide is produced in Δ*crhR*^{TR} cells at all temperatures. CrhR protein was not detected in the complete deletion Δ*crhR* strain. The 40 kDa ribosomal protein Rps1 serves as protein loading control.

4.3.2 CrhR inactivation results in deregulated expression of the *slr0082- slr0083* operon

Wild type and the two *crhR* inactivants were compared to assess for the involvement of CrhR in the regulation of *slr0082* transcript accumulation (**Fig. 4.1A**). Our previous study of *slr0083* expression suggested that *slr0082* and *slr0083* are transcribed as a dicistronic operon and
is potentially regulated by the downstream gene *slr0083* which codes for the DEAD-box RNA helicase, CrhR (Rosana *et al.*, 2012b). Complete and partial deletion of the *crhR* gene affected the basal level of *slr0082* transcript accumulation at 30^{o}C, causing a 3-5 fold increase in levels compared to those observed in wild type cells (**Fig. 4.2**). Interestingly, the magnitude of cold stress induction is not affected by *crhR* mutation, cold further enhancing accumulation of the *slr0082* transcript to the same degree, 3-4 fold, in wild type and both *crhR* mutants. The absence of a functional helicase thus resulted in a total increase in mRNA levels of 13- and 20-fold in Δ*crhR*^{TR} and Δ*crhR*, respectively (**Fig. 4.2**). A prominent stable 500 nt transcript was detected in both mutant strains, a transcript size which does not correspond to an expected size for the operon or either gene alone. At 20^{o}C, prominent 2.3 (Δ*crhR*^{TR}) and 1.5 knt (Δ*crhR*) transcripts were detected that correspond to products transcribed from the entire operon (**Fig. 4.1A**). All strains analyzed revealed a smear of transcript of varying degrees detected by the *slr0082* ORF probe (**Fig. 4.1A**) suggesting that the dicistronic transcript is rapidly processed and/or degraded. The differential mRNA accumulation observed in response to cold stress can be ascribed to either an alteration in the rate of transcription or mRNA degradation or a combination of both processes.

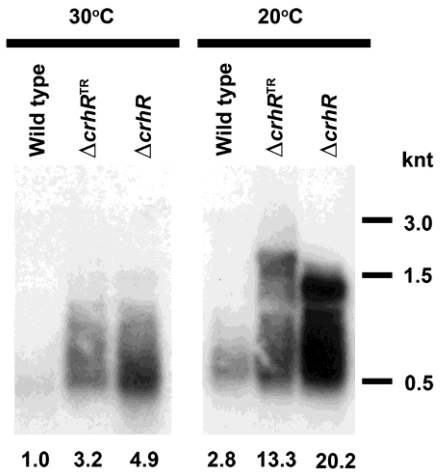

Figure 4.2 *slr0082* transcript accumulation.

Temperature dependence on *slr0082* transcript accumulation was determined by Northern analysis of total RNA (5 µg) probed with a 220 nt internal fragment of the *slr0082* open reading frame (ORF). *Synechocystis* cells (wild type, Δ*crhR*^{TR} and Δ*crhR*) were grown to mid-log phase at 30°C and cold stressed by transferring to 20°C for 20 min. Transcript levels were quantified using Image J software Version 1.45S (NIH, USA) (Schneider *et al.*, 2012) and *slr0082* accumulation, relative to that observed in illuminated wild type cells at 30°C, is indicated below each lane.

4.3.3 Transient accumulation of *slr0082* mRNA in response to cold stress is CrhR-dependent

Accumulation of the *slr0083 crhR* transcript is transient in response to cold stress, returning to basal levels after ~3 h (Rosana *et al.*, 2012b). Accumulation of the upstream *slr0082* mRNA followed a similar transitory pattern however the rate of accumulation and return to basal levels were significantly accelerated (**Fig. 4.3A**). Wild type s*lr0082* transcript accumulation is transient, reaching a maximum level after 20 min of cold stress at 20^{o}C and decreasing rapidly thereafter (**Fig. 4.3A, 4.3C**). The initial accumulation rate is similar to that observed in the Δ*crhR*^{TR} mutant for the first 20 min (**Fig. 4.3B**), suggesting that the initial cold sensing response for this operon is not affected by *crhR* inactivation. In contrast, the subsequent repression of *slr0082* accumulation is dependent on functional CrhR, as in the absence of functional CrhR, transient accumulation of *slr0082* mRNA was not observed in response to cold stress (**Fig. 4.3B**). At 20^{o}C, the enhanced *slr0082* transcript level remained elevated and constant up to 24 h (data not shown).

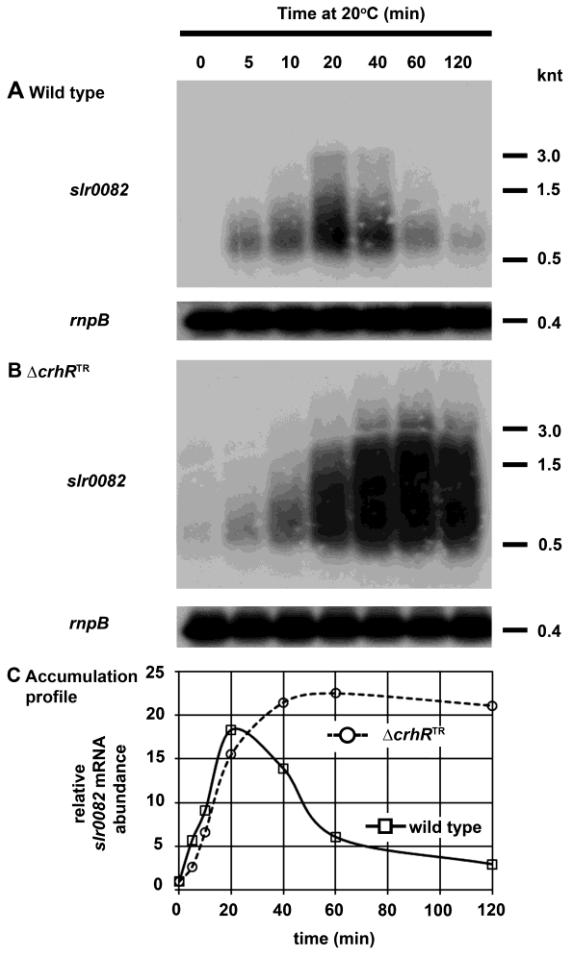

Figure 4.3 Time course of *slr0082* transcript accumulation.

A time course of crhR transcript accumulation at 20°C was performed on wild type (A) and Δ*crhR*^{TR} (B) *Synechocystis* strains were grown to mid-log phase at 30°C at which time the cultures were transferred to 20°C for the indicated times before harvesting. *slr0082* transcript was detected in total RNA as described in Fig. 2. The blots were stripped and probed with the *Synechocystis rnpB* gene as a control for RNA loading.

C) Quantification of *slr0082* transcript levels. Transcript levels were quantified as described in Fig. 2 and expressed as accumulation relative to *slr0082* abundance observed in illuminated wild type cells grown at 30^{o}C (i.e. 0 time point, set to 1.0).

4.3.4 *slr0082* transcript half-life is not affected by temperature downshift or crhR mutation

The difference in transcript accumulation between wild type and Δ*crhR*^{TR} suggest that CrhR is potentially involved in the degradation of *slr0082* mRNA. We therefore determined if *crhR* mutation affected *slr0082* transcript half-life. In wild type cells, the *slr0082* transcript half-life is temperature regulated to a slight degree, with half-lives of 2.5 and 6.0 min observed at 30^{o}C and 20^{o}C, respectively (**Fig. 4.4A**). A similar pattern was observed in Δ*crhR*^{TR} cells, there is only a marginal alteration in *slr0082* transcript half-life at both warm and cold temperatures, 5.0 and 7.5 min at 30^{o}C and 20^{o}C, respectively (**Fig. 4.4B**). Although the Δ*crhR*^{TR} has a ~3 fold higher *slr0082* transcript level (**Fig. 4.4B**), the rate of degradation is comparable irrespective of temperature. These results imply that the turnover of *slr0082* mRNA is neither dependent on the low temperature stabilization of transcript nor a direct CrhR-dependent RNA degradation pathway.

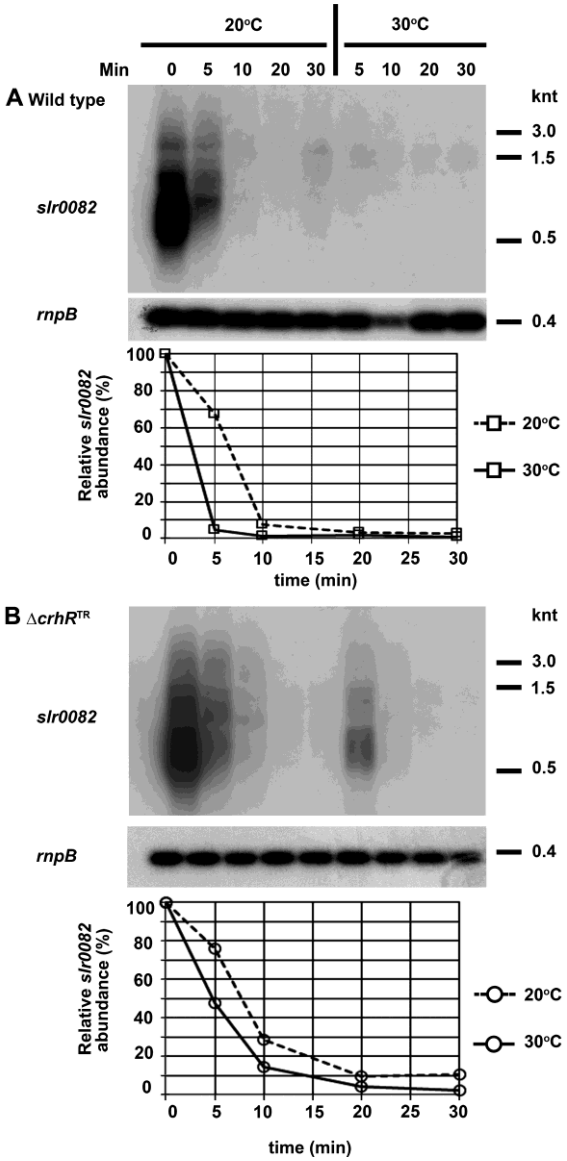

Figure 4.4. *slr0082* transcript half-life.

slr0082 transcript half-life was measured in wild type (A) and Δ*crhR*^{TR} (B) *Synechocystis* strains grown at 30°C to mid-log phase (0 min) at which time the cultures were transferred at 20°C for 20 min to induce maximal *slr0082* transcript accumulation. *de novo* RNA synthesis was subsequently inhibited by the addition of rifampicin (400 µg/ml) and half of each culture transferred back to 30°C. Aliquots for RNA extraction were harvested at the indicated times. *slr0082* and *rnpB* transcripts were detected and quantified as indicated in Fig 3. Relative *slr0082* transcript levels are indicated, normalized with respect to the level observed at time zero set to 100%.

4.3.5 His-CrhR expressing strains resulted in transient accumulation of *slr0082* mRNA in response to cold stress

The role of CrhR in the transitory accumulation of the dicistronic operon upon cold stress was further explored by complementing the two *crhR* mutants. Complementation in *trans* of the two mutants restored the transient accumulation of *slr0082* mRNA under cold stress although at a slower rate than observed in wild type cells (**Fig. 4.5**). Accumulation of *slr0082* transcript returned to the basal level in wild type cells expressing His-CrhR with *slr0082* transcript ~5 fold lower after 4 h (**Fig. 4.5A**). In contrast, *slr0082* mRNA decreased to basal levels only after 8 h in the two *crhR* mutants (**Fig. 4.5B, 4.5C**). This could be explained by the fact that the His-CrhR is not expressed at the same level as in cold stressed wild type cells (**Fig. 4.1B**).

Wild type cells expressing His-CrhR exhibited a dramatic reduction in growth rate at 30^{o}C in contrast to both *crhR* mutant strains expressing the tagged CrhR (**Fig. 4.6A**). Upon transfer to 20^{o}C, both *crhR* mutant cells were partially rescued from cold sensitivity (**Fig. 4.6B)**. His-CrhR expression in wild type and *crhR*^{TR} cells reduces the growth rate at both temperatures, indicating that expression of both forms of CrhR is detrimental to cell growth (**Fig. 4.6B**). At both temperatures, the complete deletion mutant expressing His-CrhR exhibited the most robust growth. These observations could be explained by either the over- or under-expression of CrhR in the His-CrhR strains. Accumulation of the recombinant 58 kDa His-CrhR from the constitutive pNIR promoter present in pMON 36546, was not constant in the three strains (**Fig. 4.6C**). His-CrhR abundance decreased when either the wild type or truncated forms of CrhR were expressed in the same cells (**Fig. 4.6C**). Additionally, the corresponding truncated 27kDa CrhR polypeptide also decreased in the Δ*crhR*^{TR} mutant at 30^{o}C.

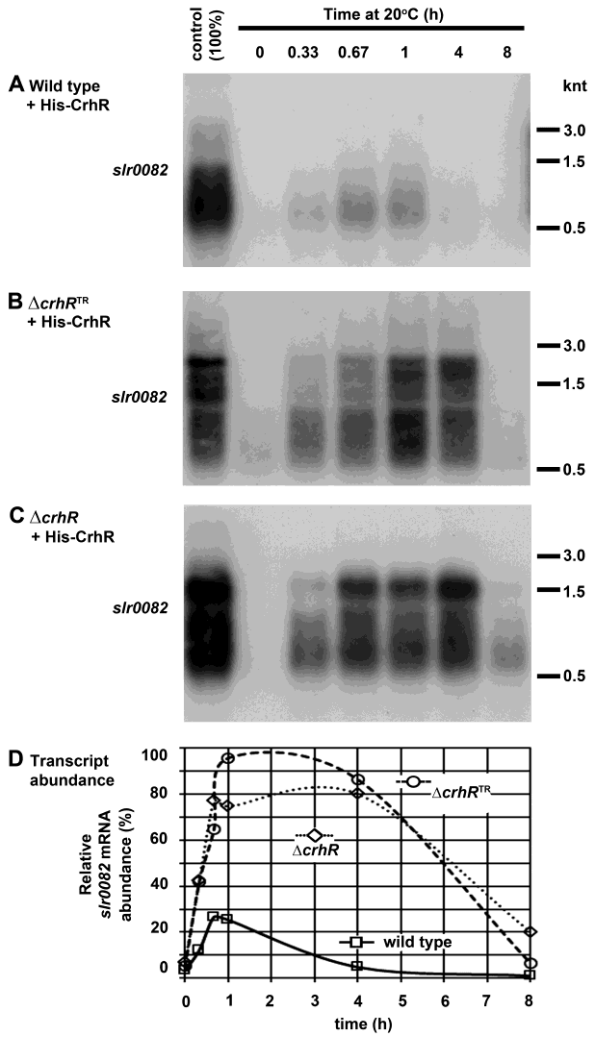

Figure 4.5 Time course of cold induced *slr0082* transcript accumulation in His-CrhR expressing strains.

The effect of wild type CrhR expression on temperature induction was assessed in wild type (A), Δ*crhR*^{TR} (B) and Δ*crhR* (C) *Synechocystis* cells transformed with pMon-His-CrhR grown at 30^{o}C to mid-log phase (0 min). Cultures were subsequent cold stressed at 20°C for the indicated times before harvesting. *slr0082* transcript was detected in total RNA as described in Fig. 2. (D) Quantification of *slr0082* transcript levels. Transcript levels were quantified as described in Fig. 2 and expressed as accumulation relative to *slr0082* abundance observed in illuminated wild type or *crhR* mutant strains not expressing His-CrhR cold stressed for 20 min (set to 100%).

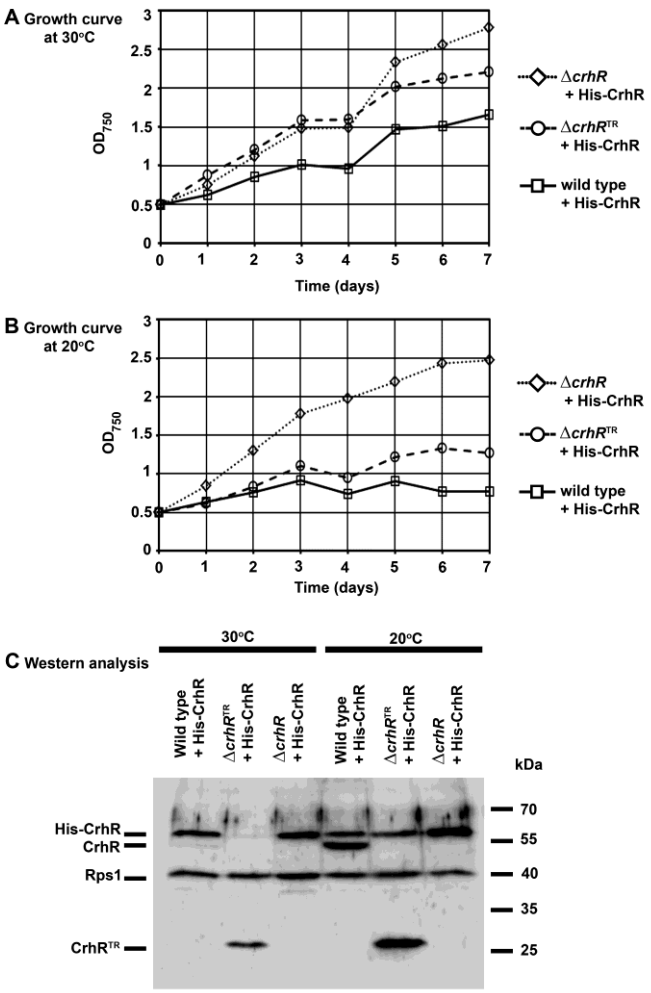

Figure 4.6 Effect of His-CrhR expression on growth and CrhR accumulation. Growth curve of His-CrhR expressing wild type, Δ*crhR*^{TR} and Δ*crhR* *Synechocystis* strains at (A) normal (30^{o}C) and (B) cold stress (20^{o}C) growth temperatures. Cell growth was estimated by measuring OD_{750nm}. (C) Western analysis. Total soluble protein (25 µg) from His-CrhR expressing cells was probed with antisera against CrhR detecting a constitutively expressed 58 kDa His-CrhR polypeptide in all strains in parallel with native CrhR (55kDa) or CrhR^{TR} (27 kDa). Simultaneous immunodecoration with an antibody against ribosomal protein Rps1 (40 kDa) was performed as a protein loading control.

3.6 Accumulation of an internal stable RNA from the open reading frame of *slr0082*

In contrast to the transient expression of the *slr0082* transcript, temperature gradient analysis of *slr0082* mRNA accumulation revealed a 500 nt stable RNA whose expression was observed at all temperatures (**Fig. 4.7**). Wild type cells accumulated constant levels of this RNA from 35^{o}C to 10^{o}C and with a concomitant detection of very minor longer transcripts (**Fig. 4.7A**). These larger transcripts were more abundant as the temperature decreased, potentially derived from slower processing of the dicistronic operon. The Δ*crhR*^{TR} cells accumulated a lower level of this internal RNA in contrast to the wild type cells, a level that also increased as the temperature decreased (**Fig. 4.7A**). Temperature downshifts resulted in enhanced accumulation of longer transcripts especially at 20 and 15^{o}C. While approximately equal transcript accumulated at 20 and 15^{o}C, the various transcripts accumulated to varying levels across the temperature gradient. At 20^{o}C, the 500 nt transcript exceeded the full length 2.3 knt transcript, a pattern that was reversed at 15^{o}C. This accumulation pattern is indicative of a temperature-induced alteration in either the transcription, processing and/or degradation of these transcripts in the absence of functional CrhR RNA helicase. When an individual cell culture was incubated at progressively decreasing temperatures from 35^{o}C to 10^{o}C for 1 h at each temperature, a differential accumulation of this stable RNA was observed (**Fig. 4.8**). In wild type cells, the 500 nt transcript decreases as temperate decreases with longer transcripts accumulating progressively as the temperature decreased (**Fig. 4.8A**). Comparably, the Δ*crhR*^{TR} cells revealed a reduced level of the 500 nt stable transcript and progressively accumulated longer transcripts as the temperature decreased (**Fig. 4.8B**). The results suggest that the Δ*crhR*^{TR} mutation dramatically affected cellular ability to process the transcripts produced from the entire operon, an effect that progressively increased as temperature decreased.

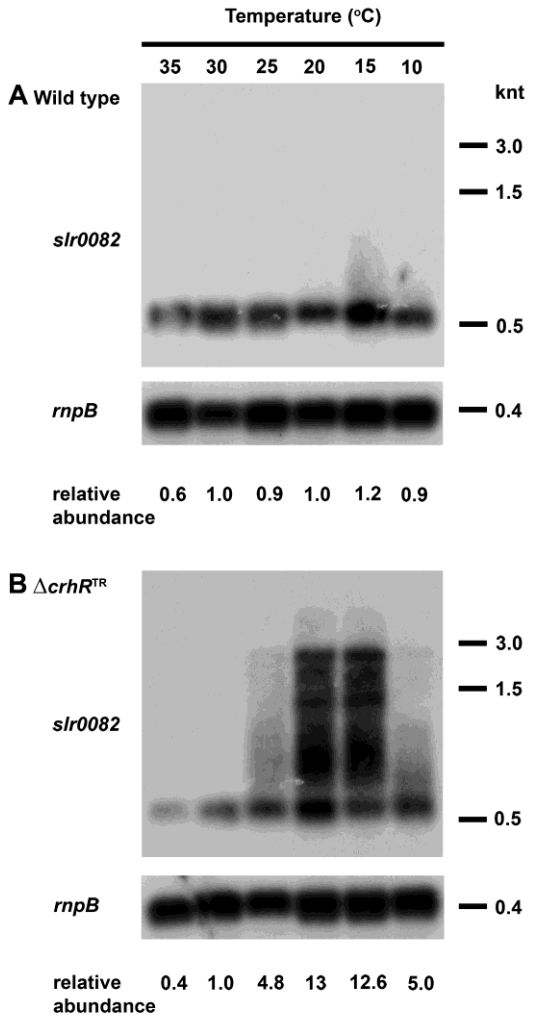

Figure 4.7 Temperature gradient of *slr0082* expression – individual culture. The effect of cold shock on *slr0082* accumulation was determined in (A) wild type and (B) Δ*crhR*^{TR} *Synechocystis* strains grown to mid-log phase at 30°C and subsequent incubation at the indicated temperature for 1 h. *crhR* transcript accumulation was determined by a northern blot analysis as described in Fig. 2. The blots were stripped and probed with the *Synechocystis rnpB* gene as a control for RNA loading. The relative level of *slr0082* abundance is provided below each lane with abundance normalized to *slr0082* levels detected from illuminated cells grown at 30°C (set to 1.0).

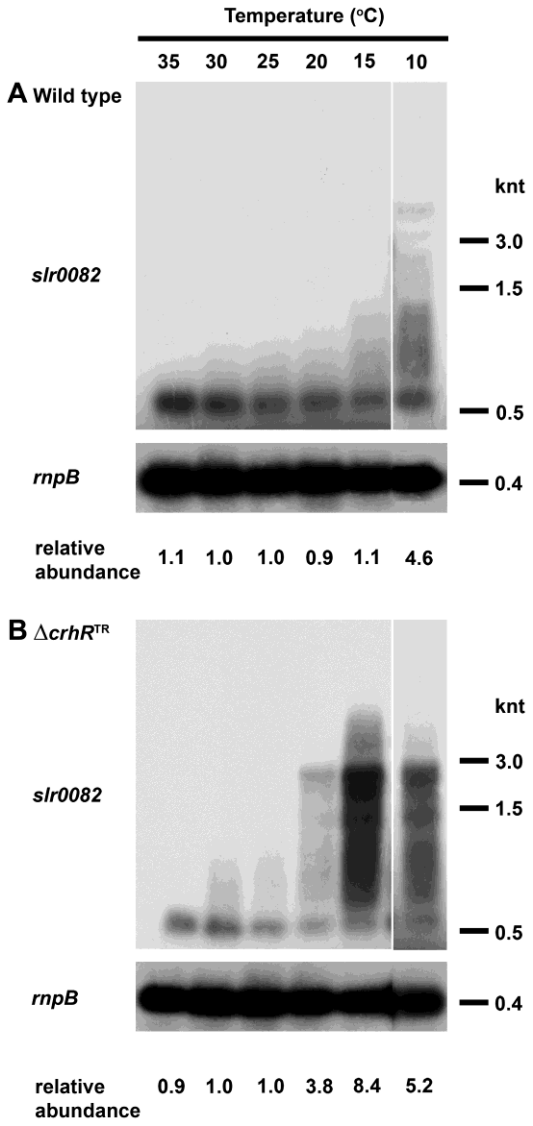

Figure 4.8 Temperature gradient of *slr0082* expression – single culture. The effect of exposure to progressively lower temperatures on *slr0082* accumulation was determined in wild type **(A)** and Δ*crhR*^{TR} **(B)** *Synechocystis* strains were grown to mid-log phase at 30°C. Cultures were exposed progressively from 35^{o}C to 10^{o}C for 1 h and aliquots taken at the indicated temperatures. *slr0082* transcript levels were quantified at each temperature as described in Fig. 2. The blots were stripped and probed with the *Synechocystis rnpB* gene as a control for RNA loading. The relative level of *slr0082* accumulation, with the abundance in illuminated, wild type cells grown at 30°C (set to 1.0) is provided below each lane.

4.3.7 5’ UTR of *slr0082* is constitutively accumulated at all temperatures.

Expression of the dicistronic operon was further analyzed by determining expression of the *slr0082* 5’ UTR that was previously mapped to contain 143 nt (Mitschke *et al*., 2011). Northern analysis using a 110 nt riboprobe from the 5’ UTR detected a 75 nt stable transcript that accumulates in wild type and mutant cells under all conditions tested (**Fig. 4.9**). Temperature gradient analysis of the 5’UTR accumulation revealed expression of this transcript increases in response to temperature downshift. Wild type cells showed efficient maturation of longer transcripts, predominately accumulating the 75 nt RNA, with minor levels of longer products progressively detected as temperature decreased (**Fig. 4.9A**). In the Δ*crhR*^{TR} mutant, a similar pattern was observed for the 75 nt transcript, however two additional, prominent stable transcripts of 120 nt and 400 nt progressively accumulated in response to temperature downshift (**Fig. 4.9B**). The results suggest that the *slr0082-crhR* dicistronic transcript is post-transcriptionally processed however the intermediate products are both not processed nor degraded as efficiently in the absence of CrhR activity.

The turnover of the stable 75 nt RNA originating from the *slr0082* 5’ UTR is more efficient in the wild type as these transcripts accumulated to a lower extent in response to growth at 20^{o}C, suggesting that processing and degradation efficiency is not affected by prolonged cold stress (**Fig. 4.10A**). Although maturation is not affected by prolonged cold stress in wild type cells, it is apparent that the abundance of all detected transcripts decreases through time. Conversely, in the Δ*crhR*^{TR} mutant cells, abundance of the 75 nt transcript increased in the first 2 h but remained steady thereafter (**Fig. 4.10B**). In parallel with this observation, is the prominent accumulation of stable 120 and 400 nt transcripts (**Fig. 4.10B**).

4.3.8 5’ RACE-RCA Analysis

In order to initiate analysis of the operon processing mechanism, 5’ RACE was utilized to identify the 5’ ends of the detected stable transcripts that accumulate in the Δ*crhR*^{TR} mutant at 20^{o}C. An analysis of *crhR* transcript expression at 20^{o}C in the Δ*crhR*^{TR} strain revealed four major accumulating transcripts (Rosana *et al.*, 2012b) detected by the 93 bp *crhR* probe (**Fig. 4.1A**). The inactivation strategy resulted in a 750 nt truncated *crhR* mRNA but northern analysis revealed three larger transcripts which the results presented above suggest originate from cotranscription with the upstream *slr0082* gene as a dicistronic message. Using 5’ RACE-RCA and inverse PCR-sequencing, the 5’ ends of the transcripts were mapped for the longest and shortest transcripts. The 2.3 knt fragment is the full length *slr0082-slr0083* operon mRNA starting at nt 28886039. Similarly, the shortest 0.75 knt mRNA was mapped to the 3’ end of *slr0082* ORF at position –137 upstream of the *slr0083* ATG. Extensive attempts to map the 5’ ends of the 1.5 and 1.3 knt transcripts were not successful, potentially a result of the multiple, single nucleotide differences between the fragment.

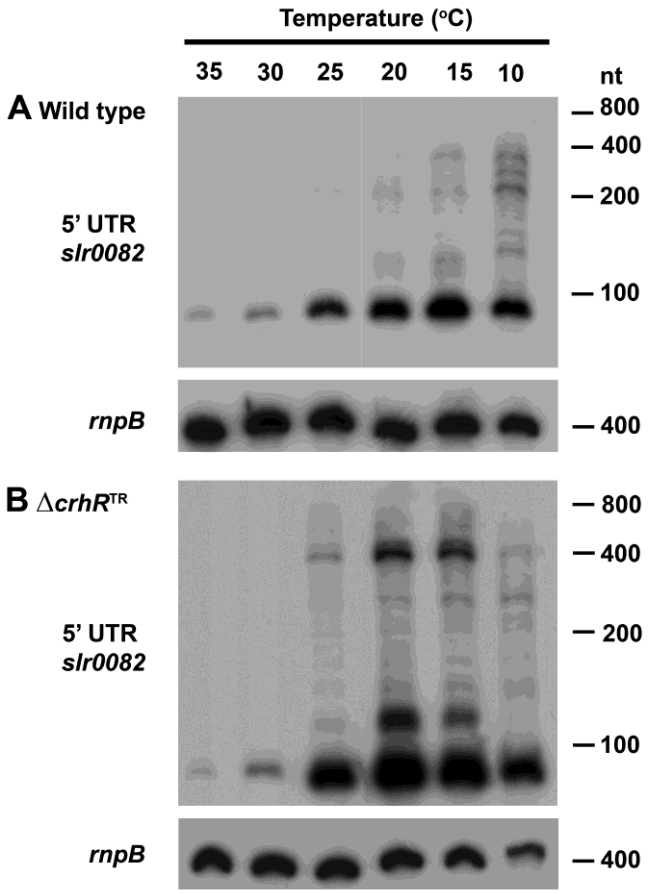

Figure 4.9 Temperature gradient accumulation of the *slr0082* 5' UTR.
Wild type **(A)** and Δ*crhR*^{TR} **(B)** *Synechocystis* strains were grown to mid-log phase at 30°C and divided into 6 aliquots, each of which was incubated at the indicated temperature for 1 h. Total RNA (5 µg) was separated on a 8M urea-8% polyacrylamide gel and probed with a 110 nt riboprobe to detect the 5' UTR. The blots were stripped and probed with the *Synechocystis rnpB* gene as a control for RNA loading.

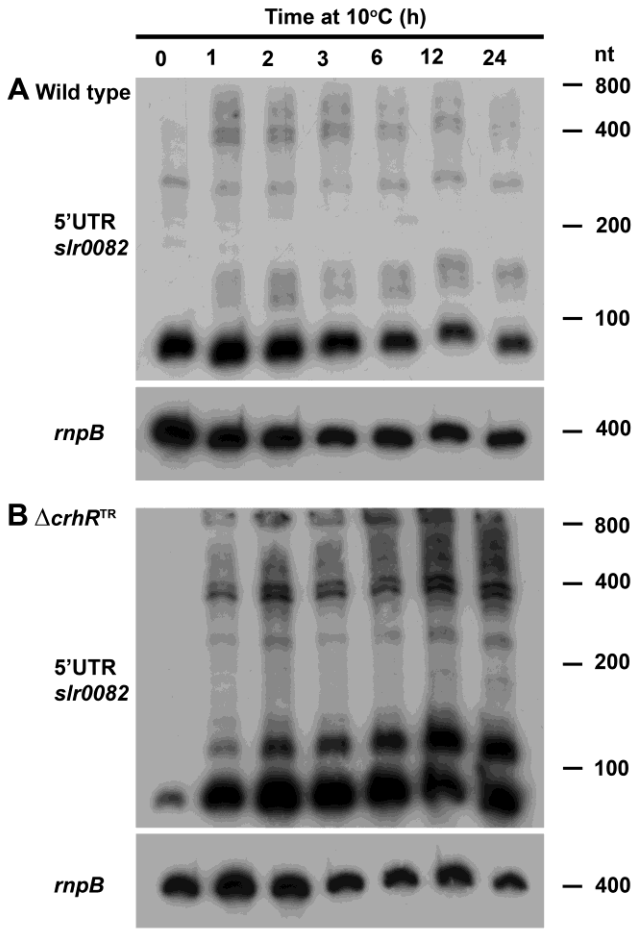

Figure 4.10 Time course of *slr0082* 5'UTR accumulation at 10°C.
Accumulation of the 75 nt transcript originating from the 5' UTR was analyzed in wild type **(A)** and Δ*crhR*^{TR} **(B)** *Synechocystis* strains grown to mid-log phase at 30°C and transferred to 10°C for the indicated times. Total RNA (5 µg) was separated on a 8M urea 8% polyacrylamide gel and probed with a 110 nt riboprobe corresponding the 5' UTR. The blots were stripped and probed with the *Synechocystis rnpB* gene as a control for RNA loading.

4.4 Discussion

Cold stress in cyanobacteria evoke the induction of a number of genes whose protein products are assumed to be important for the acclimation to the fluctuating environmental condition (Shivaji, 2013). Cold induction of *slr0082* transcript accumulation was investigated in reference to inactivation of the downstream gene *slr0083* coding for the DEAD-box RNA helicase, CrhR (Kujat and Owttrim, 2000). Experimental evidence revealed that the two genes are transcribed as a dicistronic message whose accumulation is both enhanced in response to temperature downshifts and *crhR* mutation. Analysis of *slr0082* transcript accumulation revealed complex interplay of several effectors involving regulation of mRNA transcription, processing and maturation and/or degradation which are dependent on CrhR RNA helicase activity, indicating CrhR self-regulation of operon expression.

A summary of these findings is presented in **Figure 4.11.** The differential co-expression of a putative methylthiotransferase and an RNA helicase in response to cold stress in cyanobacteria indicates the importance of these proteins in orchestrating gene expression during low-temperature adaptation. Gene expression analysis implies an intricate network involving the CrhR RNA helicase in regulating its own operon expression in response to cold stress

The data presented here, combined with deep sequencing analysis (Mitschke *et al*., 2011), suggests that *slr0082 - slr0083* form an operon expressed from a strong promoter upstream of *slr0082.* Although expression of the entire *slr0082 - slr0083* dicistronic operon is enhanced by temperature downshift, the accumulation kinetics differs significantly between the two genes. Although both genes are transiently induced at 20^{o}C (Vinnemeier and Hagemann 1999; Rosana

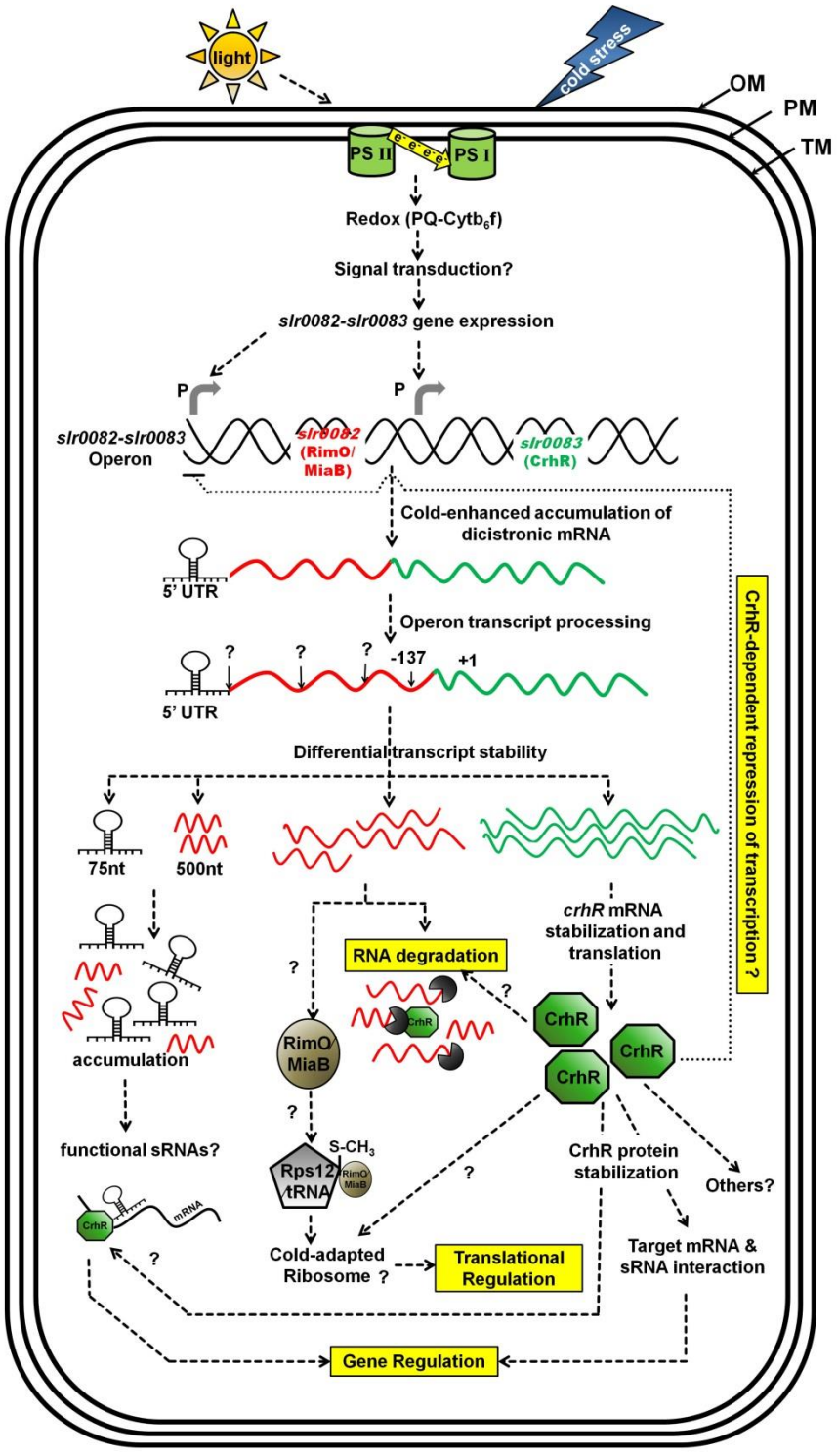
light
cold stress
OM
PM
TM
PS II
PS I
Redox (PQ-Cytb6f)
Signal transduction?
slr0082-slr0083 gene expression
P
P
slr0082-slr0083 Operon
slr0082 (RimO/ MiaB)
slr0083 (CrhR)
Cold-enhanced accumulation of dicistronic mRNA
5' UTR
Operon transcript processing
?
?
?
-137
+1
5' UTR
Differential transcript stability
75nt
500nt
accumulation
functional sRNAs?
CrhR
mRNA
?
RNA degradation
?
CrhR
RimO/ MiaB
?
S-CH3
Rps12 /tRNA
RimO/ MiaB
Cold-adapted Ribosome ?
Translational Regulation
crhR mRNA stabilization and translation
CrhR
CrhR
CrhR
CrhR protein stabilization
Others?
Target mRNA & sRNA interaction
?
Gene Regulation
CrhR-dependent repression of transcription ?

Figure 4.11. Summary of the *slr0082-slr0083* operon expression in response to light and temperature stress.

Expression of the stress-inducible dicistronic operon, *slr0082-slr0083*, is regulated by a complex network involving transcript and protein interactions. Cyanobacterial cells sense alterations in abiotic factors including light and temperature. The absence of a global cold stress response regulator makes the cascade of signals in cyanobacteria intricate. Expression of the *Synechocystis* DEAD-box RNA helicase, CrhR is regulated by the redox status of the electron transport chain together with temperature downshifts that result in further reduction of the chain. An unknown signal transduction pathway enhances accumulation of the *slr0082-slr0083* dicistronic transcript. Endonucleolytic cleavage generates variable transcript sizes whose accumulation is differentially regulated with *slr0082* being rapidly degraded while *slr0083* is stabilized. This involves half-life differences with respect to temperature as well. In addition, two stable RNAs accumulate during *slr0082* transcript degradation. The *slr0082* 5' UTR accumulates together with a 500 nt internal stable RNA originating from the ORF of *slr0082*. These stable sense RNAs could potentially act as regulatory small RNAs whose annealing to target mRNA could potentially be governed by CrhR. The modification of either ribosomal protein S12 or tRNAs by a cold-inducible methylase encoded by *slr0082* would potentially perform a role in the alteration in translation observed at low temperatures. The interaction of CrhR RNA helicase with proteins and/or RNA partners could then affect gene regulation and thus cellular adaptation to temperature stress.

et al., 2012b), the induction and subsequent degradation of *slr0082* occurs more rapidly than observed for *slr0083* (Fig. 3). Temperature contributes significantly in stabilizing both *slr0083* transcript and protein (Rosana *et al*., 2012b) but is not associated with transient expression of *slr0082* mRNA. Thus, for *slr0082*, the initial cold sensing and induction of expression are CrhR-independent, similar to *slr0083* expression (Rosana *et al*., 2012b). Similarly, the subsequent lack of transient *slr0082* transcript accumulation in the absence of functional CrhR, is reminiscent of truncated *crhR* mRNA accumulation in the Δ*crhR*^{TR} mutant (Rosana *et al*., 2012b). This result indicates that transient expression of both *slr0082* and *slr0083* are CrhR-dependent (Rosana *et al*., 2012b, Fig. 3). The magnitude of the increase in transcript abundance of both *slr0082* and *slr0083* are similar, 13-fold in response to temperature downshift, suggests that both transcripts originate from the same promoter. The lack of transient *slr0082* accumulation at low temperature is not a consequence of CrhR-regulation of transcript half-life as *slr0082* half-life is not altered by *crhR* mutation. In contrast to *slr0083* half-life, *slr0082* half-life is not influence by either temperature or *crhR* mutation. Evidence that *crhR* inactivation is the primary player in these observations is provided by their complementation by constitutive expression of His-tagged CrhR. Although the complemented *crhR* mutants still over accumulate *slr0082* transcript, the level returns to basal levels at a slower rate than in wild type cells. This can potentially be explained by the lower level of expression of His-CrhR from the constitutive pNir promoter, compared to wild type, which is observed in *crhR* mutant cells.

The presence of constitutively expressed His-CrhR provided partially complemented the cold sensitive phenotype in the complete deletion mutant, presumably again because of the observed lower level of CrhR expression from the pNIR promoter. His-CrhR reduced the cellular growth rate at 30^{o}C and more profoundly at 20^{o}C in wild type and Δ*crhR*^{TR} cells but not in Δ*crhR* deletion strains. This indicates that co-expression of wild type or truncated CrhR with His-CrhR is detrimental to cell growth at all temperatures but more significantly at 20^{o}C. This suggests that the CrhR polypeptide is acting as a dominant negative

mutant, implying that self-interaction of CrhR is required for its normal functioning. The truncated- or His-CrhR background could negatively affect multimerization and thus biochemical activities of CrhR leading to improper interaction of the oligomer with target RNA substrates and protein cofactors. Alteration of these interactions would adversely affect cell adaptation and survival. The complete deletion mutant did not exhibit this impediment since there is only His-CrhR present and hence even at a reduced level of His-CrhR expression, the cells grow exponentially at both temperatures.

The accumulation of multiple processed *slr0082* transcripts in the Δ*crhR*^{TR} suggest that CrhR is associated with processing and/or degradation of the dicistronic mRNA. Transcript half-life analysis suggests that CrhR is not directly involved in RNA degradation, since the *slr0082* transcript half-life of is not significantly extended in the *crhR* mutant, irrespective of temperature. Although *slr0082* transcript accumulates to the same level as the truncated *slr0083* in response to cold stress, cold temperature stabilizes *crhR* but not *slr0082* transcript. The different half-lives result in the observed differential accumulation of the transcripts. Full length operon transcripts are marginally detected in wild type cells in which a stable 1.5 nt *crhR* transcript accumulates but not *slr0082* mRNA is not detected (Rosana *et al*., 2012b). This suggests that the full-length dicistronic transcript undergoes endonucleolytic processing, producing two monocistronic mRNAs whose different stabilities contribute to differential accumulation.

A similar situation in which operon transcription combined with differential accumulation of individual transcript members mediated by post-transcriptional events has been observed in other systems. In the unicellular green alga, *Chlamydonomas reinhardtii*, the chloroplast genes *petD* was shown to have its own functional promoter, however *petD* is also transcribed from a promoter upstream of *petA*, producing a dicistronic *petA-petD* transcript (Sakamoto *et al*., 1994). Although endonucleolytic cleavage generates two individual mRNAs, differential accumulation of the processed products was not reported (Sakamoto *et al*., 1994). Similarly, the *E. coli* heat-shock *ibpAB* dicistronic transcript is endonucleolytically cleaved, leading to accumulation of stabilized *ibpA* while the

downstream gene *ibpB* is destabilized (Gaubig *et al*., 2011). Transcript sizes and RACE data shown here indicate that these scenarios are similar to that involved in *slr0082-slr0083* transcript maturation, with the first gene destabilized and the second stabilized by the endonucleolytic cleavage.

Accumulation of the monocistronic *crhR* transcript in cold stressed wild type cells suggest that the *slr0082-slr0083* dicistronic message was separated from the upstream *slr0082* by an unknown endonuclease (potentially RNase E or J homologue). This endonucleolytic cleavage also generates mRNA substrates with differing affinity for the mRNA decay machinery, as evidenced by the differential half-lives of the *slr0082* and *slr0083* transcripts. Furthermore, processing of the *slr0082* transcript generates shorter, stable transcripts of 75 and 500 nt. Accumulation of these partial transcripts originating from *slr0082* is CrhR-dependent, as their accumulation is significantly enhanced in the absence of CrhR RNA helicase activity. The detected internal sense RNAs originating from the *slr0082* transcript could either act as an alternative functional mRNA resulting in different protein isoform or as a regulatory RNA functioning as a sense sRNA modulating the turnover or processing of multicistronic mRNAs present in other areas of the genome (Mitschke *et al*., 2011). Stable sRNA transcripts originating from protein-coding genes have been reported previously in cyanobacteria. In *Synechocystis*, RNA sequencing data revealed the presence of hundreds of small RNAs including non-coding, antisense and internal sense RNAs (Mitschke *et al*., 2011). In addition, multiple processed, stable RNA species also originate from the *psbA* ORF in *Synechococcus* 7942 (Soitamo *et al*., 1998). It is possible that the 75 nt fragment, originating from the *slr0082* 5' UTR, is a truncated transcriptional product, as suggested for a *psbA* transcript by Soitamo et al. (1998).

Recently, small regulatory RNAs have also emerged as effectors of post-transcriptional control of operon expression in a number of bacterial model systems (Balasubramanian and Vanderpool, 2013). The ability of CrhR to anneal complimentary single-stranded RNAs *in vitro* (Chamot *et al*., 2005) combined with RNA helicase involvement in small RNA-mediated regulation has been correlated with the potential to contributes to the post-transcriptional control of

cold-induced gene regulation, however, the CrhR role performs in this regulation is yet to be analyzed.

The differential accumulation and transcript half-life between *crhR* mRNA and *slr0082* suggest that the two polypeptides are required at different times during the cold response. Although levels of the putative protein product of *slr0082*, RimO/MiaB, were not tested in this study, recent partial 2-D proteomic analysis performed on soluble polypeptides obtained from a Δ*crhR*^{TR} mutant revealed a ~4X fold increase in RimO abundance during cold acclimation (Rowland *et al.*, 2011), consistent with the *slr0082* transcript level detected in both Δ*crhR*^{TR} and Δ*crhR*. The detected cleavage site within the *slr0082* ORF transcript disrupts the ORF thereby further reducing Slr0082 protein accumulation. The enhanced accumulation of *slr0082* transcript observed in the Δ*crhR*^{TR} mutant would explain the unique detection of RimO protein only in the *crhR* mutant (Rowland *et al*., 2011) in which enhanced stabilization of a full-length *slr0082* dicistronic transcript generates enhanced translation potential.

Analysis of the co-expression of *slr0082* and *slr0083* revealed an interesting combination of control points at the transcriptional, post-transcriptional and translational levels. Transcription from a promoter upstream of slr0082 appears to be enhanced in response to a temperature downshift resulting in accumulation of the dicistronic message. The subsequent rapid endonucleolytic cleavage resulted in separation of the two transcripts, having significantly different half-lives. Different from *Streptomyces coelicolor* in which the transcripts from operon members early in the operon have enhanced stability (Laing *et al*., 2006), the *slr0082-slr0083* operon stability is reversed, *slr0083* is more stable. Instances in which downstream operon genes are expressed at elevated levels are often ascribed to the existence of alternative promoters induced by different stimuli (Gaubig *et al*., 2011). The exact mechanism(s) by which *slr0082-slr0083* is processed, presumably mediated by a combination of endo- and exo-nucleases, and the requirement for CrhR RNA helicase activity in transcript maturation have yet to be identified. The data presented here further support the autoregulation of *crhR* expression (Rosana *et al*., 2012b) and CrhR

involvement in post-transcriptional regulation and self regulation of the *slr0082-slr0083* operon in response to temperature stress.

4.5 References

Anton, B.P., Saleh, L., Benner, J.S., Raleigh, E.A., Kasif, S., and Roberts, R.J. 2008. RimO, a MiaB-like enzyme, methylthiolates the universally conserved Asp88 residue of ribosomal protein S12 in *Escherichia coli*. Proc Nati Acad of Sci USA. **105** (6): 1826-1831.

Arraiano, C. M., Andrade, J. M., Domingues, S., Guinote, I. B., Malecki, M., Matos, R. G., and Viegas, S. C. 2010. The critical role of RNA processing and degradation in the control of gene expression. FEMS Microbiol Rev. **34**(5): 883-923.

Balasubramanian, D., and Vanderpool, C. K. 2013. New developments in post-transcriptional regulation of operons by small RNAs. RNA Biol. **10**(3): 0-1.

Beckering CL, Steil L, Weber MHW, Volker U and Marahiel M. 2002. Genomewide transcriptional analysis of the cold shock response in *Bacillus subtilis*. J Bacteriol. **184** (22): 6395-6402.

Blumenthal, T. 2004. Operons in eukaryotes. Briefings in functional genomics and proteomics. **3**(3): 199-211.

Cairrão, F., Cruz, A., Mori, H., and Arraiano, C. M. 2003. Cold shock induction of RNase R and its role in the maturation of the quality control mediator SsrA/tmRNA. Mol Microbiol. **50**(4): 1349-1360.

Chamot, D., Colvin, K. R., Kujat-Choy, S. L., and Owttrim, G. W. 2005. RNA structural rearrangement via unwinding and annealing by the cyanobacterial RNA helicase, CrhR. J Biol Chem. **280**(3): 2036-2044.

Chamot, D., Magee, W. C., Yu, E., and Owttrim, G. W. 1999. A cold shock-induced cyanobacterial RNA helicase. J Bacteriol. **181**(6): 1728-1732.

Chamot, D., and Owttrim, G. W. 2000. Regulation of cold shock-induced RNA helicase gene expression in the cyanobacterium *Anabaena* sp. strain PCC 7120. J Bacteriol. **182**(5): 1251-1256.

Chinnusamy V, Zhu J and Zhu J-K. 2007. Cold stress regulation of gene expression in plants. Trends Plant Sci. **12** (10): 444-451

Cordin, O., Banroques, J., Tanner, N. K., and Linder, P. 2006. The DEAD-box protein family of RNA helicases. Gene. **367**: 17-37.

Esberg, B., Leung, H. C. E., Tsui, H. C. T., Björk, G. R., and Winkler, M. E. 1999. Identification of the *miaB* gene, involved in methylthiolation of

isopentenylated A37 derivatives in the tRNA of *Salmonella typhimurium* and *Escherichia coli*. J Bacteriol. **181**(23): 7256-7265.

Even, S., Pellegrini, O., Zig, L., Labas, V., Vinh, J., Bréchemmier-Baey, D., and Putzer, H. 2005. Ribonucleases J1 and J2: two novel endoribonucleases in *B. subtilis* with functional homology to *E. coli* RNase E. Nucleic Acids Res. **33**(7): 2141-2152.

Gaubig, L. C., Waldminghaus, T., and Narberhaus, F. 2011. Multiple layers of control govern expression of the Escherichia coli *ibpAB* heat-shock operon. Microbiol. **157**(1): 66-76.

Graumann, P., and Marahiel, M. A. 1996. Some like it cold: response of microorganisms to cold shock. Arch Microbiol. **166**(5): 293-300.

Graumann, P., Wendrich, T. M., Weber, M. H., Schröder, K., and Marahiel, M. A. 1997. A family of cold shock proteins in *Bacillus subtilis* is essential for cellular growth and for efficient protein synthesis at optimal and low temperatures. Mol Microbiol. **25**(4): 741-756.

Gualerzi, C. O., Maria Giuliodori, A., and Pon, C. L. 2003. Transcriptional and post-transcriptional control of cold-shock genes. J Mol Microbiol **331**(3): 527-539

Hernández, H. L., Pierrel, F., Elleingand, E., García-Serres, R., Huynh, B. H., Johnson, M. K., and Atta, M. 2007. MiaB, a bifunctional radical-S-adenosylmethionine enzyme involved in the thiolation and methylation of tRNA, contains two essential [4Fe-4S] clusters. Biochem. **46**(17): 5140-5147.

Horn G, Hofweber R, Kremer W and Kalbitzer HR. 2007. Structure and function of bacterial cold shock proteins. Cell Mol Life Sci **64**: 1457 – 1470

Iost, I., Bizebard, T., and Dreyfus, M. 2013. Functions of DEAD-box proteins in bacteria: Current knowledge and pending questions. Biochim Biophys Acta (BBA)-Gene Regulatory Mechanisms.

Jacob, F., Perrin, D., Sánchez, C., and Monod, J. 1960. L'opéron: groupe de gènes à expression coordonnée par un opérateur. CR Acad. Sci. Paris, **250:** 1727-1729.

Jarmoskaite, I., and Russell, R. 2011. DEAD-box proteins as RNA helicases and chaperones. Wiley Interdisciplinary Reviews: RNA. **2**(1): 135-152.

Jones, P. G., and Inouye, M. 1994. The cold-shock response—a hot topic. Mol Microbiol. **11**(5), 811-818.

Kaan, T., Homuth, G., Mäder, U., Bandow, J., and Schweder, T. 2002. Genome-wide transcriptional profiling of the *Bacillus subtilis* cold-shock response. Microbiol. **148**(11), 3441-3455.

Kaberdin, V. R., and Bläsi, U. 2013. Bacterial helicases in post-transcriptional control. Biochim Biophys Acta (BBA)-Gene Regulatory Mechanisms.

Kujat, S. L., and Owttrim, G. W. 2000. Redox-regulated RNA helicase expression. Plant Physiol. **124**(2): 703-714.

Laing, E., Mersinias, V., Smith, C. P., and Hubbard, S. J. 2006. Analysis of gene expression in operons of *Streptomyces coelicolor*. Genome Biol: **7**: R46.

Lee, J. M., and Sonnhammer, E. L. 2003. Genomic gene clustering analysis of pathways in eukaryotes. Genome Res. **13**(5): 875-882.

Linder, P. 2006. Dead-box proteins: a family affair—active and passive players in RNP-remodeling. Nucleic Acids Res. **34**(15): 4168-4180.

Liou, G. G., Chang, H. Y., Lin, C. S., ad Lin-Chao, S. 2002. DEAD box RhlB RNA helicase physically associates with exoribonuclease PNPase to degrade double-stranded RNA independent of the degradosome-assembling region of RNase E. J Biol Chem. **277**(43): 41157-41162.

Memon, D., Singh, A.K., Pakrasi, H.B., and Wangikar, P.P. 2012. A global analysis of adaptive evolution of operons in cyanobacteria. Antonie Van Leeuwenhoek. 1-16.

Mikami, K., Kanesaki, Y., Suzuki, I., and Murata, N. 2002. The histidine kinase Hik33 perceives osmotic stress and cold stress in *Synechocystis* sp. PCC 6803. Mol Microbiol. **46**(4): 905-915.

Milón, P., and Rodnina, M. V. 2012. Kinetic control of translation initiation in bacteria. Critical Rev Biochem Mol Biol. **47**(4): 334-348.

Mitschke, J., Georg, J., Scholz, I., Sharma, C. M., Dienst, D., Bantscheff, J., and Hess, W. R. 2011. An experimentally anchored map of transcriptional start sites in the model cyanobacterium *Synechocystis* sp. PCC6803. Proc Natl Acad Sci. **108**(5): 2124-2129.

Mohanty, B. K., and Kushner, S. R. 2010. Processing of the *Escherichia coli* leuX tRNA transcript, encoding tRNA Leu5, requires either the 3′→ 5′ exoribonuclease polynucleotide phosphorylase or RNase P to remove the Rho-independent transcription terminator. Nucleic Acids Res. **38**(2): 597-607.

Morgan-Kiss, R. M., Priscu, J. C., Pocock, T., Gudynaite-Savitch, L., and Huner, N. P. 2006. Adaptation and acclimation of photosynthetic microorganisms to permanently cold environments. Microbiol Mol Biol **70**(1): 222-252.

Nakao, M., Okamoto, S., Kohara, M., Fujishiro, T., Fujisawa, T., Sato, S., and Nakamura, Y. 2010. CyanoBase: the cyanobacteria genome database update 2010. Nucleic Acids Res. **38**(suppl 1), D379-D381.

Newbury, S. F., Smith, N. H., and Higgins, C. F. 1987. Differential mRNA stability controls relative gene expression within a polycistronic operon. Cell. **51**(6): 1131-1143.

Niehrs, C., and Pollet, N. 1999. Synexpression groups in eukaryotes. Nature. **402**(6761): 483-487.

Ochsner, U. A., Vasil, M. L., Alsabbagh, E., Parvatiyar, K., and Hassett, D. J. 2000. Role of the *Pseudomonas aeruginosa oxyR-recG* operon in oxidative stress defense and DNA repair: OxyR-dependent regulation of *katB-ankB, ahpB, andahpC-ahpF*. J Bacteriol. **182**(16): 4533-4544.

O'Connell, K. P., and Thomashow, M. F. 2000. Transcriptional organization and regulation of a polycistronic cold shock operon in *Sinorhizobium meliloti* RM1021 encoding homologs of the *Escherichia coli* major cold shock gene *cspA* and ribosomal protein gene *rpsU*. Appl Environ Microbiol. **66**(1): 392-400.

Owttrim, G. W. 2006. RNA helicases and abiotic stress. Nucleci Acids Res. **34**(11): 3220-3230.

Owttrim, G. W. 2012. RNA helicases in cyanobacteria: biochemical and molecular approaches. Methods Enzymol. **511:** 385-403.

Owttrim, G. W. 2013. RNA helicases: Diverse roles in prokaryotic response to abiotic stress. RNA Biol. **10**(1): 0-1.

Pedersen, M., Nissen, S., Mitarai, N., Svenningsen, S. L., Sneppen, K., and Pedersen, S. 2011. The functional half-life of an mRNA depends on the ribosome spacing in an early coding region. J Mol Biol. **407**(1), 35-44.

Polissi, A., Laurentis, W. D., Zangrossi, S., Briani, F., Longhi, V., Pesole, G. and Deho, G. 2003. Changes in *Escherichia coli* transcriptome during acclimatization to low temperature. Res Microbiol. **154**: 573–580.

Poole, K. 2012. Stress responses as determinants of antimicrobial resistance in Gram-negative bacteria. Trends Microbiol. **20**(5): 227-234.

Polidoros, A. N., Pasentsis, K., and Tsaftaris, A. S. 2006. Rolling circle amplification-RACE: a method for simultaneous isolation of 5' and 3' cDNA ends from amplified cDNA templates. Biotechniques. **41**(1): 35.

Qi, Q., Hao, M., Ng, W. O., Slater, S. C., Baszis, S. R., Weiss, J. D., and Valentin, H. E. 2005. Application of the *Synechococcus nirA* promoter to establish an inducible expression system for engineering the Synechocystis tocopherol pathway. Appl Environ Microbiol. **71**(10): 5678-5684.

Régnier, P., and Portier, C. 1986. Initiation, attenuation and RNase III processing of transcripts from the *Escherichia coli* operon encoding ribosomal protein S15 and polynucleotide phosphorylase. J Mol Biol. **187**(1): 23-32.

Rocak, S., and Linder, P. (2004). DEAD-box proteins: the driving forces behind RNA metabolism. Nat Rev Mol Cell Biol. *5*(3): 232-241.

Rosana ARR, Ventakesh M, Chamot D, Patterson-Fortin LM, Tarassova O, Espie GS and Owttrim GW. 2012a. Inactivation of a low temperature induced RNA helicase in *Synechocystis* sp. PCC 6803: Physiological and morphological consequences. Plant Cell Physiol **53**: 646–658.

Rosana ARR, Chamot D, and Owttrim GW. 2012b. Autoregulation of RNA helicase expression in response to temperature stress in *Synechocystis* sp. PCC 6803. PLoS ONE **7**(10): e48683.

Rott, R., Zipor, G., Portnoy, V., Liveanu, V., and Schuster, G. 2003. RNA polyadenylation and degradation in cyanobacteria are similar to the chloroplast but different from *Escherichia coli*. J Biol Chem. **278**(18): 15771-15777.

Rowland, J. G., Simon, W. J., Prakash, J. S., and Slabas, A. R. 2011. Proteomics reveals a role for the RNA helicase crhR in the modulation of multiple metabolic pathways during cold acclimation of *Synechocystis* sp. PCC6803. J Proteome Res. **10**(8): 3674-3689.

Sakamoto, T., and Bryant, D. A. 1997. Temperature-regulated mRNA accumulation and stabilization for fatty acid desaturase genes in the cyanobacterium *Synechococcus* sp. strain PCC 7002. Mol Microbiol. **23**(6): 1281-1292.

Sakamoto, W., Sturm, N. R., Kindle, K. L., and Stern, D. B. 1994. *petD* mRNA maturation in *Chlamydomonas reinhardtii* chloroplasts: role of 5'endonucleolytic processing. Mol Cell Biol. **14**(9): 6180-6186.

Sato, N. 1994. A cold-regulated cyanobacterial gene cluster encodes RNA-binding protein and ribosomal protein S21. Plant Mol Biol. **24**(5): 819-823.

Sato, N. 1995. A family of cold-regulated RNA-binding protein genes in the cyanobacterium *Anabaena variabilis* M3. Nucleic Acids Res. **23**(12): 2161-2167.

Sato, N., and Maruyama, K. 1997. Differential regulation by low temperature of the gene for an RNA-binding protein, rbpA3, in the cyanobacterium *Anabaena variabilis* strain M3. Plant Cell Physiol. **38**(1): 81-86.

Schneider, C. A., Rasband, W. S., and Eliceiri, K. W. (2012). NIH Image to ImageJ: 25 years of image analysis. Nat Methods. **9**(7): 671-675.

Soitamo, A. J., Sippola, K., and Aro, E. M. 1998. Expression of *psbA* genes produces prominent 5′ *psbA* mRNA fragments in *Synechococcus* sp. PCC 7942. Plant Mol Biol. **37**(6): 1023-1033.

Strader, M. B., Costantino, N., Elkins, C. A., Chen, C. Y., Patel, I., Makusky, A. J., Choy, J.S., Markey, S. P., and Kowalak, J. A. 2011. A proteomic and transcriptomic approach reveals new insight into β-methylthiolation of *Escherichia coli* ribosomal protein S12. Mol Cell Proteomics. **10**(3).

Tanner, N. K., Cordin, O., Banroques, J., Doère, M., and Linder, P. 2003. The Q motif: a newly identified motif in DEAD box helicases may regulate ATP binding and hydrolysis. Mol Cell. **11**(1): 127-138.

Vinnemeier, J., and Hagemann, M. 1999. Identification of salt-regulated genes in the genome of the cyanobacterium *Synechocystis* sp. strain PCC 6803 by subtractive RNA hybridization. Arch Microbiol. **172**(6): 377-386.

Whitton, B. A., and Potts, M. 2012. Introduction to the cyanobacteria. In Ecology of Cyanobacteria II. Springer Netherlands. 1-13.

Yu, E., and Owttrim, G. W. 2000. Characterization of the cold stress-induced cyanobacterial DEAD-box protein CrhC as an RNA helicase. Nucleic Acids Res. **28**(20): 3926-3934.

Zang, X., Liu, B., Liu, S., Arunakumara, K. K. I. U., and Zhang, X. 2007. Optimum conditions for transformation of *Synechocystis* sp. PCC 6803. J of Microbiol. **45**(3), 241.

Chapter 5: Summary and Conclusion

Cyanobacteria are primarily photoautotrophic microorganisms and therefore photosynthesis plays a crucial role in their metabolism. This prokaryotic phylum occupies diverse roles in the ecosystem as key players of aquatic food webs, global element recycling, as well as production of valuable gases such as oxygen and more recently as a source of microbial hydrogen (Paerl and Pinckney, 1996; Dutta *et al*., 2005; Gassara *et al*., 2012). Although cyanobacteria contribute significantly to primary productivity, a number of species are known toxin producers during cyanobacterial blooms, hence they are often considered as harmful microorganisms (de Figueiredo *et al*., 2004). These significant attributes in a changing habitat make it worthwhile to understand how photosynthetic microorganisms, such as cyanobacteria, respond, adapt and acclimate to their environments. Fluctuating environmental temperature is a constant stress encountered by free-living cells and deviation from the optimum growth temperature requires adaptive response to alleviate the non-permissible condition (Owttrim, 2013). As such, temperature fluctuations greatly affects the photosynthetic capabilities of aquatic photoautotrophs therefore regulating gene expression is a survival mechanism to ensure perpetuation of the species.

5.1 CrhR RNA helicase and the photosynthetic cyanobacterium *Synechocystis* sp. PCC 6803

Cyanobacterial response to temperature downshifts is not solely dependent on a single master regulator, where a few genes are implied to be under the control of an alternative signal transduction pathway (Suzuki *et al.*, 2000; Shivaji, 2013). In the photosynthetic model cyanobacterium *Synechocystis, crhR* is the most highly-induced gene upon temperature downshift (Kujat and Owttrim, 2000; Prakash *et al*., 2010) although this gene was not shown to be coordinated by the cold-gene master regulator, Hik33 (Suzuki *et al*., 2001). Inactivation of this cold-induced redox regulated DEAD-box RNA helicase is not detrimental to the cell at the optimum growth temperature (30^{o}C), but is lethal to cells transferred to cold

temperature conditions ($\leq 20^{o}$C) (Rosana *et al*., 2012a; Chapter 2) This cold-sensitive phenotype is a common theme for DEAD-box RNA helicase mutants in a number of prokaryotic systems (Iost *et al*, 2013; Kaberdin and Blassi, 2013) suggesting enhanced cellular-requirement for RNA helicase activity during bacterial cold temperature acclimation.

The *Synechocystis crhR* gene was inactivated by replacing the second RecA-like domain within the helicase core region up to the C-terminal extension by inserting a spectinomycin resistant cassette (Fig 2.1A). Functional analysis of $\Delta crhR^{TR}$ (2-76) showed remarkable phenotypic differences from the wild type including cold sensitivity, rapid cessation of photosynthesis at 20^{o}C and reduction in pigment composition. Furthermore, mutant cells are relatively smaller, contain lower DNA levels and progressively accumulate structural abnormalities (Rosana *et al*., 2012a). In contrast to *crhR* mutation in *Synechocystis*, DEAD-box RNA helicase inactivation in *E. coli* or *Bacillus*, frequently shows cold sensitivity only with no distinct morphological or physiological abnormalities noted (Pandiani *et al*., 2011). This can be ascribed to the fact that the *Synechocystis* genome only encodes a single DEAD-box RNA helicase (Owttrim, 2013) while *E. coli* or *Bacillus* have multiple DEAD-box RNA helicases which potentially perform overlapping functions (Peil *et al*., 2008; Hunger *et al*., 2008). Therefore, microorganisms with only one DEAD-box RNA helicase are excellent model systems to elucidate novel roles of RNA helicases in RNA metabolism and in studying environmental stress responses (Redko *et al*., 2013) such as temperature fluctuations (Owttrim, 2013).

The importance of DEAD-box RNA helicases in multiple abiotic stresses including freezing tolerance has also been reported in higher plant species (Kant *et al*., 2007; Kim *et al*., 2008). In tobacco chloroplasts, the DEAD-box RNA helicase Vdl, controls early plastid differentiation as well as plant morphogenesis (*Wang et al*., 2000). Similarly, two DEAD-box helicases in *Arabidopsis* control seed germination under salt- and cold-stress conditions (Kim *et al*., 2008) while an RNA helicase-like protein functions as an early regulator of transcriptional factors for the plants chilling and freezing tolerance (Gong *et al*., 2002).

The observed pleiotropic phenotype between the wild type and *crhR* mutant, both at the morphological and physiological levels, suggests that the defects are intimately associated with *crhR* inactivation in *Synechocystis*. The lack of CrhR RNA unwinding and/or annealing activity during the cold stress response presumably affects target transcripts or protein effectors such as activators or suppressors leading to the organism's inability to acclimate/adapt (Gong *et al*., 2002; Kant *et al*., 2007). Taken together, CrhR's vital role in photosynthetic capacity and cold adaptation suggest a strong link identifying RNA helicase as molecular drivers of gene regulation during photosynthesis. Although the exact mechanism by which CrhR functions in cyanobacterial photosynthetic pathways, especially during temperature downshifts, is still an enigma, elucidation of CrhR regulation during cold stress and the identification of its targets are essential aspects. Therefore, an extensive gene analysis, comparing wild type and Δ*crhR*^{TR}, during temperature stress was undertaken. Experimental analyses both at the transcript (mRNA, operon, sRNA) and protein (CrhR, protein interactome) level are reported in this thesis.

5.2 CrhR autoregulation of gene expression

CrhR RNA helicase expression is regulated by the redox poise of the electron transport chain, tightly regulated at the junction of the plastoquinone pool and cyt b_6f complex (Kujat and Owttrim, 2000). Moreover, salt stress, hyperosmotic shock and temperature downshifts all resulted in enhanced expression of *crhR* (Vinnemeier and Hagemann; Mikami *et al*., 2002; Prakash *et al*., 2010). Analysis of *crhR*^{TR} expression in response to temperature stress between wild type and Δ*crhR* revealed an autoregulatory circuit involving transcriptional and posttranscriptional controls mediated by CrhR-dependent and -independent pathways (Rosana *et al*., 2012b; Chapter 3; Fig 5.1). Transcript analysis between cold-stressed wild type and Δ*crhR*^{TR} cells revealed transient and deregulated accumulation of full length and truncated *crhR* transcript, respectively (Rosana *et al*., 2012b; Chapter 3). Temperature plays a crucial role in regulation

of *crhR* accumulation as shown by the significant extension of transcript half-life at low temperatures (20^{o}C). Transitory accumulation of cold-induced transcripts is also found in a number of prokaryotic genes involving transcriptional controls and mRNA stabilization. One classical example is the *E. coli* cold shock protein A (*cspA*) where the role of its 5' UTR and cold-box elements contributes to enhanced expression in the cold (Jiang *et al*., 1996). Similar to *crhR* stabilization, temperature dictates the stability of the *cspA* mRNA following cold shock (15^{o}C) while an unstable transcript was noted at 37^{o}C (Mitta *et al*., 1997) and therefore CspA has been implicated in its own autoregulation (Jiang *et al*., 1996; Bae *et al*., 1997; Fang *et al*., 1997, 1998). In the case of CrhR, it is theorized that after the initial cold stress when the concentration of CrhR proteins has increased, a repressor protein (e.g. CrhR, LexA-orthologue) bind the *crhR* promoter region and blocks transcription (Patterson-Fortin *et al*., 2006). The ability of CrhR to bind its own promoter is yet to be proven which also necessitates identification of the cold-responsive promoter region of *crhR*.

On the other hand, the deregulated accumulation of the truncated *crhR* transcript in the *crhR* mutant could also arise from reduced RNA degradation efficiency. Albeit there is no significant difference compared to wild type *crhR* transcript half-life, the generation of four major stable transcripts suggest that to a certain extent, RNA turnover is impaired in the *crhR* mutant. This phenomenon is potentially related to the regulation of two RNAses in *E. coli*, RNase E and PNPase. RNase E autoregulates its synthesis by controlling the degradation rate of its own mRNA (Jain and Belasco, 1995). Similarly, the cold-inducible exonuclease, PNPase, was also shown to autoregulate its own expression, post-transcriptionally by a mechanism involving RNAse III-dependent cleavage (Beran and Simons, 2001; Jarrige *et al*., 2001). The *pnp* mRNA has a long stem-loop in its leader sequence which is a substrate for RNase III resulting in a duplex with a short 3' extension which then acted upon by basal levels of PNPase (Jarrige et al., 2001).

At the protein level, proteolysis regulates the accumulation of CrhR. CrhR polypeptide is highly stable in the cold but significantly destabilized in the warm

(Rosana *et al*., 2012b; Chapter 3). The degradation of CrhR protein is dependent on CrhR activity as revealed by the enhanced expression of the truncated CrhR polypeptide observed in the mutant. This proteolytic mechanism is potentially governed by the Clp family of proteases (Tarassova, personal communication), but the mechanism is dependent on functional CrhR.

In conclusion, CrhR-dependent mechanisms regulate both the transient accumulation of *crhR* transcript at 20^{o}C and stability of the CrhR protein at all temperatures. Many of the processes are CrhR- and temperature-dependent and occur in the absence of a correlation between *crhR* transcript and protein abundance. The data provide important insights into not only how RNA helicase gene expression is regulated but also the role that rearrangement of RNA secondary structure performs in the molecular response to temperature stress.

5.3 CrhR association in RNA metabolism: processing, maturation and degradation of the *slr0082-slr0083* operon

DEAD-box RNA helicases are considered as molecular drivers of RNA metabolism since they possess the ability to reorganize RNA secondary structure (Rocak and Linder 2004). In recent years, there is increasing evidence of RNA helicase involvement in multiple aspects of RNA metabolism including RNA degradation and quality control (Hardwick and Luisi, 2013), splicing and maturation (Guan *et al*., 2013; Cordin and Beggs, 2013) and ribosome biogenesis (Iost *et al*., 2013). An evolving theme emerges where RNA helicases serves as integrators for protein-protein interactions or nucleation centers, acting as molecular clamps, maintaining RNA secondary structure in a precise configuration which then promotes formation of RNA-protein complexes (Putnam and Jankowsky, 2013; Owttrim, 2013; Linder and Fuller-Pace, 2013). DEAD-box RNA helicases are also critical players in bacterial posttranscriptional events such as RNA processing, maturation and degradation (Iost *et al*., 2013; Kaberdin and Blasi, 2013). Frequently, known prokaryotic RNA degradosome or processome

complexes have an RNA helicase component thought to be responsible for relieving stable secondary structures in target RNAs (Prud'homme-Genereux *et al*., 2004; Lehnik-Habrink *et al*., 2010; Hardwick *et al*., 2010; Redko *et al*., 2013). In eukaryotic exosomes, DEAD-box RNA helicases are also associated with RNA processing, maturation and degradation (Harwick and Luisi, 2013). A prime example of which is the chloroplast RNA helicase, RH3, which is characterized in maize and *Arabidopsis*, and shown to be involved in splicing of specific group II introns as well as plastid ribosome biogenesis (Asakura *et al*., 2012). As the evolutionary precursor of plants chloroplast (Osteryoung and Nunnari, 2003; Martin *et al*., 2012), using cyanobacteria, such as *Synechocystis*, is an excellent model system for dissection of RNA helicase function in RNA metabolism of photosynthetic organisms.

One aspect of RNA metabolism reported in this thesis is the posttranscriptional regulation of the *slr0082-slr0083* operon in *Synechocystis*. Experimental evidence supports the transcription of *slr0082-slr0083* as a dicistronic operon whose expression is enhanced both by temperature downshift and inactivation of the second gene, *slr0083*, coding for the DEAD-box RNA helicase, *crhR*. Variation in operon member mRNA accumulation involves processing of the dicistronic transcript, resulting in four transcripts that exhibit differential stability. Although both genes are transiently induced at 20^{o}C, the induction and subsequent degradation of *slr0082* occurs more rapidly than observed for *slr0083*. A major player in the differential expression involves temperature-dependent alteration of transcript half-life. Although the effectors involved in processing and degradation of the dicistronic transcript is yet to be revealed, the data suggest CrhR RNA helicase is a key player in these posttranscriptional events. The *Synechocystis* genome codes for only one DEAD-box RNA helicase, CrhR (Kujat and Owttrim, 2000) and is hypothesized to have functional multiplicity in cyanobacterial RNA processes (Lasko, 2013). Here, we propose CrhR-dependent pathways involving RNA processing and degradation based on functional similarity and expression of the effectors in *Synechocystis*.

Although there is only one DEAD-box RNA helicase, *Synechocystis* possess homologues of the major degradosome-related RNases like RNase E, J and PNPase (Nakao *et al*., 2010; Hardwick and Luisi, 2013). Nevertheless, unlike the *E. coli* or *Bacillus* degradosome, there is no established degradosome complex in *Synechocystis* (Rott *et al*., 2003), a conclusion drawn mainly from the observation that the C-terminal domain of the *E. coli* RNase E, which is responsible for degradosome assembly, is lacking in the cyanobacterial RNase E homologue. Identifying the RNases, both endo- and exonucleases, involved in *slr0082-slr0083* transcript maturation and degradation is difficult since inactivation of the known major RNases is lethal to *Synechocystis* (Rott *et al.*, 2003). The four major transcripts generated in the Δ*crhR*^{TR} mutant, suggest that the helicase is needed for the proper turnover of transcripts generated from the operon. The deleted C-terminal domain together with the C-terminal extension (V_{226}-Q_{492}) in Δ*crhR*^{TR} could potentially be important in the interaction of the helicase with its RNA targets (Lim *et al*., 2000;) or ribonucleo-protein complexes (Netterling *et al*., 2012) and/or in recruiting RNases (Lehnik-Habrink *et al*., 2010) and other proteins in the subsequent RNA maturation and/or degradation of the *slr0082* transcript. A role for RNA helicases in operon processing has been reported in the *E. coli* DEAH-box RNA helicase, HrpA (Koo *et al*., 2004). Deletion of the C-terminal domain of HrpA generates a processing defect in fimbrial operon maturation (Koo *et al.*, 2004) which is ascribed to a potential protein sequence in the domain required for targeted RNA substrate interaction or ligands for protein complex recruitment (Silverman *et al.*, 2003; Putnam and Jankowsky, 2013). The C-terminal domains in the two helicases are not conserved. The C-terminal of CrhR is unique to cyanobacteria (Owttrim, 2013) and is assumed to be involved in mRNA target specificity just like the C-terminus of the *Bacillus* DEAD-box RNA helicase, YxiN (Wang *et al*., 2006). This domain could also contribute to localization to certain regions or complexes within the cell such as the thylakoid or polysome (Appendix 6.3) similar to what is found in *Listeria monocytogenes* Lmo1722 RNA helicase where the C-terminal is known to interact with 50S ribosomal subunits (Netterling *et al*., 2012).

The persistence of multiple transcripts detected in the Δ*crhR*^{TR} mutant could be attributed to inefficient 3'- 5'exonucleolytic degradation. This pathway thus direcylt or indirectly requires RNA helicase activity as revealed by the His-CrhR expressing *crhR* mutant strains where *slr0082* transcript where degraded. The main exonucleolytic degradation pathway in *Synechocystis* and other bacteria is governed by the 3'- 5' exonucleolytic enzyme PNPase, a component of the degradosome (Rott *et al*., 2003). The absence of functional helicase could potentially affect the activity of polyadenylation and exonucleolytic degradation of structured transcripts by PNPase (Liou *et al*., 2002) and hence result in accumulation of the observed transcripts from the *slr0082-slr0083* operon in the *crhR* mutants. Cold stress has been reported to increase PNPase levels ~2-fold in both wild type and a *ΔcrhR* mutant (Rowland *et al*., 2011) but the absence of a functional helicase resulted in unregulated degradation of multiple processed transcripts in the *crhR* mutant (Rosana *et al*., 2012b). Thus, although the cold-induction of PNPase expression is not affected by *crhR* mutation, its biochemical activity is apparently affected in the absence of a functional CrhR. CrhR could directly or indirectly interact with PNPase. CrhR can potentially interact with PNPase to form a minimal degradosome similar to the *E. coli* RhlB RNA helicase and PNPase complex (Liou *et al*., 2002). Potential cold stabilization of secondary structure generated at the 3' end of the processed *slr0082-slr0083* transcripts potentially requires CrhR unwinding ability for a PNPase stimulated turnover pathway as observed in RhlB helicase-enhanced PNPase-mediated RNA degradation (Liou *et al*., 2002). Conversely, CrhR may indirectly affect the translation of structured mRNA whose protein products are involved in RNA decay pathways.

Although 3'-5' exonuclease is the only degradation pathway in *E. coli*, one cannot rule out a 5'-3' exonucleolytic degradation catalyzed by RNase J in *Bacillus* (Deikus *et al*., 2008) which is also putatively encoded in *Synechocystis* (*slr0051*). Microarray analysis revealed that cold stress increases transcript abundance of this RNaseJ homologue ~2 fold while *crhR* mutation further enhances this ~3.2 fold (Georg and Owttrim, unpublished data). It is interesting to

note that the *Synechocystis* genome encodes for both the major RNase involved in degradosome complexes in bacteria, RNase E in *E. coli* (Carpousis, 2007) and RNase J in *Helicobacter pylori* (Redko *et al*., 2013). It is possible that CrhR may interact with either RNase or both to target transcript for processing or degradation, specifically in the cold such (**Fig 5.1**).

An alternative degradosome-like complex is based on an RNase R system. *Synechocystis* encodes a single RNaseII/R homologue and biochemically was shown to catalyze exonucleolytic cleavage in the 3' to 5' direction, releasing nucleoside monophosphates (Matos *et al.,* 2012). Inactivation of this exonuclease was shown to be lethal (Rott *et al*, 2003) suggesting that its role in exonucleolytic degradation can't be compensated by PNPase. The *Synechocystis* and *E. coli* RNase II is not capable of cleaving double stranded RNA unlike the *E. coli* RNase R which is not stalled by secondary RNA structures (Awano *et al*., 2010). It is assumed that the ability to degrade RNA secondary structures, which are thermodynamically favored due to temperature downshift, is performed by RNase R through RNA helicase rearrangement of structures RNAs (Cheng and Deutscher, 2005). One can imagine CrhR RNA helicase coupling with RNase R, rearranging structured RNAs that are thermodynamically stabilized in the cold.

One aspect that is not analyzed in this thesis is the promoter region of *crhR* and *slr0082*. There could be a potential difference in the strength of the putative promoter sequence accounting for the relative difference in transcript accumulation. In the actinomycete *Streptomyces antibioticus*, the *rpsO-pnp* operon is transcribed from two separate promoters. The first transcript is a readthrough of the operon producing a dicistronic transcript while a second transcript is synthesized from a promoter located in the *rpsO-pnp* intergenic region (Bralley and Jones, 2004). Endonucleolytic cleavage is responsible for the posttranscriptional processing of the operon. This expression scenario is potentially similar to the *Synechocystis slr0082-slr0083* operon which generates a full length dicistronic transcript in the cold (**Fig 5.1**). On the other hand, a relatively weak promoter was identified in the *slr0082-slr0083* intergenic region (Hess, personal communication), which potentially gives rise to a constitutive

transcript level detected in the warm (30^{o}C) (Appendix 6.1). The identification of *slr0082* and *slr0083* monocistronic transcripts generated from either transcriptional start site or processing events by endonucleolytic cleavage requires further investigation. A strategy such as RLM-RT-PCR or RNA ligase-mediated reverse transcription-PCR, a procedure that distinguishes between transcript 5' ends generated from transcription initiation or posttrancriptional processing (Bensing *et al*., 2003), can be adapted.

The regulation of the *Synechocystis* DEAD-box RNA helicase CrhR revealed a complex network involving controls at the transcriptional, posttranscriptional, translational and potentially posttranslational levels. The induction of expression mediated by temperature downshift, which is linked to the reduction of the electron transport chain, revealed showed an autoregulatory mechanism(s) involving CrhR-independent and -dependent pathways. The sensing ability and induction of transcription are CrhR independent while the transient mRNA accumulation and protein degradation are both CrhR dependent. The established dicistronic operon with the upstream *rimO* gene, although accumulate differentially, suggest a potential RNP complex such as cold-adapted ribosome. Furthermore, the involvement of RNA helicases such as CrhR, in degradosome-polysome complexes indicates an interesting field in RNA biology where two seemingly contradictory processes, RNA degradation and translation, present yet another level of complexity to *crhR* gene regulation.

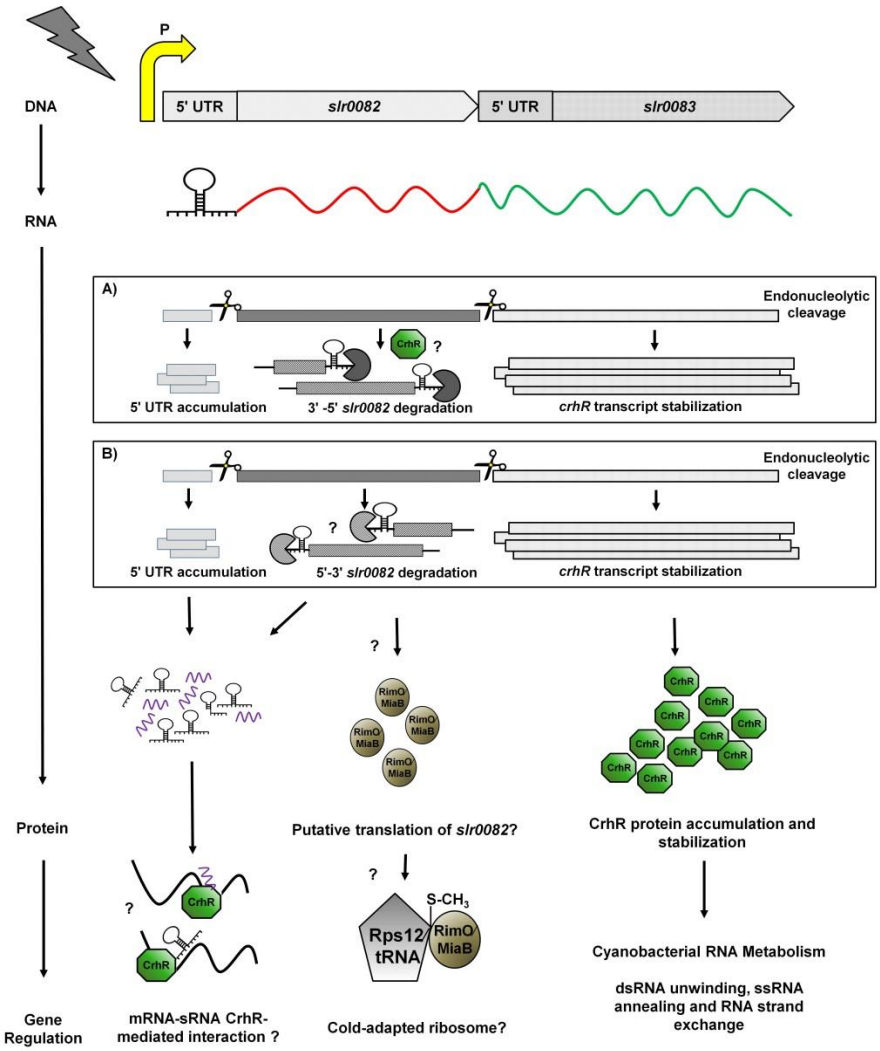

Figure 5.1 Model for *slr0082-slr0083* regulation in *Synechocystis* sp. PCC 6803. Temperature downshift enhances the expression of *slr0082-slr0083* operon generating a dicistronic transcript. This transcript is posttranscriptionally processed by an unknown endonuclease (RNase E?). *slr0083 (crhR)* mRNA is stabilized while *slr0082* is degraded. Exonucleolytic degradation is CrhR-dependent where (A) the exonuclease PNPase degrades the mRNA in a 3'-5' manner while (B) a putative 5'-3' degradation is tailored by an RNaseJ homologue. Accumulation of stable 75 and 500 nt small RNAs are generated that potentially act as regulatory RNAs. The presumed translation of *slr0082* to a methylthiotransferase modifying Rps12 could potentially give rise to a cold-adapted ribosome. CrhR polypeptide accumulate and stabilized in the cold. The ability of CrhR to unwind and anneal RNA molecules drives RNA rearrangement and thus regulate gene expression during temperature acclimation.

5.6 References

Asakura, Y., Galarneau, E., Watkins, K. P., Barkan, A., and van Wijk, K. J. 2012. Chloroplast RH3 DEAD box RNA helicases in maize and *Arabidopsis* function in splicing of specific group II introns and affect chloroplast ribosome biogenesis. Plant Physiol. **159**(3): 961-974.

Awano, N., Rajagopal, V., Arbing, M., Patel, S., Hunt, J., Inouye, M., and Phadtare, S. 2010. *Escherichia coli* RNase R has dual activities, helicase and RNase. J Bacteriol. **192**(5): 1344-1352.

Beran, R. K., and Simons, R. W. 2001. Cold-temperature induction of *Escherichia coli* polynucleotide phosphorylase occurs by reversal of its autoregulation. Mol Microbiol. **39**(1): 112-125.

Bae, W., Jones, P. G., and Inouye, M. 1997. CspA, the major cold shock protein of *Escherichia coli*, negatively regulates its own gene expression. J Bacteriol. **179**(22): 7081-7088.

Bralley, P., andJones, G. H. 2004. Organization and expression of the polynucleotide phosphorylase gene (*pnp*) of Streptomyces: processing of *pnp* transcripts in *Streptomyces antibioticus*. J Bacteriol. **186**(10): 3160-3172.

Carpousis, A. J. 2007. The RNA degradosome of *Escherichia coli*: an mRNA-degrading machine assembled on RNase E. Ann. Rev. Microbiol. **61**: 71-87.

Cordin, O., and Beggs, J. D. 2013. RNA helicases in splicing. RNA Biol. **10**(1), 82-94.

de Figueiredo, D. R., Azeiteiro, U. M., Esteves, S. M., Gonçalves, F. J., and Pereira, M. J. 2004. Microcystin-producing blooms—a serious global public health issue. Ecotox Environ Saf. **59**(2): 151-163.

Deikus, G., Condon, C., and Bechhofer, D. H. 2008. Role of *Bacillus subtilis* RNase J1 endonuclease and 5′-exonuclease activities in trp leader RNA turnover. J Biol Chem. **283**(25): 17158-17167.

Dutta, D., De, D., Chaudhuri, S., and Bhattacharya, S. K. 2005. Hydrogen production by cyanobacteria. Microb Cell Fact. **4**(36).

Fang, L., Jiang, W., Bae, W., and Inouye, M. 1997. Promoter-independent cold-shock induction of *cspA* and its derepression at 37° C by mRNA stabilization. Mol Microbiol. **23**(2): 355-364.

Fang, L., Hou, Y., and Inouye, M. 1998. Role of the cold-box region in the 5′ untranslated region of the *cspA* mRNA in its transient expression at low temperature in *Escherichia coli*. J Bacteriol. **180**(1): 90-95.

Franceschini, A., Szklarczyk, D., Frankild, S., Kuhn, M., Simonovic, M., Roth, A., Minquez, P., Doerks, T., Stark, M., Muller, J., Bork, P., and Jensen, L. J. 2013. STRING v9. 1: protein-protein interaction networks, with increased coverage and integration. Nucleic Acids Res. **41**(D1), D808-D815.

Gassara, F., Brar, S. K., Tyagi, R. D., and Surampalli, R. Y. 2012. Trends in biological degradation of cyanobacteria and toxins. In Environmental protection strategies for sustainable development. Springer Netherlands. 261-294.

Gong, Z., Lee, H., Xiong, L., Jagendorf, A., Stevenson, B., and Zhu, J. K. 2002. RNA helicase-like protein as an early regulator of transcription factors for plant chilling and freezing tolerance. Proc Natl Acad Sci. **99**(17): 11507-11512.

Guan, Q., Wu, J., Zhang, Y., Jiang, C., Liu, R., Chai, C., and Zhu, J. 2013. A DEAD Box RNA helicase is critical for pre-mRNA splicing, cold-responsive gene regulation and cold tolerance in *Arabidopsis*. Plant Cell Online. **25**(1): 342-356.

Hardwick, S. W., and Luisi, B. F. 2013. Rarely at rest: RNA helicases and their busy contributions to RNA degradation, regulation and quality control. RNA Biol. **10**(1): 0-1.

Hunger, K., Beckering, C. L., Wiegeshoff, F., Graumann, P. L., and Marahiel, M. A. 2006. Cold-induced putative DEAD box RNA helicases CshA and CshB are essential for cold adaptation and interact with cold shock protein B in *Bacillus subtilis*. J Bacteriol. **188**(1): 240-248.

Iost, I., Bizebard, T., and Dreyfus, M. 2013. Functions of DEAD-box proteins in bacteria: Current knowledge and pending questions. Biochim Biophy Acta (BBA)-Gene Regulatory Mechanisms. http://dx.doi.org/10.1016/j/bbagrm.2013.01.01

Jain, C., and Belasco, J. G. 1995. RNase E autoregulates its synthesis by controlling the degradation rate of its own mRNA in *Escherichia coli*: unusual sensitivity of the rne transcript to RNase E activity. Genes Dev **9**(1): 84-96.

Jarrige, A. C., Mathy, N., and Portier, C. 2001. PNPase autocontrols its expression by degrading a double-stranded structure in the *pnp* mRNA leader. EMBO J. **20**(23): 6845-6855.

Jiang, W., Fang, L., and Inouye, M. 1996. The role of the 5'-end untranslated region of the mRNA for CspA, the major cold-shock protein of *Escherichia coli*, in cold-shock adaptation. J of Bacteriol. **178**(16), 4919-4925.

Kaberdin, V. R., and Bläsi, U. 2013. Bacterial helicases in post-transcriptional control. Biochim Biophys Acta (BBA)-Gene Regulatory Mechanisms. http://dx.doi.org/10.1016/j.bbagrm.2012.12.005

Kant, P., Kant, S., Gordon, M., Shaked, R., and Barak, S. 2007. Stress response suppressor 1 and stress response suppressor 2, two DEAD-box RNA helicases that attenuate *Arabidopsis* responses to multiple abiotic stresses. Plant Physiol. **145**(3): 814-830.

Kim, J. S., Kim, K. A., Oh, T. R., Park, C. M., and Kang, H. 2008. Functional characterization of DEAD-box RNA helicases in *Arabidopsis thaliana* under abiotic stress conditions. Plant Cell Physiol. **49**(10): 1563-1571.

Komarek J and Hauer T. 2013. CyanoDB.cz – On-line database of cyanbacterial genera. World-wide electronic publication. Univ of South Bohemia and Inst of Botany AS CR. http:///www.cyanodb.cz

Koo, J. T., Choe, J., and Moseley, S. L. 2004. HrpA, a DEAH-box RNA helicase, is involved in mRNA processing of a fimbrial operon in *Escherichia coli*. Mol Microbiol. **52**(6): 1813-1826.

Kujat, S. L., and Owttrim, G. W. 2000. Redox-regulated RNA helicase expression. Plant Physiol. **124**(2), 703-714.

Lasko, P. 2013. The DEAD-box helicase Vasa: Evidence for a multiplicity of functions in RNA processes and developmental biology. Biochim Biophys Acta (BBA)-Gene Regulatory Mechanisms. http://dx.doi.org/10.1016/j.bbagrm.2013.04.005.

Lehnik-Habrink, M., Pförtner, H., Rempeters, L., Pietack, N., Herzberg, C., and Stülke, J. 2010. The RNA degradosome in *Bacillus subtilis*: identification of CshA as the major RNA helicase in the multiprotein complex. Mol Microbiol. **77**(4): 958-971.

Linder, P., and Fuller-Pace, F. 2013. Looking back on the birth of DEAD-box RNA helicases. Biochim Biophys Acta (BBA)-Gene Regulatory Mechanisms. http://dx.doi.org/10.1016/j.bbagrm.2013.03.007

Lim, J., Thomas, T., and Cavicchioli, R. 2000. Low temperature regulated DEAD-box RNA helicase from the antarctic archaeon, *Methanococcoides burtonii*. J Mol Biol. **297**(3): 553-567.

Liou, G. G., Chang, H. Y., Lin, C. S., and Lin-Chao, S. 2002. DEAD box RhlB RNA helicase physically associates with exoribonuclease PNPase to degrade double-stranded RNA independent of the degradosome-assembling region of RNase E. J Biol Chem. **277**(43): 41157-41162.

Mao, F., Dam, P., Chou, J., Olman, V., and Xu, Y. 2009. DOOR: a database for prokaryotic operons. Nucleic Acids Res. **37:** D459-D463.
Martin, W., Roettger, M., Kloesges, T., Thiergart, T., Woehle, C., Gould, S., and Dagan, T. 2012. Modern endosymbiotic theory: Getting lateral gene transfer in-to the equation. J Endocytobiosis Cell Res. 1-5.

Matos, R. G., Fialho, A. M., Giloh, M., Schuster, G., and Arraiano, C. M. 2012. The *rnb* gene of *Synechocystis* PCC6803 encodes a RNA hydrolase displaying RNase II and not RNase R enzymatic properties. PloS ONE **7**(3): e32690.

Mikami, K., Kanesaki, Y., Suzuki, I., and Murata, N. 2002. The histidine kinase Hik33 perceives osmotic stress and cold stress in *Synechocystis* sp. PCC 6803. Mol Microbiol. **46**(4) 905-915.

Mitta, M., Fang, L., and Inouye, M. 1997. Deletion analysis of *cspA* of *Escherichia coli*: requirement of the AT-rich UP element for *cspA* transcription and the downstream box in the coding region for its cold shock induction. Mol Microbiol. **26**(2): 321-335.

Nakao, M., Okamoto, S., Kohara, M., Fujishiro, T., Fujisawa, T., Sato, S., and Nakamura, Y. 2010. CyanoBase: the cyanobacteria genome database update 2010. Nucleic Acids Res. **38:** D379-D381.

Netterling, S., Vaitkevicius, K., Nord, S., and Johansson, J. 2012. A *Listeria monocytogenes* RNA helicase essential for growth and ribosomal maturation at low temperatures uses its C terminus for appropriate interaction with the ribosome. J Bacteriol. **194**(16): 4377-4385.

Osteryoung, K. W., and Nunnari, J. 2003. The division of endosymbiotic organelles.
Sci. **302**(5651): 1698-1704.

Owttrim, G. W. 2013. RNA helicases: Diverse roles in prokaryotic response to abiotic stress. RNA Biol. **10**: 96-11.

Paerl, H. W., and Pinckney, J. L. 1996. A mini-review of microbial consortia: their roles in aquatic production and biogeochemical cycling. Microb Ecol. **31**(3): 225-247.

Pandiani, F., Brillard, J., Bornard, I., Michaud, C., Chamot, S., and Broussolle, V. 2010. Differential involvement of the five RNA helicases in adaptation of *Bacillus cereus* ATCC 14579 to low growth temperatures. Appl Environ Microbiol. **76**(19): 6692-6697.

Patterson-Fortin, L. M., Colvin, K. R., and Owttrim, G. W. 2006. A LexA-related protein regulates redox-sensitive expression of the cyanobacterial RNA helicase, *crhR*. Nucleic Acids Res. **34**(12): 3446-3454.

Peil, L., Virumäe, K., and Remme, J. 2008. Ribosome assembly in *Escherichia coli* strains lacking the RNA helicase DeaD/CsdA or DbpA. FEBS J. **275**(15): 3772-3782.

Prakash, J. S., Krishna, P. S., Sirisha, K., Kanesaki, Y., Suzuki, I., Shivaji, S., and Murata, N. 2010. An RNA helicase, CrhR, regulates the low-temperature-inducible expression of heat-shock genes *groES, groEL1* and *groEL2* in *Synechocystis* sp. PCC 6803. Microbiol. **156**(2): 442-451.

Prud'homme-Généreux, A., Beran, R. K., Iost, I., Ramey, C. S., Mackie, G. A., and Simons, R. W. 2004. Physical and functional interactions among RNase E, polynucleotide phosphorylase and the cold-shock protein, CsdA: evidence for a 'cold shock degradosome'. Mol Microbiol. **54**(5): 1409-1421.

Putnam, A. A., and Jankowsky, E. 2013. DEAD-box helicases as integrators of RNA, nucleotide and protein binding. Biochim Biophys Acta (BBA)-Gene Regulatory Mechanisms. http://dx.doi.org/10.1016/j.bbagrm.2013.02.002.

Redko, Y., Aubert, S., Stachowicz, A., Lenormand, P., Namane, A., Darfeuille, F., Thibonnier, M., and De Reuse, H. 2013. A minimal bacterial RNase J-based degradosome is associated with translating ribosomes. Nucleic Acids Res. **41**(1): 288-301.

Rocak, S., and Linder, P. 2004. DEAD-box proteins: the driving forces behind RNA metabolism. Nat Rev Mol Cell Biol. **5**(3), 232-241.

Rosana, A. R. R., Ventakesh, M., Chamot, D., Patterson-Fortin, L. M., Tarassova, O., Espie, G. S., and Owttrim, G. W. 2012a. Inactivation of a low temperature-induced RNA helicase in *Synechocystis* sp. PCC 6803: physiological and morphological consequences. Plant Cell Physiol. **53**(4): 646-658.

Rosana ARR, Chamot D, and Owttrim GW. 2012b. Autoregulation of RNA helicase expression in response to temperature stress in *Synechocystis* sp. PCC 6803. PLoS ONE **7**(10): e48683.

Rott, R., Zipor, G., Portnoy, V., Liveanu, V., and Schuster, G. 2003. RNA polyadenylation and degradation in cyanobacteria are similar to the chloroplast but different from *Escherichia coli*. J Biol Chem. **278**(18): 15771-15777.

Rowland, J. G., Simon, W. J., Prakash, J. S., and Slabas, A. R. 2011. Proteomics reveals a role for the RNA helicase *crhR* in the modulation of multiple metabolic pathways during cold acclimation of *Synechocystis* sp. PCC6803. J Proteome Res. **10**(8): 3674-3689.

Shivaji, S. 2013. Sensing and molecular responses to low temperature in cyanobacteria. Stress biology of cyanobacteria: Molecular mechanisms to cellular responses 155.

Silverman, E., Edwalds-Gilbert, G., and Lin, R. J. 2003. DExD/H-box proteins and their partners: helping RNA helicases unwind. Gene. **312**: 1-16.

Suzuki, I., Kanesaki, Y., Mikami, K., Kanehisa, M., and Murata, N. 2001. Cold-regulated genes under control of the cold sensor Hik33 in *Synechocystis*. Mol Microbiol. **40**(1): 235-244.

Tsai, Y. C., Du, D., Domínguez-Malfavón, L., Dimastrogiovanni, D., Cross, J., Callaghan, A. J., Garcia-Mena, J., and Luisi, B. F. 2012. Recognition of the 70S ribosome and polysome by the RNA degradosome in *Escherichia coli*. Nucleic Acids Res. **40**(20): 10417-10431.

Vinnemeier, J., and Hagemann, M. 1999. Identification of salt-regulated genes in the genome of the cyanobacterium *Synechocystis* sp. strain PCC 6803 by subtractive RNA hybridization.
Arch Microbiol. **172**(6): 377-386.

Wang, S., Hu, Y., Overgaard, M. T., Karginov, F. V., Uhlenbeck, O. C., and McKay, D. B. 2006. The domain of the *Bacillus subtilis* DEAD-box helicase YxiN that is responsible for specific binding of 23S rRNA has an RNA recognition motif fold. RNA. **12**(6): 959-967.

Wang, Y., Duby, G., Purnelle, B., and Boutry, M. 2000. Tobacco VDL gene encodes a plastid DEAD box RNA helicase and is involved in chloroplast differentiation and plant morphogenesis. Plant Cell Online. **12(**11),:2129-2142.

Chapter 6: Appendix

6.1 Translational control of CrhR expression

The unregulated accumulation of the inactive, truncated CrhR polypeptide in the mutant suggest that CrhR is potentially involved in the regulation of its own abundance through an unknown regulation of the proteolytic machinery (Rosana *et al*., 2012b; Chapter 3; Tarassova and Owttrim, unpublished). Using differential translation inhibitors, specifically targeting initiation or elongation, the requirement for *de novo* protein synthesis for CrhR induction was assessed in cold-stressed wild type and Δ*crhR*^{TR} cells. The translation of CrhR is not inhibited by antibiotics affecting translation initiation (Figure 6.1A) suggesting that the effect of the antibiotic was by-passed. This observation was also observed for the induction of the major *E. coli* cold-shock protein, CspA (Etchegaray and Inouye, 1999). On the contrary, elongation inhibitors block the synthesis of the CrhR polypeptide. This differential result is not due to inactivated antibiotic as the cells tested were all sensitive to the indicated antibiotics, except the *crhR* mutant which is the spectinomycin resistant (Twomey and Owttrim, unpublished data). From the data generated, two hypotheses are proposed. It is theorized that the basal transcript detected in the warm has already initiated translation and upon transfer to cold elongation of the pre-initiated CrhR polypeptide was resumed. This scenario is similar to D1 (PsbA) translation where the nascent D1-polysome complex is targeted to the thylakoid membrane and is completed (Tyystjärvi *et al*., 1996). Second, the potential generation of an alternative ribosome binding site through the formation of an IRES (internal ribosome entry site) could generate the observed effect. Northern analysis revealed two *crhR* transcripts (Figure 6.1A), a ~1.6- and 1.5 knt fragment, where the 1.6 knt mRNA provided maximum CrhR polypeptide level. This double transcript is also observed repeatedly in several experiments (Figure 6.2D; Whitford and Owttrim, unpublished) and identification of the 5' end of these transcripts may shed light to the differential effect observed affecting translation initiation or elongation.

6.2 Phylogenetic analysis of *rimO-crhR* operon

To date, the *in vivo* targets of the *Synechocystis* CrhR RNA helicase are

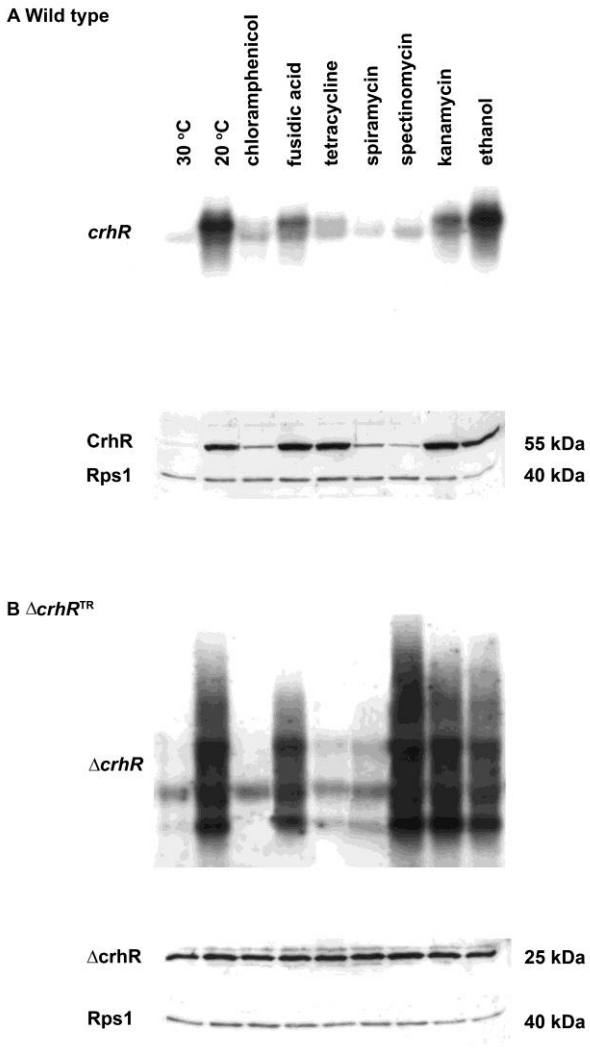

Figure 6.1 *de novo* CrhR synthesis. Wild type (A) and Δ*crhR*^{TR} (B) *Synechocystis* cells were grown to mid-log phase at 30^{o}C (0 min). Indicated antibiotics (150 mg/ml) were added and continued for an additional 1h at 30^{o}C to fully inhibit *de novo* protein synthesis. Cultures were then transferred to 20^{o}C and incubated for 2 h for maximum induction of CrhR synthesis. Samples for RNA and soluble protein extraction were harvested. Northern and western analyses were performed as described previously (Rosana *et al*., 2012b). *crhR* transcript was detected from total RNA probed with a 93 bp *Hinc*II-*Sac*II internal fragment of *crhR*. Western blots were simultaneously probed with antibodies against CrhR (55 kDa) and *E. coli* ribosomal protein S1 (Rps1, 40 kDa), used as a control for protein loading.

still unknown. Genome-wide transcriptional profiling using a custom microarray comparing wild type and *crhR*^{TR} cells suggest a CrhR-specific regulon (Georg and Owttrim, unpublished data). This approach detects the expression level of both non-coding transcripts (e.g. 5' UTR, asRNAs, ncRNAs) as well as the mRNAs making a comprehensive profile of the *Synechocystis* transcriptome responding to both abiotic stress and *crhR* inactivation. Both *slr0082* and *slr0083* transcripts responded to temperature downshift with similarly high induction levels supporting the notion of autoregulated expression as well as an operon structure (Chapter 4). Having a small intergenic region (130 bp) separating the two genes, DOOR (Database of PrOkayotic OpeRons) ver 2.0 (Mao *et al*., 2009) predicted an operon assembly and is further supported by specific riboprobing (**Figure 6.2**) and 5'RACE analysis. The co-expression of the upstream gene, *slr0082*, which is theorized to be controlled by a temperature-regulated promoter, generating a dicistronic message with *crhR*, adds another level of complexity to *crhR* expression. The conservation of this methylthiotransferase-RNA helicase operon structure is mainly limited to cyanobacterial phylum represented by three major orders (**Figure 6.3**). *Synechocystis* belongs to order Chroococcales, while the other two groups are represented by Nostocales and Oscillatoriales. Clustering of the dicistronic operon into three orders was supported by high bootstrap values (100), suggesting a strong sequence and gene structure conservation in each of the clades. Interestingly, gene structure of *rimO-crhR* is specific to the cyanobacterial clade. The only other genomes possessing an operon similar to *rimO-crhR* occurs in *Chitinophaga pinensis* DSM2588 and *Desulfovibrio salexigens* DSM2638. The latter two species although have a predicted operon similar to *Synechocystis rimO-crhR*, sequence analysis of these two potential operons revealed a number of insertion elements in the intergenic region between the two member genes. Overall, the phylogram generated from the operon structure reported here agrees with the pleotropic nomenclature used for cyanobacterial species (Komarek and Hauer, 2013) and identifies the *rimO-crhR* operon as a diagnostic predictor of cyanobacterial lineage .

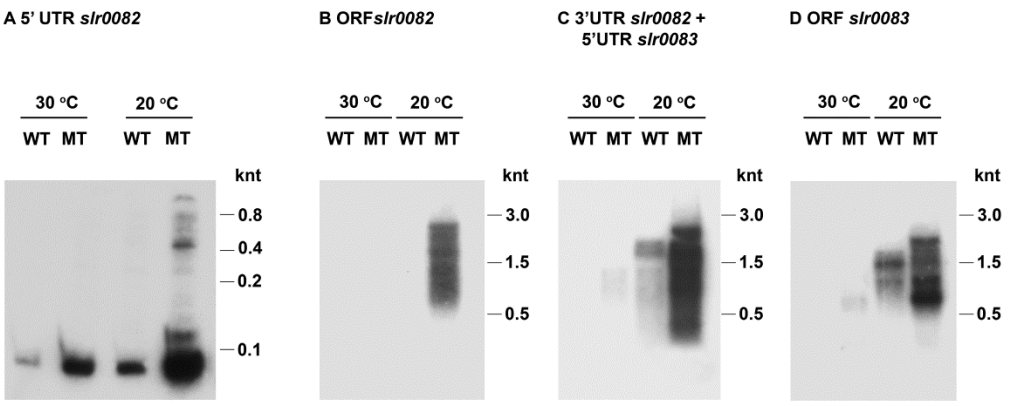

Figure 6.2 Multiple riboprobing of the *Synechocystis slr0082-slr0083* transcript accumulation in wild type (WT) and Δ*crhR*^{TR} (MT) in response to temperature stress (1 hr at 20^{o}C). 5 µg total RNA was resolved on either 8M-10% polyacrylamide gel (A) or formaldehyde 1.2% agarose gel (B-D) and transferred to a nylon membrane (Amersham). Each blot was hybridized by the indicated ^{32}P-labelled riboprobe:

(A) 110 nt riboprobe specific for the *slr0082* 5`UTR

(B) 220 nt riboprobe was hydridized internal to the *slr0082* open reading frame

(C) 345 nt riboprobe detecting the intergenic region encompassing the 3'end of *slr0082* and the 5'UTR of slr0083, and

(D) 93 nt riboprobe hybridizing with the internal *Hinc*II-*Sac*II fragment of the *crhR* open reading frame

6.3 Localization of CrhR in *Synechocystis* sp. PCC 6803: co-sedimentation with the polysome and thylakoid membrane

6.3.1 CrhR RNA helicase co-sediments with the cyanobacterial polysome complex

Ribosome complex was isolated from warm-grown (30^{o}C) and cold-stressed (20^{o}C) wild type and Δ*crhR*^{TR} mutant cells using chloramphenicol-sucrose ultracentrifugation to inhibit the elongation of an actively translating ribosome (Tyystjärvi *et al.*, 2001). After separating the cell lysate on a 1.0 M sucrose cushion, five differentially pigmented layers were harvested (Fig 6.4A,B) and a crude greenish-brown polysome containing pellet was collected (Fig 6.4A). Although concentrated protein (~100 µg) was resolved from these five layers (Fig 5.1C), western blot analysis revealed a 55 kDa CrhR protein detected only in the polysome fraction (Fig 6.1D). Interestingly, a ~65kDa and ~30 kDa polypeptides cross-reacted with the CrhR antibody in layers 1 and 4. The greenish pellet collected from the cushion showed potential thylakoid membrane contamination, since pure polysomes have a brown-glassy appearance. The purity of the polysome fraction therefore necessitates more stringent fractionation. To address this concern, a more extensive CrhR fraction profiling was performed on wild type and Δ*crhR*^{TR} cells to identify CrhR localization within the *Synechocystis* cell lysate (Fig 6.5, 6.6). This was accomplished by treating the isolated polysome with polyoxy-10-tridecyl ether and performing a second sucrose cushion ultracentrigation. Wild type cells grown at 30^{o}C revealed CrhR is present in the ultracentrifugation (UC1) pellet but not in the polysome fraction although the ribosomal protein small subunit S1 (Rps1) confirms the presence of ribosomal complexes in the polysome (Fig 6.5A). The membrane fraction (UC1), hypothesized to be predominantly thylakoid membrane, revealed a strong ~65 kDa band cross reacting with the anti-CrhR antibody (Fig 6.5A). Conversely, cold stressed cells revealed CrhR in both membrane and polysome fractions, with differential size of ~65 and 55 kDa, respectively (Fig 6.5B).

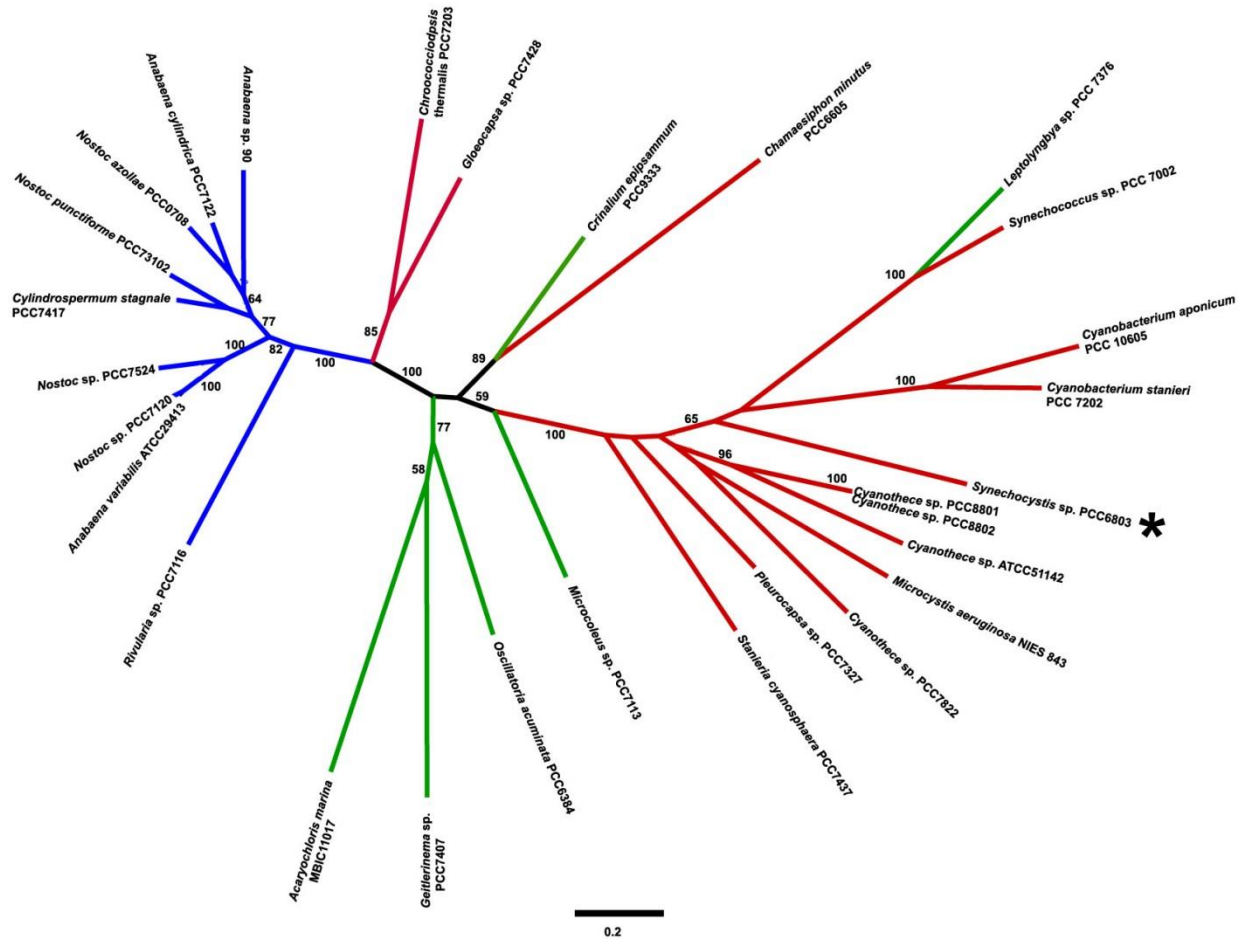

Figure 6.3 Maximum likelihood phylogenetic tree of *Synechocystis* sp. PCC 6803 *slr0082-slr0083* operon structure in phylum cyanobacteria. Scale bar represents 1 nucleotide change every 10 nucleotide sequence. Bootstrap values support greater than 50 of 100 replicates is indicated at the nodes. Three distinct clades are represented by the colored clusterings: order Nostocales (blue), order Oscillatoriales (green) and Chroococcales (red). *Synechocystis* sp PCC 6803 is indicated by *.

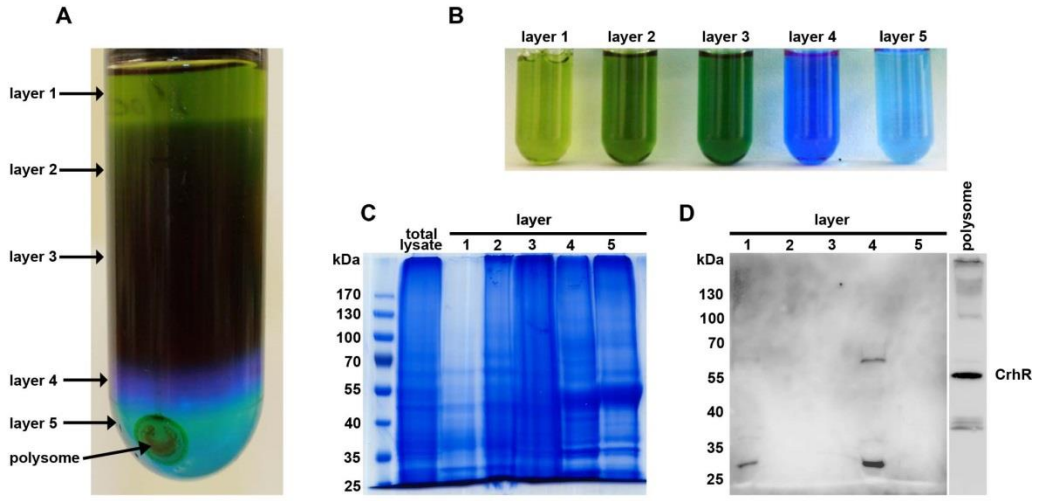

Figure 6.4 Pigmented ultracentrifugated fractions of *Synechocystis* sp. PCC 6803 total cell lysate from polysome isolation. (A) Ultracentrifuge tube showing five distinct colored fractions and greenish-brown polysome pellet. (B) Aliquots of five distinct layers in cuvettes: light green, green, blue green, royal blue, and light blue layers. (C) Coomassie-stained gel showing SDS-PAG resolved protein from the colored fractions. (D). Western analysis of fractionated cell lysate (100 ug) and ribosomal fraction (A_{260}=100). Membrane was probed with anti-CrhR antibody and detected using chemiluminescence method.

6.3.2 Truncated CrhR impairs CrhR cellular localization

A similar polysome analysis was performed on the Δ*crhR*^{TR} to identify the potential role of the C-terminal extension in CrhR localization. A very striking and interesting difference is that the truncated polypeptide was detected in all layers obtained after ultracentrifugation (Fig 6.5C, D). As reported previously (Rosana *et al*., 2012), the truncated polypeptide is present irrespective of temperature (Fig 6.5C,D) with slightly higher levels detected in the cold stress cells (Fig 6.5D).

6.3.3 CrhR RNA helicase localized in the thylakoid region of *Synechocystis*

The presence of the ~60 kDa polypeptide cross-reacting with the CrhR antibody in the membrane fractions necessitated analysis of the individual membrane found in this cyanobacterium. A commonly used discontinuous sucrose gradient method (El-Fahmawi and Owttrim, 2003) was performed to separate the three membrane systems in *Synechocystis* namely: outer membrane (OM, 10% sucrose), plasma membrane (PM, 30% sucrose) and the photosynthetic network, thylakoid membrane (TM, 39% sucrose). Multiple congruent western analyses using membrane specific antibodies against known membrane-associated protein was used to assess the purity of the fractionated membranes and confirm CrhR localization (Fig 6.6).

The thylakoid-associated integral protease FtsH, responsible for the turnover of a number of photosystems protein such as D1 and its intermediates was used as a marker for thylakoid membrane layers (REF). The anti-FtsH antibody against *Arabidopsis* (a kind gift from Z. Adam, Hebrew University of Jerusalem) cross-reacted with two *Synechocystis* FtsH isomers from the 39% sucrose layer (Fig. 6.6) together with the detection of the ~60 kDa CrhR polypeptide in the same layer. The presence of both FtsH and CrhR from the thylakoid membrane fraction coupled with an immunogold electron microscopic analysis (Tarassova and Owttrim, unpublished; Lang and Owttrim, unpublished) further verify the localization of CrhR in the thylakoid region.

We utilized the vesicle inducing protein Vipp1 which is involved in thylakoid biogenesis as marker for plasma membrane. A strong ~36 kDa band immunodecorated by the anti-Vipp1 antibody (a gift from W. Hess, University of Freiburg) was detected at the 30% sucrose layer where CrhR is not found (Figure 6.6). This layer in the sucrose step gradient is where majority of the cyanobacterial plasma membrane is concentrated (Murata and Omata, 1988).

Unlike the CrhC RNA helicase in *Anabaena* sp. PCC 7120 which is localized in the pole of the cell (El Fahmawi and Owttrim 2003), CrhR doesn't seemed to localize in the plasma membrane. Interestingly, three bands were observed in the thylakoid fraction (39%) and a single but slow migrating polypeptide was established in the cell wall pellet. Though the Vipp1 was annotated to have a 28 kDa weight, the protein most likely has several post translational modifications for it to localize in the plasma membrane hence migrating differentially in an SDS-PAG. This observation is similar with Westphal *et al*, 2001 where only the recombinant Vipp1 exemplified the theoretical molecular weight while the actual protein isolated from *Synechocystis* was detected at around 36 kDa. One striking difference is that cold induction reduces the expression of this vesicle inducing protein, perhaps in response to membrane freezing. Furthermore, tiling microarray analysis of wild type cells supports the low level of Vipp1 protein in the cold in congruence with *vipp1* mRNA whose level decreases ~2.2 fold upon temperature downshift (Georg, unpublished data).

An extensive proteomic analyses of *Synechocystis* has been done including the soluble fraction (Simon *et al*, 2002), thylakoid membrane (Norling *et al*, 1998; Srivastava *et al*, 2005), plasma membrane (Huang et al, 2002) and outer membrane (Huang et al, 2004). None of these studies revealed CrhR RNA helicase to localize in any of the three membrane systems nor the cytoplasm. This is most likely due to the fact that these studies resolved the isolated proteins from the membranous fractions using a 2D-gel analysis which limits the isoelectric pH

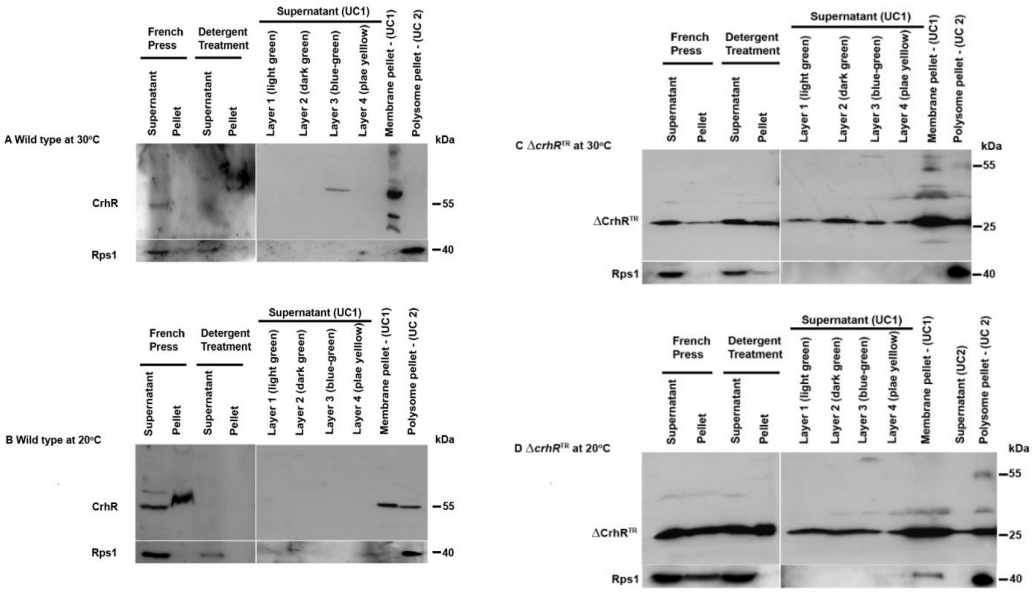

Figure 6.5. Western analysis of ultracentrifuge-fractionated total wild type (A,B) and Δ*crhR*^{TR} (C,D) *Synechocystis* sp. PCC 6803 cell lysate. Soluble cell lysate was overlaid on 1M sucrose cushion and ultracentrifuged at 37 000 rpm for 16 h at 4^{o}C. Western analysis with the anti-ChR antibody revealed a 55 kDa CrhR polypeptide co-sedimenting with the polysome pellet in conjunction with a 40 kDa polypeptide cross reacting with *E. coli* anti-RpS1 antibody. Cells grown at 30^{o}C (A,C) and cells cold shocked at 20^{o}C for 2 h (B,D).

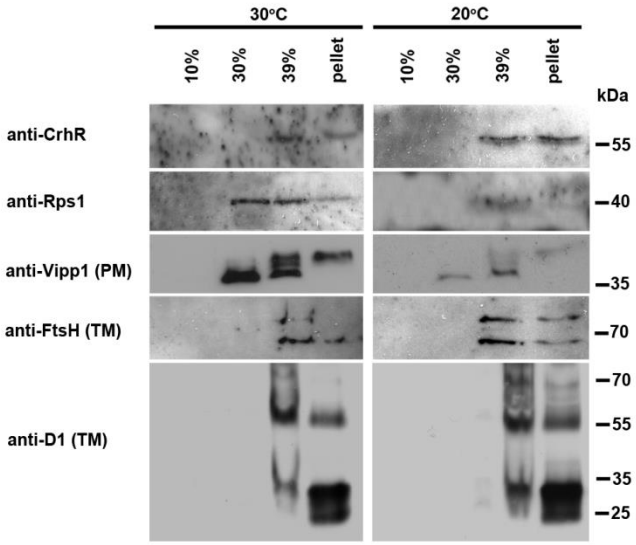

Figure 6.6. Discontinuous sucrose gradient analysis of *Synechocystis* membranes. Total membrane was harvested from warm grown and cold shocked wild type cells and overlay on a discontinuous sucrose gradient and ultracentrifuge at 37000 rpm for 16 hr at 4^{o}C. Equal volume of each fraction was resolved on 10% SDS-PAG and electroblotted on a nitrocellulose membrane. Parallel western analyses were performed using anti-CrhR antibody (*Synechocystis*), anti-Rps1antibody (*E. coli*), anti-Vipp1 antibody (*Synechocystis*), anti-FtsH antibody (*Arabidopsis thaliana*), and anti-D1 antibody (*Synechocystis*).

range to 4-7. The calculated isoelectric pH of CrhR is around 8.7 which then remove it from the gel cut-off. Furthermore, the proteomics studies utilized cells grown at the optimum temperature of 30-34^{o}C, temperatures at which CrhR may not have been abundant enough to detect.

6.4 CrhR Protein Interactome: Effectors of transcription, processing and translation

DEAD-box RNA helicases are often associated with multisubunit complexes performing diverse function in RNA metabolism (Owttrim, 2013). Several attempts were performed to identify interacting polyeptides with CrhR using both native and truncated CrhR. Approaches such as FLPC (fast phase liquid chromatography) revealed CrhR RNA helicase is co-immigrating as a multi-subunit complex eluting at around ~600 kDa (Skeik and Owttrim, unpublished data) while co-immunoprecipitation and affinity column purification (Tarassova and Owttrim, unpublished data) as well as polysome sucrose cushion ultracentrifugation (Rosana and Owttrim, unpublished) revealed a plethora of proteins identified by mass spectrometry. A common theme arising from these endeavours is the co-localization of CrhR with the ribosomal subunit. All polysome pellet revealed an extensive pool of ribosomal proteins from both the 30s and 50s ribosomal subunits (Fig 6.7). Interestingly, RNases reported to interact with DEAD-box RNA helicases as well as thylakoid-associated polypeptides were also detected. A very interesting and emerging trend with RNA helicase complexes from other bacterial systems is the coupling of three seemingly contradictory processes, transcription, translation and degradation. The *E. coli* degradosome assembled through the endonuclease, RNase E is recognizing the 70S ribosomal subunit as well as an actively translating polysome (Tsai *et al*., 2012). A second account associated the sole DExD-box RNA helicase, RhpA with an RNaseJ-based degradosome was found interacting with the translating polysome in Helicobacter pylori (Redko *et al*., 2013).

Although CrhR has not been demonstrated conclusively to interact with either the translational or RNA degrading machineries, bioinformatic predictions supports a protein interactome involving effector proteins involved in transcription, mRNA processing and degradation as well as translation (Table 6.1). The transcription factor, SigB, could potentially be responsible for the transient expression of *crhR*, where CrhR binds this positive regulator and represses operon transcription. RNA polymerase subunits (α, β) were also detected in the *Synechocystis* polysome preparation similar to the *Helicobacter* RNaseJ-RhpA-polysome tandem affinity purification (Redko *et al*., 2013).

Another compelling protein predicted was the exoribonuclease, PNPase, which then potentially act as a minimum degradosome with CrhR for specific cold-stabilized transcript degradation which was previously demonstrated *in vitro* for the *E. coli* Pnpase- RhlB RNA helicase RNA degradation pathway (Liou *et al*., 2002). A number of translational apparatus components (Rps15, Rps2) or the cold-inducible ribosomal binding factors (RbfA) are also predicted to interact with CrhR (Table 5.1). If these association(s) will be demonstrated *in vivo,* CrhR will be the first helicase from a prokaryotic photosynthetic organism to support a cold-adapted ribosome/ degradosome complex, similar to the CsdA-mediated cold-specific ribosome in *E. coli* (Prud'homme-Genereux *et al*., 2004).

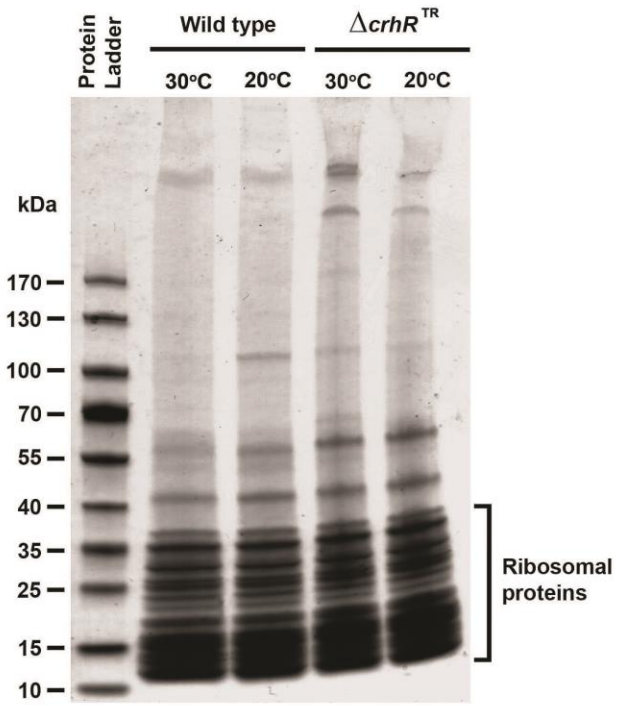

Figure 6.7 Polysome isolation in warm-grown and cold-stress wild type and Δ*crhR*^{TR} *Synechocystis* cells using sucrose cushion ultracentrifugation. Polysome was isolated as described in Tyystjari *et al* (2001) with slight modifications. Three liter cell culture pellet (equivalent to 100 µg chl *a* per ml) was passed through a continuous French press cell press (American Instrument Company) system at 20 000 psi three times. The lysate was clarified twice at 10 000 rpm. Clarified supernatant was layered on top of 1M sucrose cushion buffer and centrifuge at 37 000 rpm at 4^{o}C for 16 h in a swing-bucket SW40Ti rotor using L8-60M ultracentrifuge (Beckman). Polysome pellet suspension (A_{260} = 100U) was resolved on an SDS-4-15% PAG and stained with colloidal comassie. Differentially represented polypeptide was excised or the whole lane was cut into 10 equal sections for total protein mass spectrometry analysis. Mass spectrometry was performed by the Institute of Biomolecular Design at the University of Alberta.

Table 6.1 Predicted CrhR protein interactome using the STRING ver 9.05 (Franceschini *et al*., 2013) algorithm with confidence scoring set to ≥ 0.85

Predicted CrhR-interacting protein	**Function (by homology)**	**Score**
SigB (*sll0306*)	RNA polymerase sigma factor; Sigma factors are initiation factors that promote the attachment of RNA polymerase to specific initiation sites and are then released	0.97
Pnpase (*sll1043*)*	Ppolynucleotide phosphorylase/polyadenylase; Involved in mRNA degradation. Hydrolyzes single-stranded polyribonucleotides processively in the 3'- to 5'-direction	0.95
RbfA (*sll0754*)	Ribosome-binding factor A; Associates with free 30S ribosomal subunits (but not with 30S subunits that are part of 70S ribosomes or polysomes). Essential for efficient processing of 16S rRNA. May interact with the 5'-terminal helix region of 16S rRNA	0.94
RimO (*slr0082*)	Ribosomal protein S12 methylthiotransferase; Catalyzes the methylthiolation of an aspartic acid residue of ribosomal protein S12	0.92
Nth (*slr1822*)	Endonuclease III; Possess an apurinic and/or apyrimidinic endonuclease activity and a DNA N-glycosylase activity. Incises damaged DNA at cytosines, thymines and guanines. Acts on a damaged strand, 5' from the damaged site	0.90
Slr1031	Tyrosyl-tRNA synthetase; Catalyzes the attachment of tyrosine to tRNA(Tyr) in a two-step reaction: tyrosine is first activated by ATP to form Tyr- AMP and then transferred to the acceptor end of tRNA(Tyr)	0.89
RpsB (*sll1260*)*	30S ribosomal protein S2	0.89
PheS (*sll0454*)‡	Phenylalanyl-tRNA synthetase subunit alpha	0.88
RpsO (ssl1784)*	30S ribosomal protein S15; One of the primary rRNA binding proteins, it binds directly to 16S rRNA where it helps nucleate assembly of the platform of the 30S subunit by binding and bridging several RNA helices of the 16S rRNA	0.85
TypA (*sll1105*)*	Elongation factor EF-G; Probably interacts with the ribosomes in a GTP dependent manner	0.85

* polypeptide detected from polysome isolated from 2h-cold stress WT cells
‡ Phenylalanyl-tRNA synthetase subunit beta was detected from polysome isolated from 2h-cold stress WT cells

6.3 CrhR and RNA-folding predictions

The 5' ends of both the *slr0082-slr0083* dicistronic transcript and the processed *crhR* transcript were identified using 5' RACE analysis (Chapter 4). The folding of the processed *crhR* was compared with the transcriptional start site reported previously (Vinnemeier and Hagemann, 1999). RNA-folding of the transcripts was predicted using M-fold analysis (Zuker, 2003) at the optimum growth temperature (30^{o}C) and cold-stress conditions (20^{o}C). RNAs folded at the 20^{o}C is significantly stabilized, as indicated by lower Gibbs free energies (ΔG), frequently resulting in a more complex secondary structures such as multi-branched hairpin/stem loops (Fig 6.8C) or a ROSE-like element (Fig 6.9A,B,C; Chowdhury *et al*., 2006). The generation of these structured RNA regions in the *crhR* transcript potentially contributes to its stabilization in the cold. Furthermore, the translation of these structured RNAs require RNA chaperones such as CrhR RNA helicases or Rps1, especially the ribosome binding site (RBS) is predicted to be restricted by a stem loop (Fig 6.9). For a number of cyanobacterial transcripts lacking the Shine-Dalgarno sequence (Mutsuda and Sugiura, 2006), Rps1 recruits the ribosome complex. Here we propose that CrhR RNA helicase relieves the secondary structure for the proper functioning of the translational apparatus assemblage, supporting a cold-adapted ribosome.

The *slr0082* 5' untranslated region (UTR) accumulates in both wild type and Δ*crhR*^{TR} at all temperatures with approximately 8-10 fold enhancement at 20^{o}C (Chapter 4). Processing of the dicistronic transcript by an endonucleolytic cleavage generates this stable small RNA species. Accumulation of the 5' UTR could act as regulatory small RNA potentially targeting other transcripts from the genome, which then necessitate the identification of its sequence. This can be done by either circle ligation – sequencing approach (Polidoros *et al*., 2006) or small RNA enrichment coupled TOPO cloning (Rosas-Cardenas *et al*., 2007). The current data also shows that the accumulation of this small stable RNA in the warm while *slr0082* ORF is undetected (Chapter 4) could suggest a potential attenuation of transcription in the warm and alleviation to give an operon read-through in the cold.

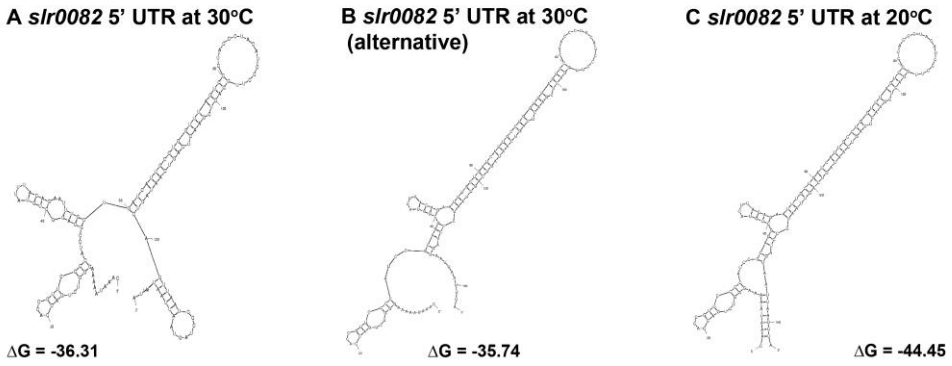

Figure 6.8 Predicted RNA folding (Zuker, 2012) of the 147 nt 5' UTR of *slr0082-slr0083* operon. Calculated Gibbs-free energy (ΔG) are indicated.

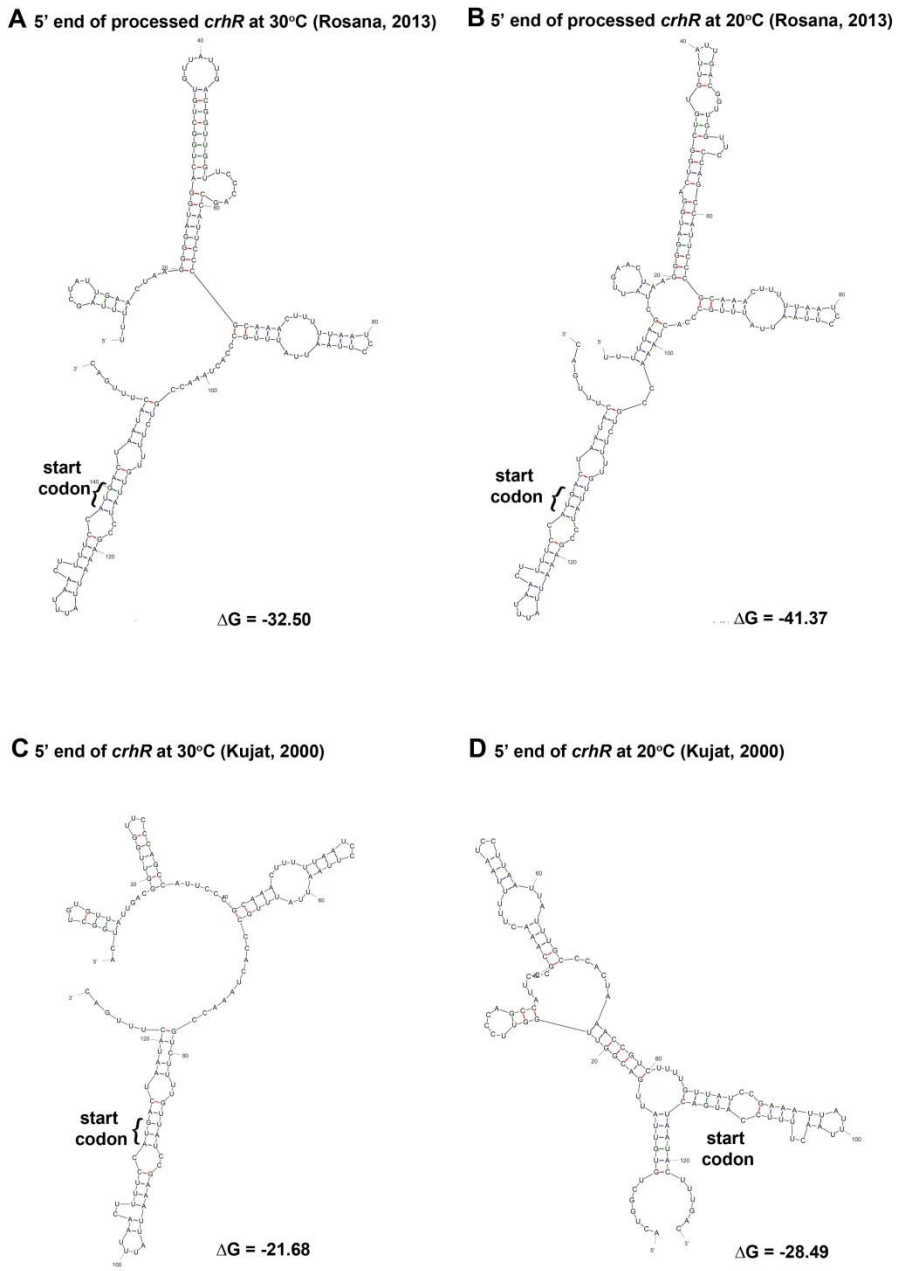

Figure 6.9 Predicted RNA folding (Zuker, 2012) of the *crhR* transcript identified by 5' RACE (A,B) (Chapter 4) and primer extension analysis (C,D) (Kujat and Owttrim, 2000). Start codon and calculated Gibbs-free energy (ΔG) are indicated.

6.5 References

Chowdhury, S., Maris, C., Allain, F. H., and Narberhaus, F. 2006. Molecular basis for temperature sensing by an RNA thermometer. EMBO **25**(11): 2487-2497.

El-Fahmawi, B., and Owttrim, G. W. 2003. Polar-biased localization of the cold stress-induced RNA helicase, CrhC, in the cyanobacterium *Anabaena* sp. strain PCC 7120. Mol Microbiol. **50**(4): 1439-1448.

Etchegaray, J. P., and Inouye, M. 1999. CspA, CspB, and CspG, major cold shock proteins of *Escherichia coli*, are induced at low temperature under conditions that completely block protein synthesis. J Bacteriol. **181**(6): 1827-1830.

Franceschini, A., Szklarczyk, D., Frankild, S., Kuhn, M., Simonovic, M., Roth, A., Lin, J., and Jensen, L. J. 2013. STRING v9. 1: protein-protein interaction networks, with increased coverage and integration. Nucleic Acids Res. **41**(D1): D808-D815.

Komárek, J., and Hauer, T. 2013. CyanoDB. cz—On-line database of cyanobacterial genera. http://www.cyanodb.cz/

Kujat, S. L., & Owttrim, G. W. 2000. Redox-regulated RNA helicase expression. Plant Physiol. **124**(2), 703-714.

Huang, F., Parmryd, I., Nilsson, F., Persson, A. L., Pakrasi, H. B., Andersson, B., and Norling, B. 2002. Proteomics of *Synechocystis* sp. strain PCC 6803 identification of plasma membrane proteins. Mol Cell Proteomics. **1**(12): 956-966.

Huang, F., Hedman, E., Funk, C., Kieselbach, T., Schröder, W. P., & Norling, B. 2004. Isolation of outer membrane of *Synechocystis* sp. PCC 6803 and its proteomic characterization. Mol Cell Proteomics. **3**(6): 586-595.

Liou, G. G., Chang, H. Y., Lin, C. S., and Lin-Chao, S. 2002. DEAD box RhlB RNA helicase physically associates with exoribonuclease PNPase to degrade double-stranded RNA independent of the degradosome-assembling region of RNase E. J Biol Chem. **277**(43): 41157-41162.

Mao, F., Dam, P., Chou, J., Olman, V., and Xu, Y. 2009. DOOR: a database for prokaryotic operons. Nucleic Acids Res. **37:** D459-D463.

Murata, N., and Omata, T. 1988. Isolation of cyanobacterial plasma membranes. Met Enzymol. **167:** 245.

Mutsuda, M., and Sugiura, M. (2006). Translation initiation of cyanobacterial mRNAs requires the 38-kDa ribosomal protein S1 but not the Shine-Dalgarno

sequence: Development of a cyanobacterial in vitro translation system. J Biol Chem. **281**(50): 38314-38321.

Norling, B., Zak, E., Andersson, B., and Pakrasi, H. 1998. 2D-isolation of pure plasma and thylakoid membranes from the cyanobacterium *Synechocystis* sp. PCC 6803. FEBS Lett. **436**(2): 189-192.

Owttrim GW. 2013. RNA helicases: Diverse roles in prokaryotic response to abiotic stress. RNA Biol. 10:96-110.

Prud'homme-Généreux, A., Beran, R. K., Iost, I., Ramey, C. S., Mackie, G. A., and Simons, R. W. 2004. Physical and functional interactions among RNase E, polynucleotide phosphorylase and the cold-shock protein, CsdA: evidence for a 'cold shock degradosome'. Mol Microbiol. **54**(5): 1409-1421.

Redko, Y., Aubert, S., Stachowicz, A., Lenormand, P., Namane, A., Darfeuille, F., Thibonnier, M., and De Reuse, H. 2013. A minimal bacterial RNase J-based degradosome is associated with translating ribosomes. Nucleic Acids Res. **41**(1): 288-301.

Rosana, A. R. R., Chamot, D., and Owttrim, G. W. 2012. Autoregulation of RNA helicase expression in response to temperature stress in *Synechocystis* sp. PCC 6803. PloS ONE **7**(10): e48683.

Simon, W. J., Hall, J. J., Suzuki, I., Murata, N., and Slabas, A. R. 2002. Proteomic study of the soluble proteins from the unicellular cyanobacterium *Synechocystis* sp. PCC6803 using automated matrix-assisted laser desorption/ionization time of flight peptide mass fingerprinting. Proteomics. **2:**17351.

Skeik, R. and Owttrim G.W. 2012. Dimerization of the DEAD-Box cyanobacterial RNA helicase Redox, CrhR. Thesis. University of Alberta. 1-185.

Srivastava, R., Pisareva, T., and Norling, B. 2005. Proteomic studies of the thylakoid membrane of *Synechocystis* sp. PCC 6803. Proteomics. **5**(18): 4905-4916.

Tsai, Y. C., Du, D., Domínguez-Malfavón, L., Dimastrogiovanni, D., Cross, J., Callaghan, A. J., Mena, J.G. and Luisi, B. F. 2012. Recognition of the 70S ribosome and polysome by the RNA degradosome in *Escherichia coli*. Nucleic Acids Res. **40**(20): 10417-10431.

Tyystjärvi, T., Mulo, P., Mäenpää, P., and Aro, E. M. 1996. D1 polypeptide degradation may regulate *psbA* gene expression at transcriptional and translational levels in *Synechocystis* sp. PCC 6803. Photosynthesis Res. **47**(2): 111-120.

Vinnemeier, J., and Hagemann, M. 1999. Identification of salt-regulated genes in the genome of the cyanobacterium *Synechocystis* sp. strain PCC 6803 by subtractive RNA hybridization. Arch Microbiol. **172**(6): 377-386.

Westphal, S., Heins, L., Soll, J., and Vothknecht, U. C. 2001. Vipp1 deletion mutant of *Synechocystis*: a connection between bacterial phage shock and thylakoid biogenesis. Proc Natl Acad Sci. **98**(7): 4243-4248.

Zuker, M. 2003. Mfold web server for nucleic acid folding and hybridization prediction. Nucleic Acids Res. **31**(13): 3406-3415.